

Modular Approaches to Assemble Macrocycles and Pyridinophanes Containing P/N, Al/N, B/N and Zn/N Connectivity in the Framework

Chandrakala Negi

*A thesis submitted for the partial fulfilment of
the degree of Doctor of Philosophy*



Department of Chemical Sciences

Indian Institute of Science Education and Research Mohali, India

Knowledge city, Sector 81, SAS Nagar, Manauli PO, Mohali 140306, Punjab, India

April 2024

*Dedicated to my beloved
parents and brothers*

DECLARATION

The work presented in this thesis titled “**Modular Approaches to Assemble Macrocycles and Pyridinophanes Containing P/N, Al/N, B/N and Zn/N Connectivity in the Framework**” has been carried out by me under the supervision of **Prof. Sanjay Singh** in the Department of Chemical Sciences, Indian Institute of Science Education and Research (IISER) Mohali, Mohali. This work has not been submitted in part or full for a degree, diploma or a fellowship to any other university or institute. Whenever contributions of others are involved, every effort is made to indicate this clearly with due acknowledgments of collaborative work and discussions. This thesis is a bonafide record of original work done by me and all sources listed within have been detailed in the bibliography.

Chandrakala Negi

Date:

Place:

In my capacity as the supervisor of the candidate's thesis work, I certify that the above statements by the candidate are true to the best of my knowledge.

Dr. Sanjay Singh

Professor

Department of Chemical Sciences

Indian Institute of Science Education and Research Mohali

Date:

Place:

Acknowledgements

First, I would like to express my sincere appreciation and gratitude to my Ph.D. thesis supervisor, Dr. Sanjay Singh, Professor, Department of Chemical Sciences, for his valuable guidance, encouragement, and constant support throughout my Ph.D. I am forever thankful and indebted to him for allowing me to work in his lab and for sharing his knowledge, expertise, guidance, and consistent encouragement throughout this Ph.D. journey. Without his guidance and constant support, I would have never been able to complete this journey. Though I had minimal exposure to fundamental lab techniques, limited knowledge about sensitive research going on in the lab at the beginning of my Ph.D., his teaching improved my practical skills during my research period. I feel privileged to submit my Ph.D. thesis under his unconditional supervision.

Further, I extend my gratitude to my Doctoral Committee Members, Prof. R. Vijaya Anand, and Dr. Debashis Adhikari, Department of Chemical Sciences, for their valuable discussions, feedback, and constructive advice and for evaluating my research progress yearly by spending their valuable time. I express my sincere gratitude to Dr. Angshuman Roy Choudhury for teaching and help in X-ray crystallography.

I want to thank former Directors of IISER Mohali, Professor N. Sathyamurthy, Professor Debi P. Sarkar, and the current Director, Professor J. Gawarishankar, for providing the world-class infrastructure and facilities. I want to thank former Heads of Department, Chemical Sciences, Prof. K. S. Viswanathan, Prof. S. Arulananda Babu, Prof. Sanjay Singh and current Head of Department, Prof. Sripada S. V. Ramasastry, for providing the necessary facilities at the Department of Chemical Sciences. I also acknowledge IISER Mohali for NMR, HRMS, IR, XRD, and other facilities.

I am also thankful to Mr. Balbir and Mr. Triveni for their help. I want to acknowledge the chemistry teaching lab assistants, especially Mr. Mangat, Mr. Prahlad, Mr. Bahadur, Mr. Ankit and Mr. Ajay for their co-operation during my research period.

I would like to give my special thanks to lab senior Dr. Deependra Bawari for teaching me experimental techniques at the initial stages and his constant support during my Ph.D. work. I am highly thankful to all the former and current lab members Dr. Bhupendra Goswami, Dr. Deepika Tyagi, Dr. Krishna Kumar Manar, Dr. Mamta Bhandari, Dr. Sandeep Rawat, Dr. Mandeep Kaur, Mr. Nitish Garg, Dr. Soumydeep Chakraborty, Dr. Vishal Kumar Porwal, Mr. Rohit Kamte, Ms. Darsana Prakash, Ms. Surbhi Bansal, Ms. Alisha Sharma, Ms. Simranjeet Kaur, Mr. Yuvraj Yogesh, Ms. Mansi, Ms. Anju, Ms. Manisha, Mr. Soumya, Ms. Devika and

Ms. Gopika for creating a fun-filled and healthy environment in the lab which makes research enjoyable. I also acknowledge all the summer trainees who worked with me in the lab.

I feel extremely lucky to have friends like Dr. Sandeep Kumar Thakur, Mr. Manu Adhikari, and Ms. Manu Goyal as lab mates, and eternally grateful for their love and unwavering support in lab work as well as for sharing ups and downs in life. Thanks for always being there for me and for all the cherished moments spent together. I would like to give my special thanks to Ms. Manu Goyal for her cooperation and help in lab work.

Words are inadequate to explain my gratitude to all my friends, especially Dr. Prateek Ahuja, Dr. Lona Dutta, Ms. Nisha Bamola, Dr. Prabhakar Singh, Dr. Gurdeep Singh, Dr. Ankit Kumar Gaur, Dr. Rekha, Dr. Bara Singh, Dr. Pavit, Dr. Yogesh Pankhade, Dr. Pooja Bhatt, Dr. Narendra Bisht, Dr. Jyotsana Ojha, Mr. Arjun Bisht, Dr. Yogendra Nainwal, Ms. Sonam Suwasia and all the friends at IISER-Mohali and outside for being with me during good and bad phases of my life. I am grateful to have friends like Dr. Sonam Sharma and Dr. Feroz Ahmad. Your support, encouragement, and laughter have kept me going up, even on the most challenging days.

I am also grateful to all my teachers from the bottom of my heart for their guidance and inspiration from the tender stage of my career. I wish to express my sincere gratitude to my beloved mother, father and brothers (Mr. Harish Singh and Mr. Tajber Singh) who have always believed me, stood with me, and supported me in all circumstances with unconditional love throughout my life. Their love, encouragement, and unwavering belief in me have been a constant source of strength, inspiration, and motivation, and I am deeply grateful for their love and support. Their continuous prayers for me and my progress have allowed me to complete this journey.

Finally, I bow down to ALMIGHTY GOD for giving me the health and energy to complete this work successfully. Completing my Ph.D. journey has been an incredible experience, full of challenges, triumphs, and moments of self-doubt. But through it all, I have been blessed with the support, encouragement, and love of many incredible people. I thank all whom I haven't acknowledged here, and I am eternally grateful for their direct or indirect help. Your love, encouragement, and belief in me have meant more than words can express. Thank you all for being a part of this unforgettable journey.

वागर्थाविव संपृक्तौ वागर्थप्रतिपत्तये।
जगतः पितरौ वन्दे पार्वतीपरमेश्वरौ॥

में शब्द और अर्थ की सिद्धि के लिए, शब्द और अर्थ के समान जुड़े हुए जगत के माता-
पिता पार्वती एवं शंकर को प्रणाम करता हूं।

*For the accomplishment of word and meaning, I bow to Parvati-Shankar (almighty god),
the parents of world who are connected like word and meaning.*

नास्ति विद्यासमो बन्धुर्नास्ति विद्यासमः सुहृत्।
नास्ति विद्यासमं वित्तं नास्ति विद्यासमं सुखम्॥

विद्या के समान कोई बन्धु नहीं है, विद्या के समान कोई मित्र है, विद्या के समान कोई
धन नहीं है और विद्या के समान कोई सुख नहीं है।

*There is no brother like knowledge, there is no friend like knowledge, there is no wealth
like knowledge and there is no happiness like knowledge*

“उत्तिष्ठत जाग्रत प्राप्य वरान्निबोधत।

उठो, जागो और लक्ष्य की प्राप्ति तक मत रुको

Arise, awake and don't stop until you achieve your goal.

Table of Contents

Chapter 1. Cyclodiphosph(III)azane Based Bicyclic Macrocycles: An Attempt to Mimic The Conventional Cryptands.....	1
1.1 Introduction	3
1.1.1. Choice of ligand and bond energy considerations	5
1.1.2. Examples of macrocycles and cryptands containing phosphorous	6
1.2 Results and Discussion.....	10
1.3 Conclusions	21
1.4. Experimental Section	22
1.4.1 General procedure	22
1.4.2 Physical measurements	22
1.4.5 Synthetic procedure.....	23
1.5 Crystallographic Data.....	27
Table 1.5.1 Crystallographic data for bicyclic macrocycles 1, 2 and 4'	27
1.6 References	28
Chapter 2A. Aluminum Bridged [3.3](2,6)Pyridinophanes and Organoaluminum Complexes.....	32
2A.1 Introduction	34
2A.1.1 Choice of Ligand Scaffold	35
2A.2 Results and Discussion.....	40
2A.3 Conclusions	47
2A.4 Experimental Section	48
2A.4.1 General procedure	48
2A.4.2 Starting materials.....	48
2A.4.3 Physical measurements.....	48
2A.4.4 Synthetic procedure.....	49
2A.5 Crystallographic Data.....	52
Table 2A.5.1. Crystallographic data for compounds 1-4.	52
2A.6. References	53

Chapter 2B. Macrocycles Assembled via Hydroborative Dearomatization and Self-sorting of Triazine Rings	58
2B.1 Introduction	60
2B.2 Results and Discussion	64
2B.3 Conclusions	76
2B.4 Experimental Section.....	77
2B.4.1 General procedure.....	77
2B.4.2 Starting materials.....	77
2B.4.3 Physical measurements.....	77
2B.4.4 Synthetic procedure	78
2B.5 Crystallographic Data	81
Table 2B.5.1. Crystallographic data for compounds 2 and 3.....	81
Table 2B.5.2. Crystallographic data for compounds 4 and 5.....	82
2B.6 References	83
Chapter 3. Modular Approach to Macrocycles and Cluster Topologies Assembled Around Zinc Centers	88
Abstract	89
3.1 Introduction	90
3.2 Results and Discussion.....	93
3.3 Conclusions	113
3.4 Experimental section	113
3.4.1 General methods.....	113
3.4.2 Starting materials.....	114
3.4.3 Physical measurements	114
3.4.4 Synthetic procedures	114
3.5 Crystallographic Data.....	121
Table 3.5.1 Crystallographic data of Compounds 1-3.	121
Table 3.5.2 Crystallographic data of Compounds 4-6.	122
Table 3.5.3 Crystallographic data of Compounds 7-9.	123
3.6 References	124
List of Publications.....	127

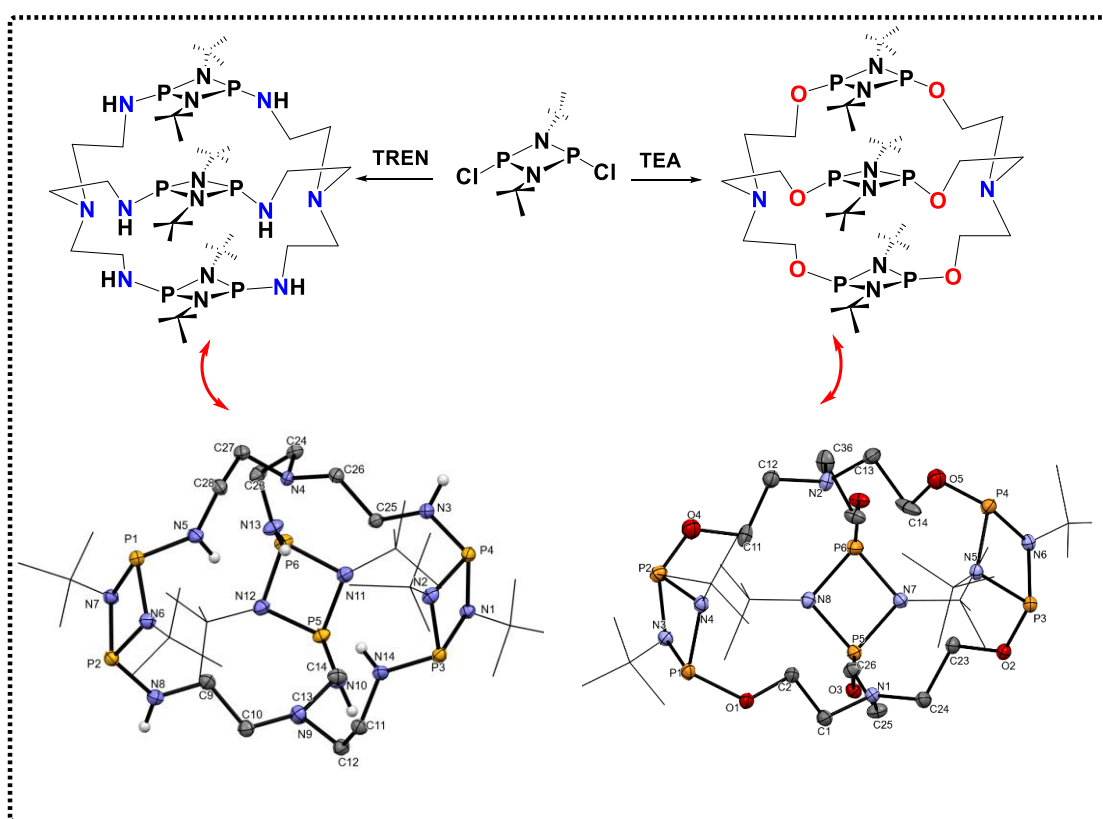
List of Symbols and Abbreviations

Å	Angstrom
Ar	Aryl
avg	Average
ⁿ Bu	Normal butyl
^t Bu	<i>tert</i> -butyl
°C	Degree celsius
DFT	Density function theory
m-CPBA	meta-chloroperbenzoic acid
Et	Ethyl
g	Gram
V	Volume
HOMO	Highest occupied molecular orbital
LUMO	Lowest unoccupied molecular orbit
Hz	Hertz
IR	Infrared
ⁱ Pr	<i>iso</i> -propyl
K	Kelvin
kcal	Kilocalorie
LA	Lewis acid
m	Multiplet
<i>m/z</i>	mass/charge
<i>M</i> ⁺	Molecular ion
Me	Methyl
mol	Mole
M.p.	Melting point
J	coupling constant
ⁿ J _{AB}	n-Bond coupling constant between A and B
NMR	Nuclear magnetic resonance
MS	Mass spectrometry, mass spectra
Ph	Phenyl
ppm	Parts per million

δ	Chemical shift
d	Doublet
s	Singlet
t	Triplet
q	Quartet
m	multiplet
Br	broad
bap	bis(trimethylsilyl)-N,N'-2,6-diaminopyridine
BDMT	2,4-N,N-bisilylateddiamino-6-methyltriazine
Py	Pyridine
R,R',R''	Organic substituents
SiMe ₃	Trimethylsilyl
Eqv.	equivalents
Calcd.	calculated
h	hours
Min.	minutes
RT	Room temperature
THF	Tetrahydrofuran
TMS	Trimethylsilane
BDT	bis(trimethylsilyl)-N,N'-2,4-diamino-1,3,5-triazine

Chapter 1

Cyclodiphosph(III)azane Based Bicyclic Macrocycles: An Attempt to Mimic The Conventional Cryptands



C. Negi,[‡] M. Goyal,[‡] S. Singh,* New members in cryptand family: Cyclophosphazane based bicyclic macrocycles. *Unpublished results*

Abstract: In the past two decades, series of hybrid organic-inorganic cyclodiphosph(III)azane based macrocycles have been experimentally and theoretically highlighted, while the analogous bicyclic counterparts are lagging behind. This chapter of the thesis presents a completely new macrocyclic family of cyclodiphosph(III)azane with the bicyclic framework analogous to cryptands. These are assembled via [3:2] condensations of {[CIP(μ -N^tBu)]₂} building blocks and tripodal linkers TEA (triethanolamine), N(CH₂CH₂OH)₃ or TREN [tris(2-aminoethyl)amine], N(CH₂CH₂NH₂)₃. The successful synthesis of cryptands has been achieved by the removal of HCl in the presence of triethylamine base. The formation of these cryptands were investigated by various spectroscopic techniques, including multinuclear NMR, HRMS, IR, and the solid-state structures were confirmed from single crystal X-ray diffraction. All the new cryptands have symmetrical structures where the arms of tripodal linkers connect three units of [P(μ -N^tBu)]₂ in such a way that it forms like a hollow three-dimensional spherical cage. The progressive increase in building block complexity not only generates future developments in both the phosphazane and main group chemistry but also in the fields of supramolecular chemistry.

1.1 Introduction

Macrocyclic chemistry has expanded remarkably since 1960s. Macrocycles have fascinating ring structures and are attractive candidates for molecular recognition, having incredible complexation properties with vital implications for host-guest and supramolecular chemistry. Nature being an important source of bioactive macrocycles, many synthetic macrocyclic complexes mimic the naturally occurring macrocyclic systems such as porphyrins, metalloproteins, cobalamines, and a number of natural products like vancomycin and erythromycin. Decades ago, in 1987, Donald J. Cram, Jean-Marie-Lehn, and Charles J. Pedersen won the Nobel Prize for their remarkable efforts in discovering and determining the ability of macrocycles to recognize guests. The common examples of traditional macrocycles include crown ethers, azacrowns, cryptands, calixarenes etc. (Figure 1.1).^[1]

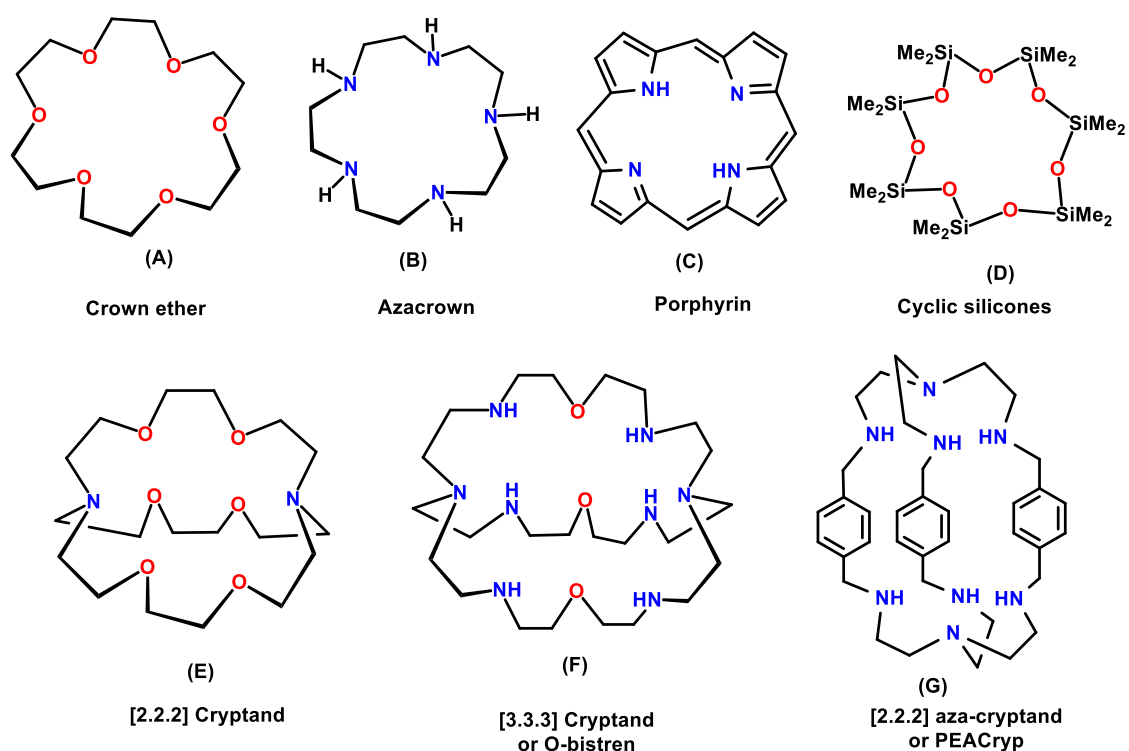


Figure 1.1. Examples of some common macrocycles (top) and some common bicyclic macrocycles (bottom).

Cryptands, are similar in structure to crown ethers, differing in the addition of a bridge that reaches across the ring to give football-shaped structures. The cryptands were first prepared in 1969 by Jean-Marie-Lehn and formed a series of well-defined host-guest complexes (cryptates) with alkali and alkaline-earth metals and were found to be more selective for the guest ions depending on the nature of donor sites and cavity size.

On the basis of atoms in the cyclic core, macrocycles are categorized into three classes: (i) organic, (ii) inorganic, and (iii) hybrid organic-inorganic macrocycles. Families of organic macrocycles have a significant influence on many areas of molecular and supramolecular chemistry, including coordination chemistry, material chemistry, and a wide range of biological disciplines. Comparatively, the field of inorganic macrocycles, in which the cyclic core is composed of elements other than carbon, are far less investigated. The hybrid organic-inorganic macrocycles contain both carbon and elements other than carbon in the core.^[1] The targeted synthesis of inorganic macrocycles is challenging, and the crucial reasons for the steady progression of macrocycles containing inorganic elements in the core ring are (i) the availability of various oxidation states of inorganic elements as compared to carbon; (ii) a broad range of accessible orbitals and hybridization state leads to a mismatch of orbital sizes and results in the weaker bonding interactions within elements from different groups or periods; (iii) simultaneous formation of multiple products; (iv) moisture sensitivity and hydrolytic instability of these compounds which hampers the separation and purification of multiple products; (v) lack of general synthetic strategy for inorganic systems compares to the organic derivatives; (vi) polar nature of bonds leads to kinetically labile and thermodynamic less stable frameworks.^[2] Apart from these challenges, the main difficulty in synthesizing a stable macrocycle is controlling the ring size of the desired macrocycle. In general, the ring-closing processes do not encourage the formation of

large rings; instead, small rings or acyclic polymers tend to form. This problem can be addressed to some extent by adopting a high dilution condition that favors intramolecular reaction leading to cyclization over intermolecular oligomerization/polymerization. The vital prerequisite for macrocycle synthesis is that the substrate or building block should be pre-organized and rigid. However, challenges persist in the intricate synthesis, purification, and characterization of these compounds, which demand substantial expertise and resources. Despite of many hurdles stated above, it has been possible to design inorganic macrocycles.^[2]

1.1.1. Choice of ligand and bond energy considerations

During the last decades, appreciable efforts have been made to assemble inorganic macrocyclic systems. Among these, the P-N phosphazane frameworks are of particular interest due to the robustness stemming from the thermodynamic stability of the P-N bonds (293 kJ.mol⁻¹ comparable to C-C single bond energy 335 kJ.mol⁻¹).

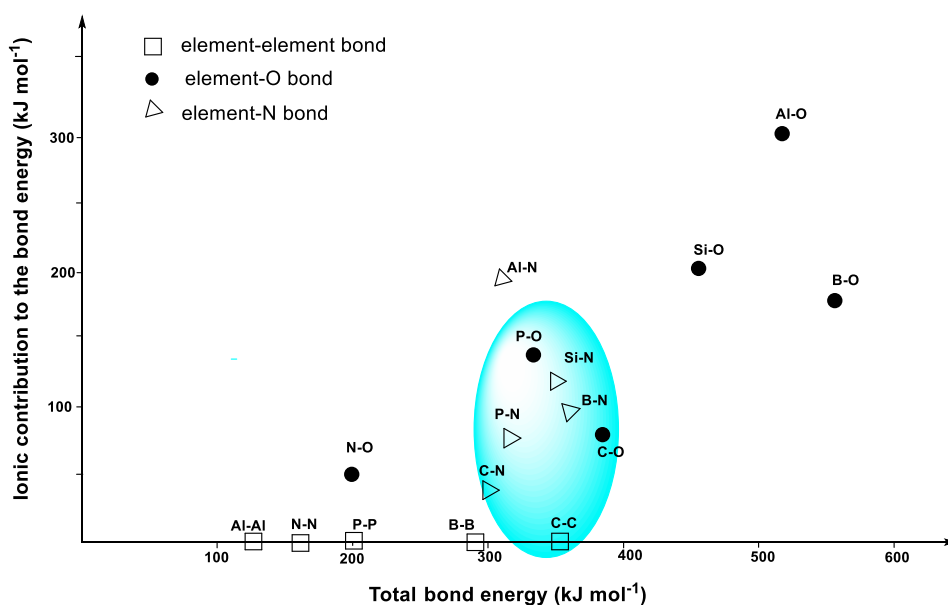


Figure 1.2. Graph for bond energy and bond polarity, adapted from *Chem. Eur. J.* **2018**, *24*, 3073.

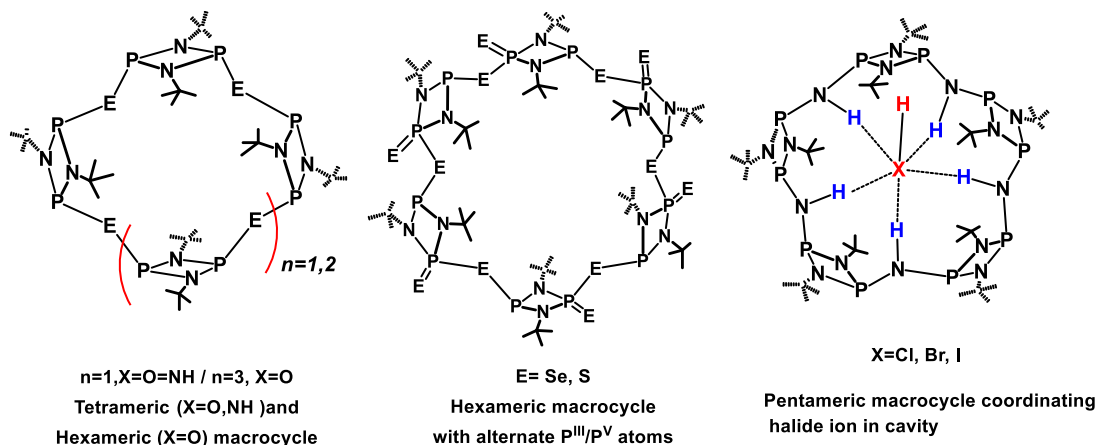
Wright and co-workers compared the bond energy versus the ionic character of covalent bonds and contemplated the importance of these fundamental points to assembling stable inorganic macrocyclic systems. The graph of “heteroatomic bond energy” versus “the ionic contribution to the bonds energy” guides for the range of element-element, element-O, and element-N bonds (Figure 1.2).^[2] The kinetic and thermodynamic stability of carbon-based macrocycles can be considered by relatively low ionic contribution to the bond character, and the bonds in the range of classical organic region are relatively stable and they named it as ‘*sweet spot*’ as illustrated in Figure 1.2. One of the stable P-N bonded building blocks is cyclodiphosph(III)azane $[\text{CIP}(\mu\text{-N}^t\text{Bu})_2]$, and it exists in two isomeric forms, *cis* and *trans*.^[3a] It is found to be the robust building block to assemble macrocyclic systems $[\{\text{P}(\mu\text{-NR})\}_2(\mu\text{-LL}')_n]$ (where LL' is an organic linker), as it fulfills the challenge of being reactive, thermodynamically stable *cis* form is pre-organized and highly symmetrical cyclic four-membered moiety with a rigid framework. It acts as a versatile neutral and anionic ligand in coordination chemistry as well as scaffolds for supramolecular chemistry.^[3]

1.1.2. Examples of macrocycles and cryptands containing phosphorus

In the last two decades, $[\text{CIP}(\mu\text{-N}^t\text{Bu})_2]$ based various inorganic and hybrid organic-inorganic macrocycles have been prepared by its reaction with bifunctional linkers, especially hybrid macrocycles have attracted particular interest due to their dual inorganic-organic nature. The size of the macrocyclic products formed (e.g., di-, tri- and tetrameric species) is strictly determined by the nature of the bifunctional linkers employed (Figure 1.3).^[2-6,8] Using cyclodiphosph(III)azane, Wright and co-workers reported inorganic and hybrid organic-inorganic macrocyclic systems (some of those also act as hosts for anionic and neutral guest molecules).^[2,4] Balakrishna and co-workers have used the donor property of phosphorus atoms to form homo or hetero-

polynuclear complexes, metal-based macrocycles, and coordination polymers.^[2c,5] Chivers, Garcia and co-workers have reported P^{III}/P^V macrocycles of different ring sizes depending on the steric and electronic demand of molecules.^[2a,6]

Cyclodiphosphazane based inorganic macrocycles



Cyclodiphosphazane based hybrid organic-inorganic macrocycles

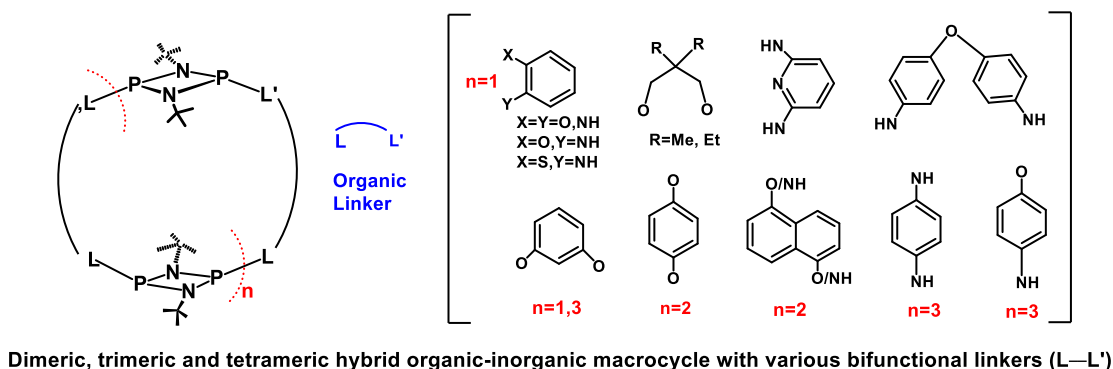


Figure 1.3. Some examples of cyclodiphosphazane $[P(\mu-N^tBu)]_2$ based inorganic macrocycles with different ring sizes (top); hybrid organic-inorganic macrocycles with different linkers and ring sizes (bottom) [$n = 1$ (dimer), $n = 2$ (trimer) and $n = 3$ (tetramer)].

In this area of macrocycles, various phosph(III)azanes based inorganic and inorganic-organic hybrid macrocycles have been reported in the past two decades.^[7,8] However, the analogous bicyclic macrocycles (cryptands) have not been investigated so far. Apart from cyclodiphosphazanes, Majoral and co-workers synthesized various phosphorous-containing macrocycles and cryptands in 1996 (A, Figure 1.4).^[7a] Sinyashin and co-workers have reported the phosphorous-containing bicyclic

macrocycles (or cryptands) using PCl_3 and POCl_3 and an example of stereoselective self-assembly of a cryptand having four asymmetric phosphane groups (**B**, **C**, **D**, Figure 1.4).^[7b,d] Von Hanisch and co-workers have reported the donor-type Si-O-P- bonded [2.1.1] inorganic cryptand (**E**, Figure 1.4).^[7c]

Phosphorous containing cryptands

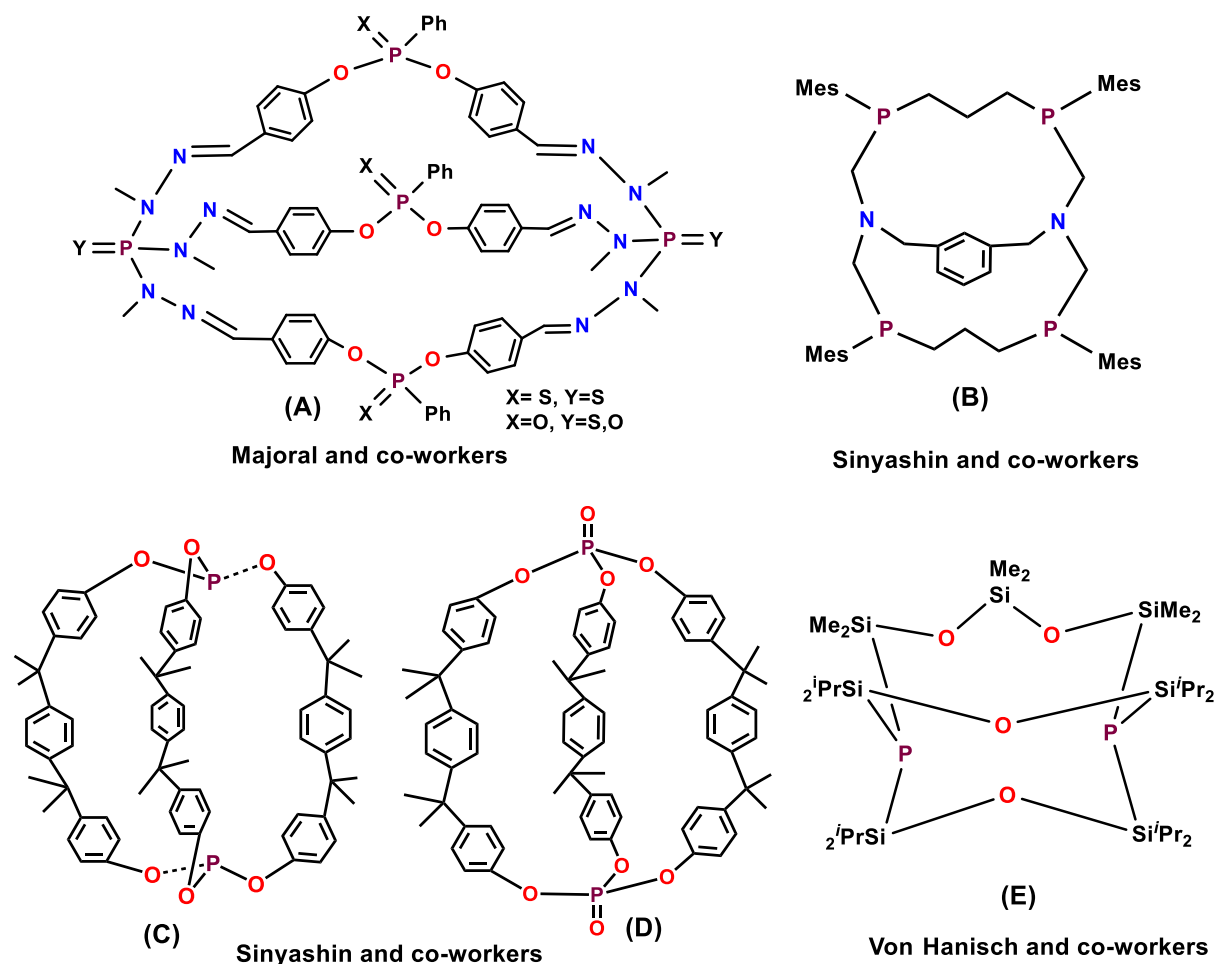


Figure 1.4. Examples of phosphorous containing cryptands.

Since the 2000s, despite various reports on cyclodiphosphazanes-based hybrid organic-inorganic macrocycles, no experimental report has been published on the host-guest and supramolecular interaction of those molecules. The first fully inorganic NH-bridged pentameric macrocycle was reported in 2002,^[3e] however, its first implementation as a host for small organic molecules was experimentally demonstrated in 2019.^[9] The longer timespan taken could be due to their polar bonding nature, air-

moisture sensitivity, number of atoms in bonding proximity, and size of the macrocycle. If the intensity of some of the hurdles reduces, it could be possible that inorganic frameworks can perform like traditional organic analogs in supramolecular chemistry. Like bidentate ligands have better coordination ability than monodentate ligands, and the additional bridge in cryptand across the ring facilitates more effective encapsulation of metal ions. Consequently, cryptands have enhanced binding and selectivity for guests compared to crown ethers. Motivated by the above idea, we were interested in synthesizing the hybrid inorganic-organic cryptands as they can be the key scaffold to develop the novel supramolecular chemistry of main group species. For that, various tripodal linkers and different reaction pathways have been investigated. Both aromatic [1,1,1-*tris*(4-hydroxyphenyl)ethane (THPE)] as well as aliphatic (tris(hydroxymethyl)ethane (THME), triethanolamine (TEA), *tris*(2-aminoethyl)amine (TREN)) linkers have been examined. The reaction with 1,1,1-*tris*(4-hydroxyphenyl)ethane (THPE) does not give a clean product, while in the case of 1,1,1-*tris*(hydroxymethyl)ethane (THME), the dimeric 16 membered macrocyclic product obtained leaving one arm unreacted rather than the expected bicyclic macrocycle. The bicyclic molecules {TEA₂-[P₂(μ-N^tBu)₂]₃} (**1**) and {TREN₂-[P₂(μ-N^tBu)₂]₃} (**2**) have been successfully assembled with TEA and TREN, respectively. Among the bases, using triethylamine (NEt₃) as a base seems to be a more convenient route over *n*BuLi. In literature, TEA and TREN have been used as linkers with organic partners to synthesize organic bicyclic molecules.^[1] These bicyclic molecules structurally resemble the conventional organic multidentate bicyclic molecules called cryptands. The common example N[CH₂CH₂OCH₂CH₂OCH₂CH₂]₃N is called [2.2.2]cryptand, where the numbers indicate the number of binding sites (ether oxygen atoms) in each of the three bridges between the amine nitrogen caps. Similarly, the macrobicycle, {TEA₂-

$[P_2(\mu-N^tBu)_2]_3$ (**1**) contains two oxygen atoms in each arm, and the nitrogen analogue, $\{TREN_2-[P_2(\mu-N^tBu)_2]_3\}$ (**2**) contains two nitrogen atoms in each arm between the amine nitrogen caps. Figure 1.5 illustrates the structural comparison between conventional organic cryptands and novel bicyclic compounds.^[1]

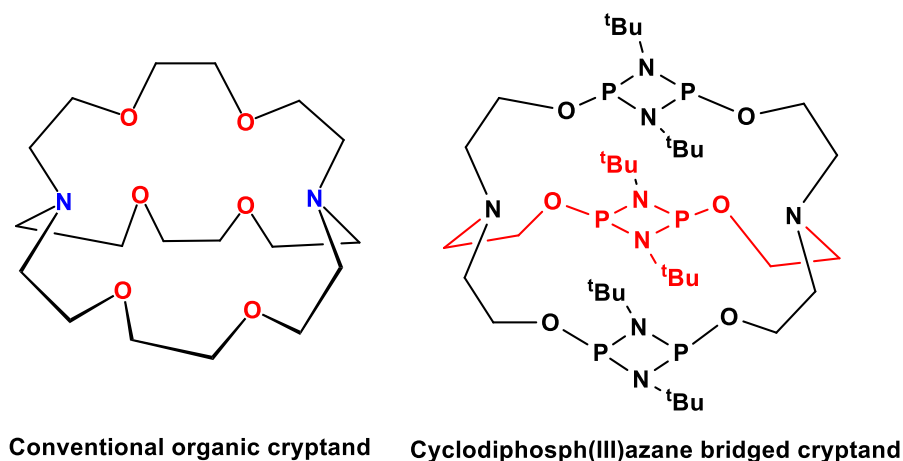
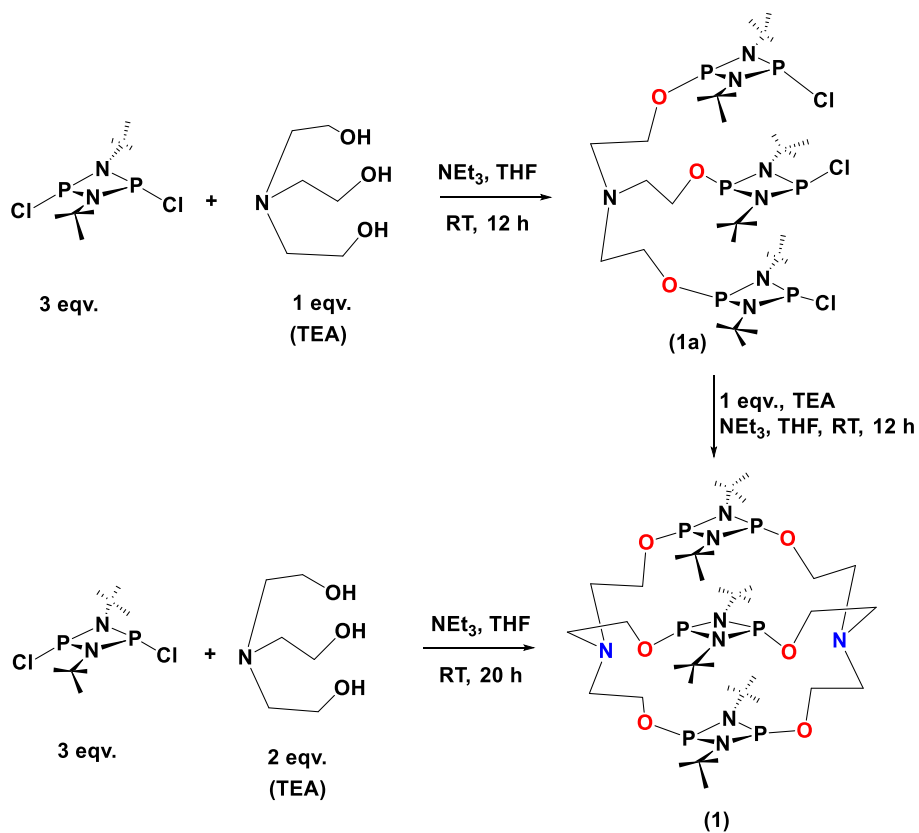


Figure 1.5. Comparison of a conventional and common organic [2.2.2] cryptand with the newly synthesized cyclodiphosph(III)azane bridged cryptand where the central ethylene bridges are replaced by the $[P_2(N^tBu)_2]$ moieties.

1.2 Results and Discussion

The 1:3 reaction of TEA (triethanolamine) with $cis-[CIP(\mu-N^tBu)]_2$, in THF in the presence of slightly excess amounts of triethylamine for 12 h at room temperature (Scheme 1.1) showed two equal intensity doublets in the *in-situ* $^{31}P\{^1H\}$ NMR spectrum at 187.5 and 138 ppm ($^3J_{P-P} = 40$ Hz), indicating the presence of two types of phosphorus centers in the product **1a**. In the second step, another equivalent of TEA and Et_3N was added to the reaction mixture at low temperature and subsequent overnight stirring at room temperature followed by work-up afforded a white fluffy product, $\{TEA_2-[P_2(\mu-N^tBu)_2]_3\}$ (**1**). In the $^{31}P\{^1H\}$ NMR spectrum, only one signal at 124.9 ppm reveals the symmetrical environment around all the phosphorous atoms (Figure 1.6). In the 1H

NMR spectrum, the signals for $-O-CH_2$ and $-N-CH_2-$ moieties appeared at 3.90 and 2.74 ppm as triplets, each for twelve protons of the TEA linker arm.



Scheme 1.1. Synthesis of the cryptand $\{TEA_2-[P_2(\mu-N^tBu)_2]_3\}$ (**1**).

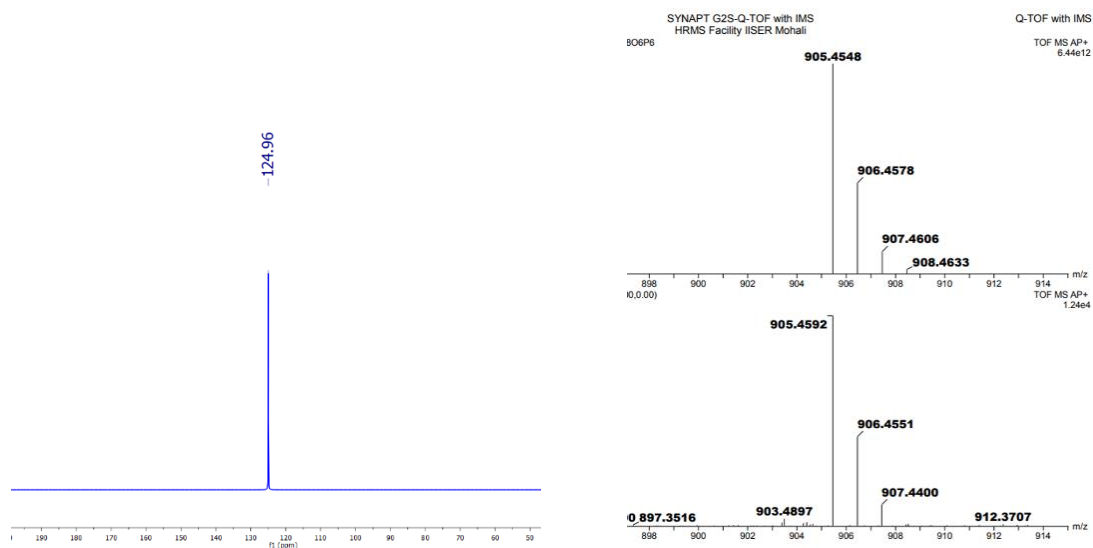


Figure 1.6. $^{31}P\{^1H\}$ NMR ($CDCl_3$, 162 MHz) spectrum (left) and HRMS spectrum (right) of $\{TEA_2-[P_2(\mu-N^tBu)_2]_3\}$ (**1**).

The earlier reported hybrid organic-inorganic macrocycles have been assembled *via* one-step synthesis. Similarly, the direct one-pot synthetic route has also been employed and optimized for the synthesis of bicyclic macrocycle. The stoichiometry was maintained as 2:3 equivalent for TEA and *cis*-[CIP(μ -N'Bu)]₂ in THF in the presence of triethylamine as a base under high dilution conditions (Scheme 1.1). After overnight stirring at room temperature, a white slurry was obtained containing triethylammonium chloride salt in the reaction mixture, which was removed after workup and pure compound **1** extracted was in hexane. Moreover, the absence of OH signal in IR and ¹H NMR spectrum indicated the elimination of HCl through the condensation reaction of TEA and *cis*-[CIP(μ -N'Bu)]₂. Eventually, the formation of cryptand **1** was seen by HRMS spectrum with *m/z* of 905.4592 (calcd. 905.4548) for [M+H]⁺ and later, the bicyclic structure was confirmed by the single crystal X-ray diffraction analysis as depicted in Figure 1.7. Compound **1** crystallized in the monoclinic system with *P*2₁/*n* space group. The well-diffracting crystals were obtained from the solvent mixture (pentane and DCM at 20 °C) using the layering method, and the molecule crystallized with one dichloromethane molecule. As reported in the literature, such tripodal linkers are known to show an interesting feature, namely, *in* and *out* isomerism. The *in* isomers have residues pointing inwards, and the *out* isomer has residue pointing outwards with respect to the cavity of the macrobicyclic system.^[3] The macrobicyclic system has the probability of three types of homeomorphic isomers (*out,out*, *in,in* and *in,out*).^[3] The single crystal X-ray structure of **1** showed the *in-in* isomer, where both the nitrogen atom (N1 and N2) of TEA are pointing inwards the cavity of the cryptand. The three arms are connected through the bridge of three [P(μ -N'Bu)]₂ units oriented in space symmetrically in a spherical fashion, and the symmetry can also be assigned through the ³¹P{¹H} NMR spectrum that showed

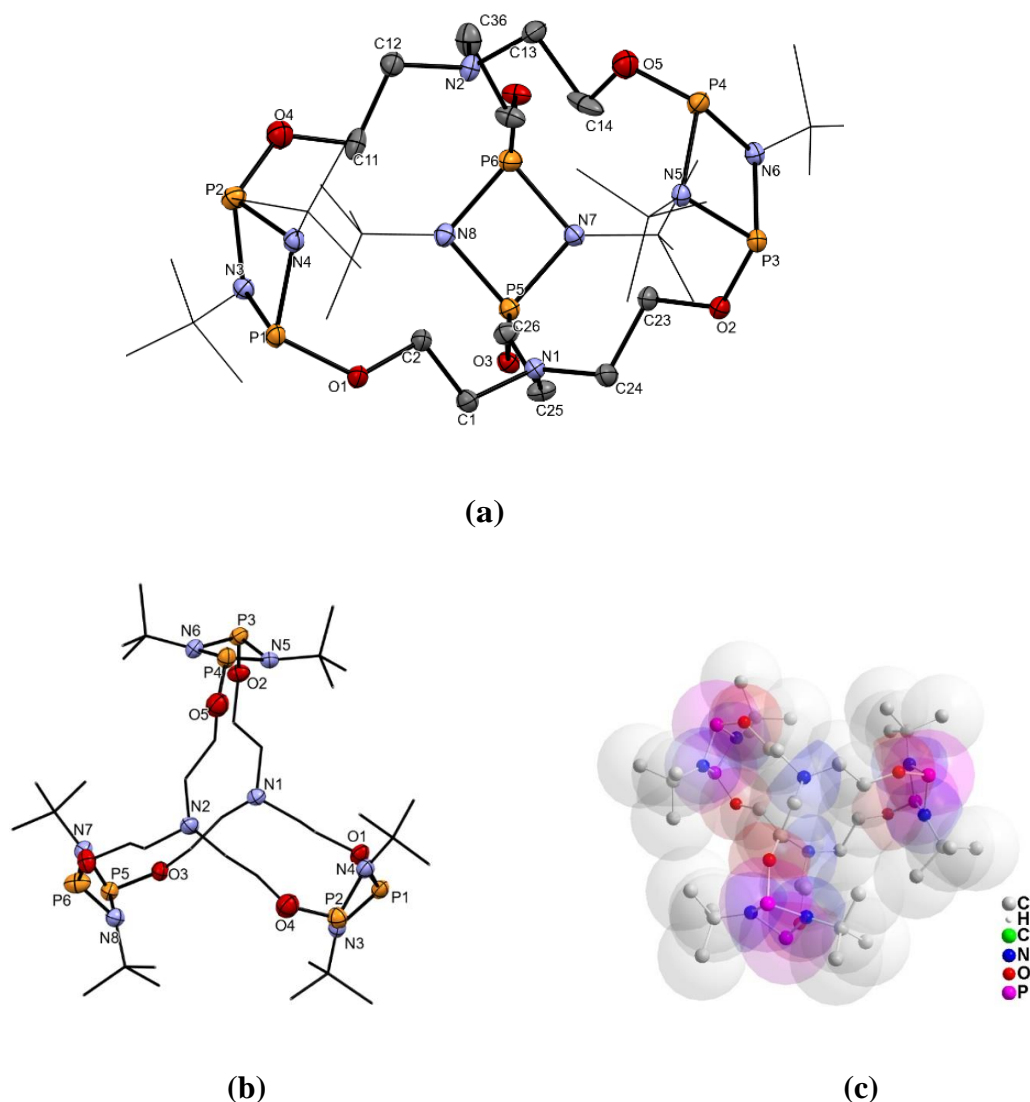
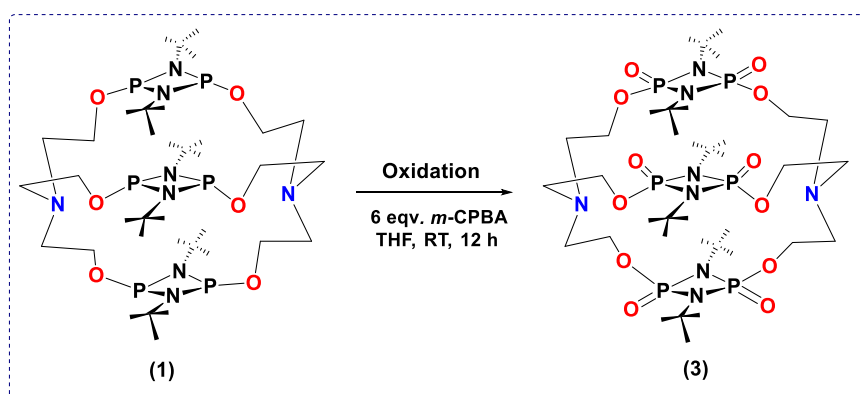


Figure 1.7. Solid-state structure of $\{\text{TEA}_2\text{-}[\text{P}_2(\mu\text{-N}'\text{Bu})_2]_3\}$ (**1**); *(a)* view showing the orientation of P_2N_2 ring and *in,in* connectivity around N of TEA ; *(b)* side view showing two rings each of 22 atoms $[\text{N}_6\text{P}_4\text{O}_4\text{C}_8]$ in the core; *(c)* superimposed space-filling model with ball-and-stick structure All hydrogen atoms have been omitted for clarity. Selected bond lengths [\AA] and bond angles [$^\circ$]: P1-O1 1.617(4), P1-N3 1.726(5), P1-N4 1.734(5), O1-C2 1.449(7), N1-C1 1.459(7), N1-C25 1.428(7), N1-C1 1.459(7), N1-C24 1.460(8), P5-P6 2.560(2), P5-O3 1.628(4), P5-N8 1.711(5), P5-N7 1.713(5), P3-P4 2.585(2), P3-O2 1.605(4), P3-N5 1.724(5), P3-N6 1.726(5); P1-O1-C2 125.3(4), O1-P1-N3 107.9(2), N3-P1-N4 80.4(2), C1-N1-C25 114.4(5), C1-N1-C24 113.2(5), C25-N1-C24 114.9(5), O3-P5-N7 106.8(2), N8-P5-N7 81.2(2), C26-O3-P5 125.0(4), C23-O2-P3 123.8(4), C2-O1-P1 125.3(4), C11-O4-P2 124.7(5).

only one signal. The core of each cycle contains twenty-two atoms $\text{P}_4\text{N}_6\text{C}_8\text{O}_4$ involving two $[\text{P}(\mu\text{-N}'\text{Bu})_2]$ rings and as a whole, the cryptand contains thirty-two atoms

$P_6N_8C_{12}O_6$ in the bicyclic framework. This cryptand has a football-like structure similar to the conventional organic cryptand (say [2.2.2] cryptand).^[13] The distance between nitrogen atoms of TEA (N1 and N2) in cryptand **1** is around 5.3 Å, and oxygens are found at a distance of around 6.2-6.4 Å and phosphorous of two neighbouring P_2N_2 units are at a distance of around 8.4-8.6 Å. Whereas, capped nitrogen of [2.2.2] cryptand are at a distance of 6.03 Å and oxygen centers are around 4.37 Å. In [2.2.2] cryptate, mainly oxygen atoms bind to K^+ ion which are at a distance of around 4.0-4.2 Å.

The P^{III} center-containing frameworks are sensitive to air and moisture, and in order to attribute aerobic stability to the cryptand, we have attempted to oxidise P^{III} to P^V using *meta*-chloroperbenzoic acid (*m*-CPBA).^[10] The 1:6 reaction of compound **1** with *m*-CPBA results in the oxidation of all the six $P(III)$ centers to $P(V)$ and afforded $TEA_2-[(O=P_2(\mu-N^tBu)_2)]_3$ (**3**) at room temperature (Scheme 1.2). Multinuclear NMR and HRMS measurements confirmed the oxidation of all P^{III} centers to P^V (Figure 1.8).



Scheme 1.2. Oxidation of P^{III} centers in cryptand **1** to P^V form and the formation of $\{TEA_2-[(O=P_2(\mu-N^tBu)_2)]_3\}$ (**3**).

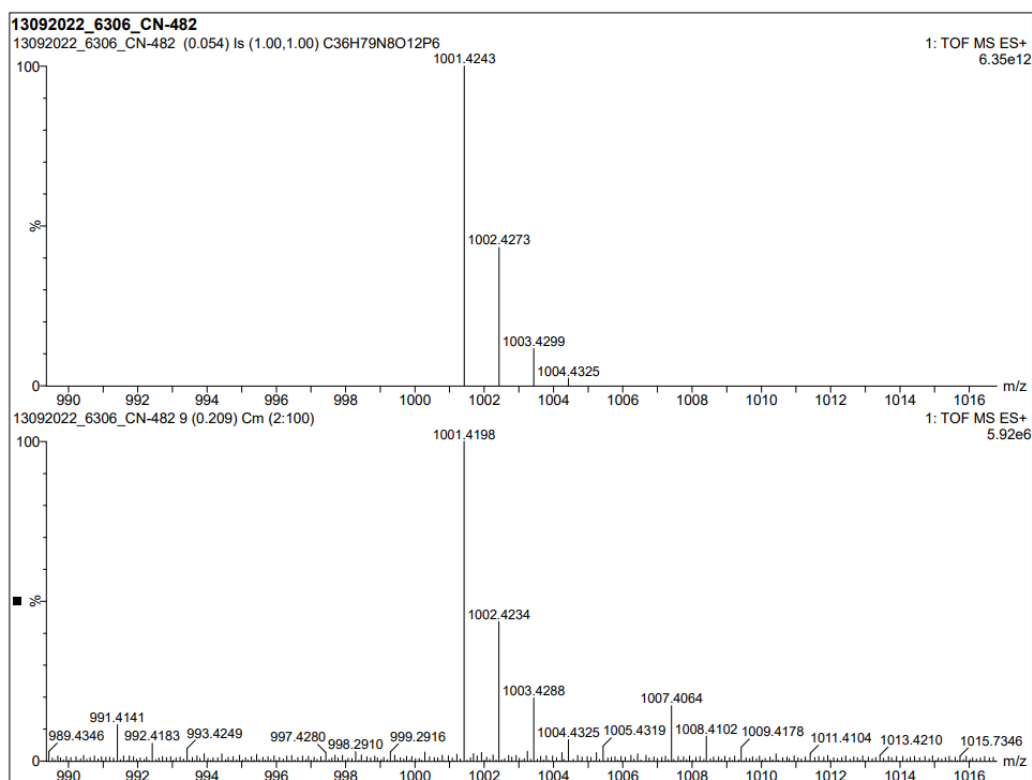
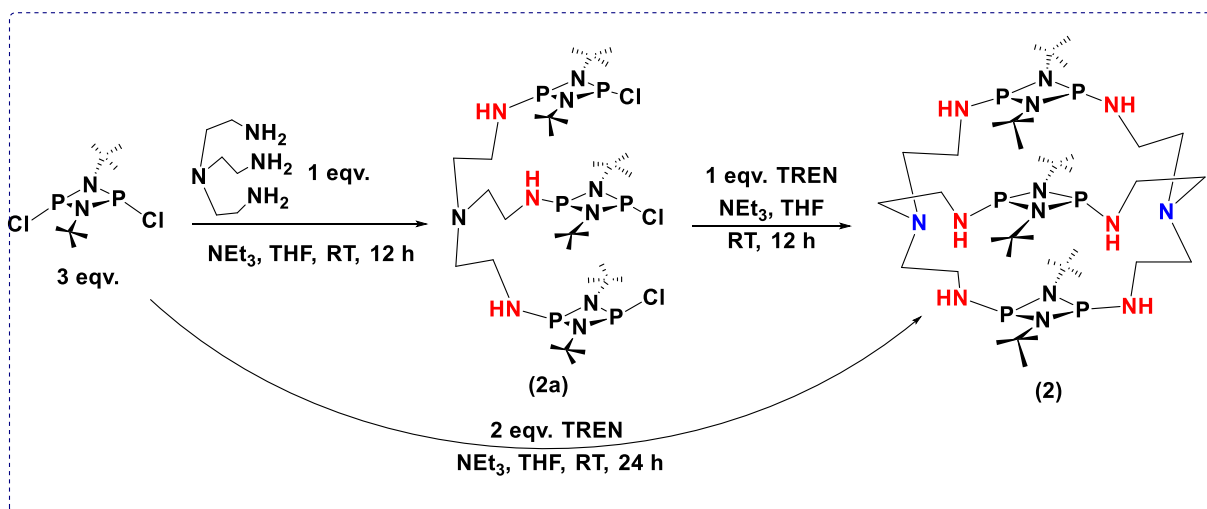


Figure 1.8. HRMS spectrum of $\{\text{TEA}_2\text{-}[\text{O}=\text{P}_2(\mu\text{-N}^t\text{Bu})_2]_3\}$ (**3**).

Similarly, another tripodal linker TREN, (*tris*(2-aminoethyl)amine) has also been used to assemble the bicyclic molecule. Following the stepwise path, a 1:3 reaction of TREN and $[\text{CIP}(\mu\text{-N}^t\text{Bu})]_2$ was performed in the presence of slightly excess triethylamine base at room temperature for 12 h. The formation of trisubstituted **2a** was confirmed by two signals at 192 and 119 ppm in the *in-situ* $^{31}\text{P}\{^1\text{H}\}$ NMR spectrum of the reaction mixture. The complete cryptand formation was carried out by the addition of another equivalent of TREN linker and triethylamine base to **2a** in the second step. Alternatively, the direct reaction route (one pot synthesis) has also been employed, the reaction of 2:3 equivalent of TREN (and *cis*- $[\text{CIP}(\mu\text{-N}^t\text{Bu})]_2$ in THF in the presence of slight excess of triethylamine as a base under high dilution conditions has been performed at room temperature (Scheme 1.3). A white slurry was obtained containing triethylammonium chloride salt in the reaction mixture which was removed during workup and pure compound was obtained in hexane.



Scheme 1.3. Synthesis of cryptand $\{TREN_2-[P_2(\mu-N^tBu)_2]_3\}$ (**2**).

Only one signal in the $^{31}P\{^1H\}$ NMR spectrum was attributed to the symmetrical environment around all the P atoms. In 1H NMR spectrum, the signals for $-NH-CH_2$ and $-N-CH_2$ at 3.03 and 2.37 ppm, respectively appeared as triplets each for twelve methylene protons of TREN and one signal for the tBu group at 1.25 ppm indicating the symmetrical environment around linker in solution (Figure 1.9).

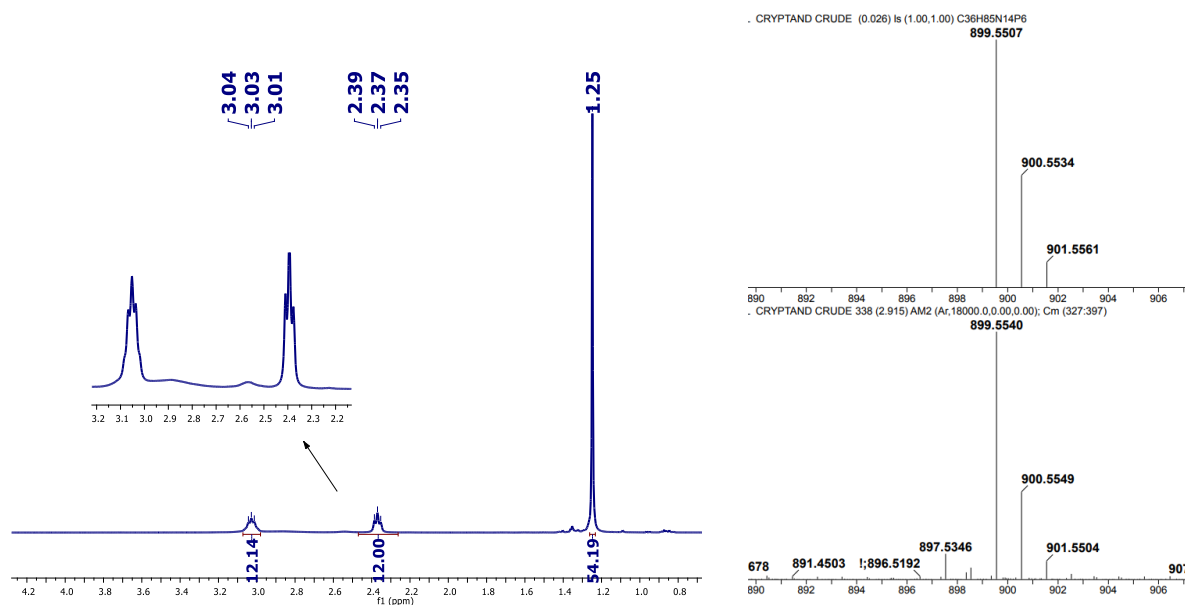


Figure 1.9. 1H NMR (CDCl₃, 400 MHz) spectrum (left) and HRMS spectrum (right) of $\{TREN_2-[P_2(\mu-N^tBu)_2]_3\}$ (**2**).

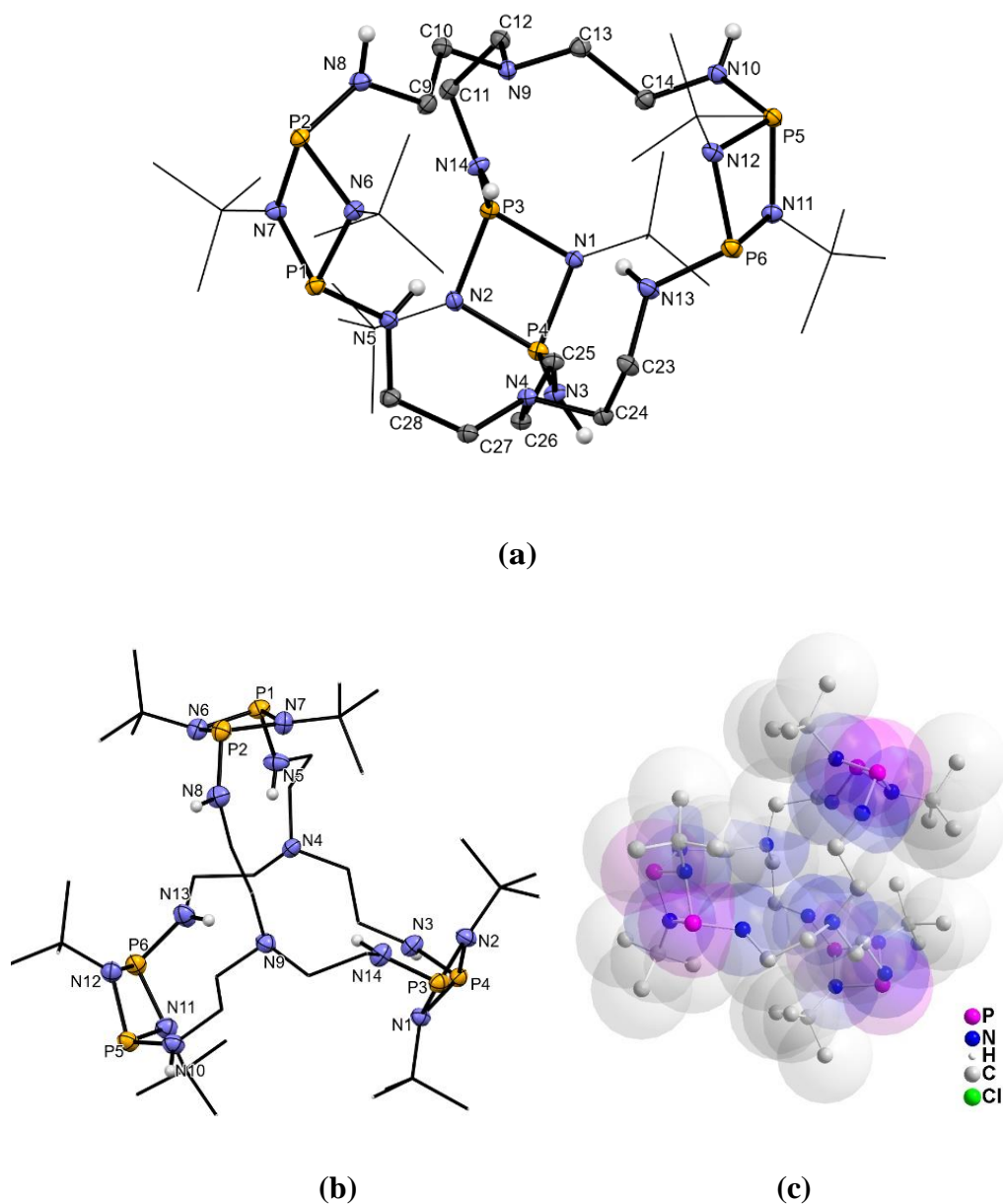
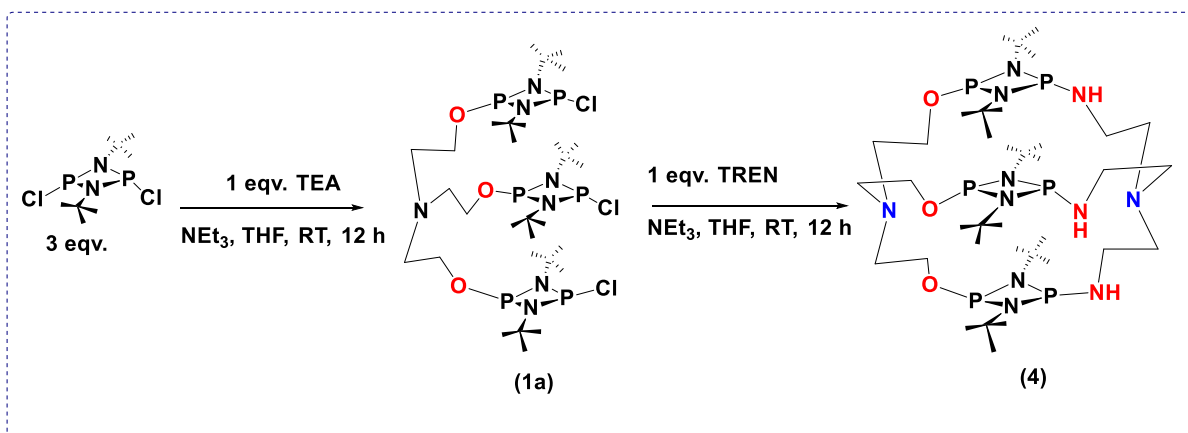


Figure 1.10. Solid-state structure of cryptand, $\{\text{TREN}_2\text{-}[\text{P}_2(\mu\text{-N}^i\text{Bu})_2]_3\}$ (**2**); (a) view showing orientation of P_2N_2 and *in,in* connectivity around N of TREN ; (b) side view showing two rings each of 22 atoms $[\text{N}_{10}\text{P}_4\text{C}_8]$ in the core; (c) superimposed space-filling model with ball-and-stick structure All hydrogen atoms (except relevant N-H bond) have been omitted for clarity. Selected bond lengths [\AA] and bond angles [$^\circ$]: P2-N8 1.661(4), P2-N6 1.736(4), P4-N1 1.728(4), P4-N3 1.658(4), P4-N2 1.718(4), P3-N1 1.720(4), P3-N2 1.717(4), P3-N14 1.656(4), N4-C27 1.480(5), N4-C24 1.472(5), N4-C26 1.462(5); N8-P2-N6 106.8(2), N5-P1-N6 104.8(2), N7-P2-N6 80.75(18), P1-N6-P2 97.49(19), C10-N9-C12 110.9(4), N14-C11-C12 112.0(4), N3-C25-C26 110.3(4), C24-N4-C27 109.4(3), C26-N4-C27 110.9(3), C26-N4-C24 110.9(3), C10-N9-C12 110.9(4), C10-N9-C13 112.0(4), C13-N9-C12 111.6(4).

Further, the formation of the complete cryptand was observed by HRMS technique, which showed the signal at $m/z =$ at 899.5540 (calcd. 899.5507) for $[M+H]^+$ and the bicyclic structure of **2** was confirmed by the single crystal X-ray diffraction analysis.

Compound **2** crystallized in the monoclinic system with $P2_1/c$ space group along with one molecule of $CHCl_3$. The cryptand seems to be symmetrical as speculated by spectroscopic characterization, and the three arms are oriented in space, forming a spherical cage-like structure. The solid-state structure of **2** showed that there is *in-in* orientation around the nitrogen caps of TREN where both the nitrogen atoms (N4 and N9) point inwards the macrobicyclic cavity. The core of each cycle is twenty-two membered, including two $[P(\mu-N^tBu)]_2$ units, and as a whole, the cryptand contains thirty-two atoms ($C_{12}N_{14}P_6$) in the core of the bicyclic framework (Figure 1.10). Out of six hydrogen atoms on N-H, three are pointing toward the cavity, while three hydrogen atoms are oriented outwards. The distance between nitrogen atoms of TEA (N1 and N2) is around 5.3 Å, while the distance between nitrogen atoms of TREN (N4 and N9) is around 5.9 Å, and the two $[P(\mu-N^tBu)]_2$ units are at a distance of around 8 Å in both cryptand **1** and **2**.

Along this series, we have attempted to synthesize a hybrid cryptand containing both TEA and TREN linkers. Following the stepwise path, the 1:3 reaction of TEA and $[ClP(\mu-N^tBu)]_2$ was performed in the presence of slight excess of triethylamine base at room temperature for 10 hours. The formation of trisubstituted **1a** was perceived by two signals at 187 and 138 ppm in the *in-situ* $^{31}P\{^1H\}$ NMR spectrum, and then in second step one equivalent of TREN and triethylamine was added to the reaction mixture to get a hybrid cryptand $\{(TREN)(TEA)-[P_2(\mu-N^tBu)_2]_3\}$ (**4**) (Scheme 1.4).



Scheme 1.4. Synthesis of cryptand $\{(\text{TREN})(\text{TEA})\text{-}[\text{P}_2(\mu\text{-N}^t\text{Bu})_2]_3\}$ cryptand (4).

This molecule also authenticates the stepwise method and intermediate **1a** and **2a**. In the $^{31}\text{P}\{^1\text{H}\}$ NMR spectrum, the signal at 115 ppm was attributed to the phosphorous connected to O-CH_2 of *TEA*, and the signal of phosphorous connected to -NH-CH_2 of *TREN* appeared at 100 ppm. In the ^1H NMR, there are four signals of equal intensity, each for 6H for four types of methylene $\text{-CH}_2\text{-}$ units of linkers.

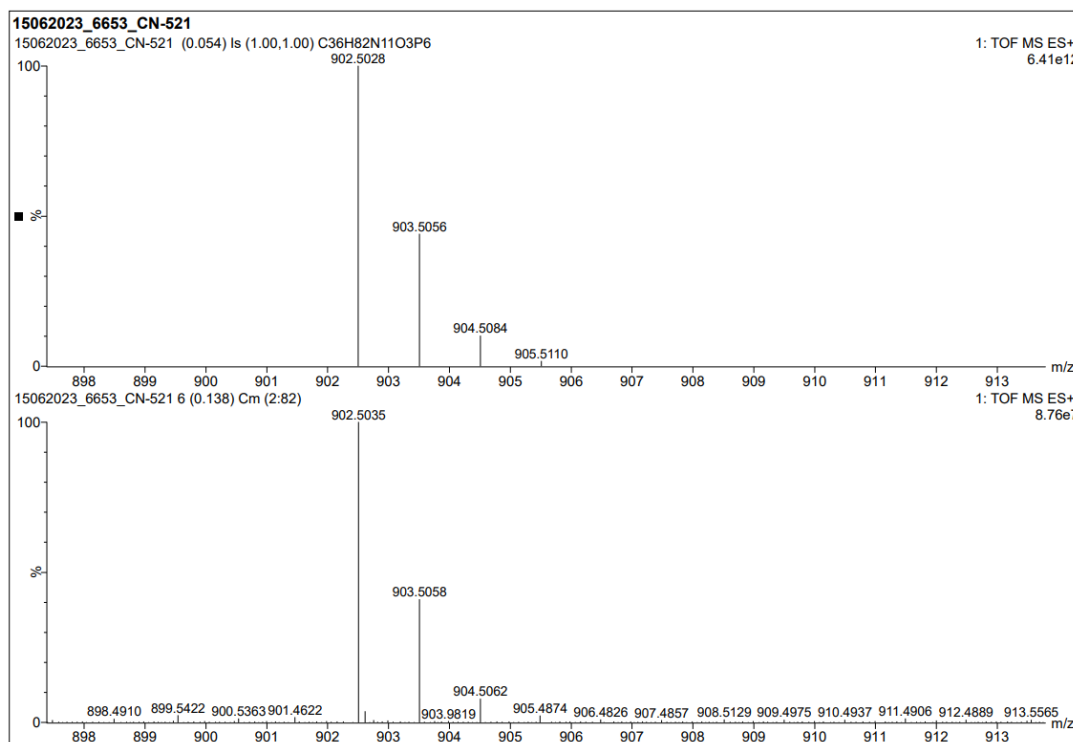


Figure 1.11. HRMS spectrum of cryptand $\{(\text{TREN})(\text{TEA})\text{-}[\text{P}_2(\mu\text{-N}^t\text{Bu})_2]_3\}$ (4).

The formation of hybrid cryptand was also observed by HRMS spectrum having a signal at m/z 902.5035 (calcd. 902.5028) for $[M+H]^+$ (Figure 1.11), and later the bicyclic nature of **4** was confirmed by the structure of partially oxidised hybrid cryptand **4'** by the single crystal X-ray diffraction analysis (Figure 1.12). The P^{III} atom of cryptand attached to TREN linker (-NH) of compound **4** due to aerial oxygen got oxidized to P^V during crystallization to give **4'**.

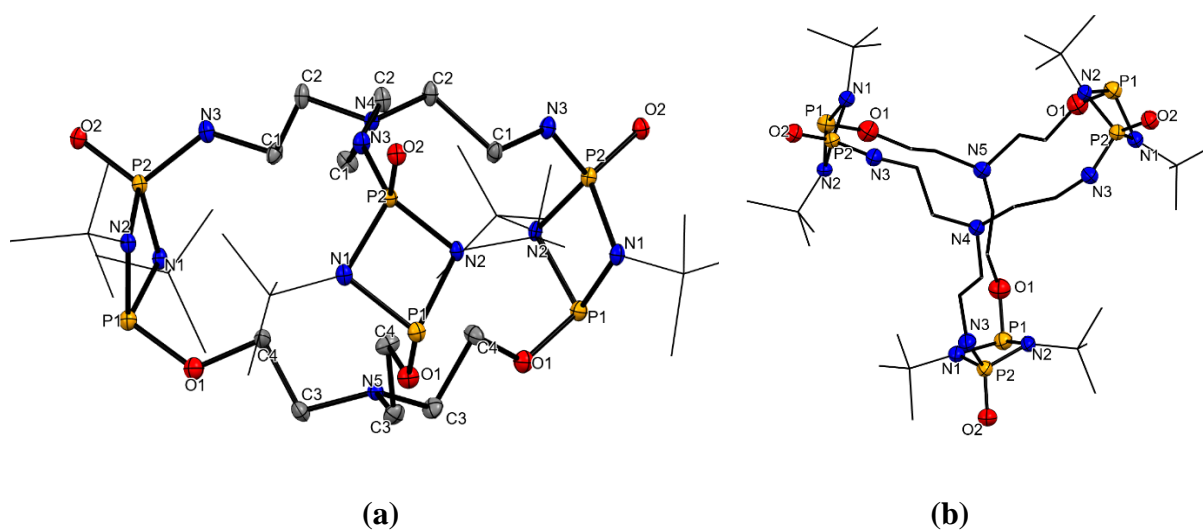


Figure 1.12. Solid-state structure of $[(TREN)\{(O=)P(\mu-N^tBu)_2P\}_3(TEA)]$ cryptand (**4'**); (a) view showing orientation of P_2N_2 and *in,in* connectivity around TREN and TEA nitrogen atom; (b) side view showing two rings each of 22 atoms $[N_8P_4O_2C_8]$ in the core. All hydrogen atoms have been omitted for clarity. Selected bond lengths [\AA] and bond angles [$^\circ$]: P1-O1 1.592(8), P1-N1 1.721(8), P1-N2 1.749(7), P2-P1 2.544(4), P2-O2 1.481(6), P2-N1 1.671(8), P2-N2 1.670(7), P2-N3 1.614(8), O1-C3 1.366(11), N1-C5 1.510(12), N2-C9 1.486(10); O1-P1-P2 122.7(3), O1-P1-N1 108.1(4), O1-P1-N2 108.9(4), N1-P1-P2 40.7(3), N1-P1-N2 80.0(4), N2-P1-P2 40.8(2), O2-P2-P1 122.9(3), O2-P2-N1 119.5(4), O2-P2-N2 119.9(3), O2-P2-N3 105.5(4), N1-P2-P1 42.2(3), N2-P2-P1 43.1(2), N2-P2-N1 83.8(4), N3-P2-P1 131.6(4), N3-P2-N1 113.4(4), N3-P2-N2 114.1(4), C3-O1-P1 125.5(7), P2-N1-P1 97.1(4), C5-N1-P1 125.9(7), C5-N1-P2 131.7(8), P2-N2-P1 96.1(3), C9-N2-P1 125.3(6), C9-N2-P2 129.6(6).

Compound **4'** crystallized in the triclinic system with $P1$ space group. In an asymmetric unit, only one arm was crystallized, and the cryptand seemed symmetrical and formed a cage-like structure. The three arms are oriented in space in a spherical manner. The

solid-state structure of **4'** shows that there is *in-in* orientation around N4 nitrogen of TREN and N5 nitrogen of TEA where the nitrogen atom is directed inwards the macrocycle cavity. The core of each cycle contains twenty-two atoms, including two $[P_2(\mu-N'Bu)_2]$ rings, and as a whole, the cryptand contains thirty-two atoms in the core of the bicyclic framework, including $C_{12}N_{11}O_3P_6$ atoms. The distance between nitrogen atom N4 of TEA and N5 of TREN is around 5 Å, while the two $[P_2(\mu-N'Bu)_2]$ units are at a distance of around 8 Å. In all the cryptands **1**, **2**, and **4**, the N-N distance of capped nitrogen of TEA and TREN was found to be nearly around 5 Å.

1.3 Conclusions

In summary, we have synthesized and characterized the first phosph(III)azane based bicyclic macrocycles $\{TEA_2-[P_2(\mu-N'Bu)_2]_3\}$ (**1**), $\{TREN_2-[P_2(\mu-N'Bu)_2]_3\}$ (**2**), $\{TEA_2-[(P=O)_2(N'Bu)_2]_3\}$ (**3**) and $\{(TREN)(TEA)-[P_2(\mu-N'Bu)_2]_3\}$ (**4**) cryptand. The successful synthesis of bicyclic macrocycles has been achieved by the condensation reaction between the preorganized cyclodiphosph(III)azane and the tripodal flexible spacer linkers having -OH and -NH₂ reaction sites, i.e., TEA and TREN, respectively. These new cryptands have structural similarities with the conventional [2.2.2] cryptands regarding the number of oxygens available for coordinating a suitable host in the core; additionally, the novel cryptand family contains donor phosphorous (III) atoms. Both have three-dimensional football-type structures and represent a negatively charged cavity. The coordinating donor atoms (oxygen and phosphorous) in new cryptands are at relatively longer distances than those of [2.2.2] cryptand (whose cavity size is well suited for K⁺ ion).^[13] Various attempts to encapsulate the cation in cavity are currently being pursued.

It has been verified that organic macrobicycles have greater coordination ability and selectivity for a suitable guest compared to analogous macrocyclic crown ethers. Similarly, the increase in building block complexity, number of cycles, and coordinating atoms in cyclodiphosph(III)azanes macrocycles not only generate future prospects in the main group and phosphazane chemistry but also in the field of supramolecular chemistry and may be capable of performing like traditional organic building blocks. This work motivates us to invest greater efforts in developing cyclodiphosph(III) azanes based bicyclic macrocycles of the main group containing building blocks, which we predict will play a crucial role in developing novel supramolecular chemistry.

1.4. Experimental Section

1.4.1 General procedure

All manipulations were performed under an inert atmosphere of nitrogen/argon using Schlenk line or glove box techniques. All the glassware were dried at 120 °C in an oven. Solvents were purified by MBRAUN solvent purification system MB SPS-800. All chemicals were purchased from commercial sources and used without further purification. The starting material $[\text{CIP}(\mu\text{-N}^t\text{Bu})_2]$ was prepared as per the reported procedure.^[3a]

1.4.2 Physical measurements

High resolution mass spectra were recorded on a Waters SYNAPT G2-S instrument. The ^1H , $^{13}\text{C}\{^1\text{H}\}$, and $^{31}\text{P}\{^1\text{H}\}$ NMR spectra were recorded with a Bruker 400 MHz spectrometer; chemical shift values are reported in ppm. IR spectra of the complexes were recorded in the range 4000-400 cm^{-1} using a Perkin Elmer Lambda 35-spectrophotometer. The absorption of only characteristic functional groups were

assigned. Melting points were obtained in sealed capillaries on a Büchi B–540 melting point instrument.

Single crystal X-ray diffraction data of complexes **1**, **2** and **4'** were collected using a Rigaku XtaLAB mini diffractometer equipped with Mercury375M CCD detector. The data were collected with MoK α radiation ($\lambda = 0.71073 \text{ \AA}$) using omega scans. During the data collection, the detector distance was 49.9 mm (constant), and the detector was placed at $2\theta = 29.85^\circ$ (fixed) for all the data sets. The data collection and data reduction were done using CrysAlisPro 1.171.38.46 and all the crystal structures were solved through OLEX2^[12]. All figures were generated using Mercury 2022.1.0.

1.4.5 Synthetic procedure

Synthesis of cryptand {TEA₂-[P₂(μ -N^tBu)₂]₃} (1**):** (*Stepwise synthesis*) A solution of [CIP(μ -N^tBu)]₂ (9.0 mmol, 2.5 g) in THF (50 mL) added slowly to the solution of TEA (3.0 mmol 0.45 g) in THF (50 mL) at -78 °C in the presence of slightly excess triethylamine (10.0 mmol, 1.0 g, 1.5 mL) base. The reaction mixture was allowed to warm to room temperature and stirred for another 12 h to afford **1a**. Then, in the second step, a THF solution of another equivalent of TEA (3.0 mmol 0.45 g) was added to the reaction mixture at -78 °C in the presence of slightly excess triethylamine (10.0 mmol, 1.0 g, 1.5 mL) base, the reaction mixture was allowed to warm to room temperature and stirred for 12 h. After the removal of all the volatiles, compound **1** was extracted in hexane.

Alternative synthesis (direct one step synthesis); In the solution of [CIP(μ -N^tBu)]₂ (9.0 mmol, 2.5 g) in THF (80 mL), the solution of TEA (6.0 mmol 0.9 g) in THF (40 mL) at -78 °C was added slowly in the presence of triethylamine (20.0 mmol, 2.0 g, 3 mL) base. The reaction mixture was allowed to warm to room temperature and stirred for another

20 h. The mixture was then filtered to remove triethylammonium chloride salt, and all the volatiles were removed under vacuum. The pure colourless crystal of Compound **1** was obtained from the mixture of pentane and DCM using the layering method at -20°C. Yield: 1.1 g (41 %). Mp: 120-123 °C. IR (nujol) ν : 2958, 2926, 2854, 1459, 1363, 1211, 1023, 894, 794, 730, 650, 594 cm^{-1} . ^1H NMR (400 MHz, CDCl_3): δ = 3.90 (poorly resolved triplet signals, 12H, $-\text{OCH}_2-$), 2.74 (12H, $-\text{NCH}_2-$), 1.30 (m, 54H, $-\text{tBu}$) ppm; $^{31}\text{P}\{^1\text{H}\}$ NMR (162 MHz, CDCl_3) δ = 124.9 ppm, *In situ* $^{31}\text{P}\{^1\text{H}\}$ NMR of **1a** δ = 187.5, 138.0 (d, $^2J_{\text{P-P}}$ = 40 Hz) ppm; $^{13}\text{C}\{^1\text{H}\}$ NMR (100 MHz, CDCl_3): δ = 60.0, 57.8, 51.3, 31.2, 1.0 ppm. HRMS (AP^+): m/z calcd. for $[\text{C}_{36}\text{H}_{78}\text{N}_8\text{O}_6\text{P}_6]$: (905.4548) $[\text{M}+\text{H}]^+$; found: (905.4592).

Synthesis of cryptand $\{\text{TREN}_2\text{-}[\text{P}_2(\mu\text{-N}^t\text{Bu})_2]_3\}$ (2**):** (*Stepwise synthesis*) A solution of $[\text{ClP}(\mu\text{-N}^t\text{Bu})_2]$ (9.0 mmol, 2.5 g) in THF (50 mL) was added slowly to the solution of TREN (3.0 mmol 0.45 g) in THF (40 mL) at -78 °C in the presence of slightly excess triethylamine (10.0 mmol, 1.0 g, 1.5 mL) base. The reaction mixture was allowed to warm to room temperature, and further stirring for 12 h afforded **2a**. Then, in the second step, THF solution of another equivalent of TREN (3.0 mmol 0.45 g) was added to the reaction mixture at -78 °C in the presence of slightly excess triethylamine (10.0 mmol, 1.0 g, 1.5 mL) base, the reaction mixture was allowed to warm to room temperature and stirred for 12 h. After the removal of all the volatiles, compound **2** was extracted in hexane.

Alternative synthesis (direct one-step synthesis); In the solution of $[\text{ClP}(\mu\text{-N}^t\text{Bu})_2]$ (9.0 mmol, 2.5 g) in THF (80 mL) the solution of TREN (6.0 mmol, 0.90 g) in THF (50 mL) was added slowly at -78°C in the presence of triethylamine (20 mmol, 2. g, 3 mL) base. The reaction mixture was allowed to warm to room temperature and stirred for 24 h. The mixture was then filtered to remove triethylammonium chloride salt and all the

volatiles were removed under vacuum, the pure product **2** was extracted in hexane. The colourless crystal of compound **2** was obtained in an NMR tube in CDCl₃. Yield: 0.65 g (24 %). Mp: 105 °C. IR (nujol) ν in cm⁻¹: 2922, 2858, 1696, 1624, 1559, 1459, 1375, 1279, 1207, 1095, 1043, 958, 922, 822, 806, 762, 726, 650, 586, 462. ¹H NMR (400 MHz, CDCl₃): δ = 3.03 (t, 12H, -NH-CH₂-), 2.37 (t, 12H, -NCH₂-), 1.25 (m, 54H, -^tBu) ppm; ³¹P{¹H} NMR (162 MHz, CDCl₃): δ = 87 ppm, *In-situ* ³¹P{¹H} NMR of **2a** δ = 192.9, 119.8 ppm; ¹³C{¹H} NMR (100 MHz, CDCl₃): δ = 59.0, 51.2, 31.1, 14.0 ppm. HRMS (AP⁺): m/z calcd. for [C₃₆H₈₄N₁₄P₆]: (899.5507) [M+H]⁺; found: (899.5540).

Synthesis of cryptand {TEA₂-(P=O)₂(μ -N^tBu)₂]₃} (3**):** A solution of *meta*-chloroperbenzoic acid (1.04 g, 6.0 mmol) in 30 mL THF was added to the solution of {TEA₂-(P₂(^tBuN)₂)₃} (0.9 g, 1.0 mmol) of cryptand **1** at -78 °C and then stirred at room temperature for 12 h. Even after several attempts, the molecule could not crystallize. Yield: 0.38 g (38 %). ¹H NMR (400 MHz, CDCl₃): δ = 4.19 (m, 12H, -OCH₂-), 3.02 (m, 12H, -NCH₂-), 1.42, 1.39 (m, 54H, -^tBu) ppm; ³¹P{¹H} NMR (162 MHz, CDCl₃): δ = -3.8, -5.2 ppm; ¹³C{¹H} NMR (100 MHz, CDCl₃): δ = 67.9, 55.1, 30.2, 25.0, 0.5 ppm. HRMS (ESI): m/z calcd. for [C₃₆H₇₉N₈O₁₂P₆]: [M+H]⁺ 1001.4243; found 1001.4198.

Synthesis of cryptand {(TEA)(TREN)[P₂(μ -N^tBu)₂]₃} (4**):** A solution of TEA (3.0 mmol, 0.5 g) in 50 mL THF was added slowly to the solution of [CIP(μ -N^tBu)]₂ (9.0 mmol, 2.5 g) in THF (50 mL) at -78 °C in the presence of slightly excess triethylamine (10.0 mmol, 1.0 g, 1.5 mL) base. The reaction mixture was allowed to warm to room temperature and stirred for another 12 h to afford **1a**. In the second step, the THF solution of another equivalent of TREN (3.0 mmol 0.4 g) was added to the reaction mixture at -78 °C in the presence of slightly excess triethylamine (10 mmol, 1.0 g, 1.5 mL) base, the reaction mixture was allowed to warm to room temperature and stirred for further 12h. After the removal of all the volatiles, compound **4** was extracted in

hexane. Yield: 0.76 g (28 %). Mp: 130-132 °C. ^1H NMR (400 MHz, CDCl_3): $\delta = 3.83$ (m, 6H), 3.10 (m, 6H), 2.83(m, 6H), 2.52 (m, 6H), 1.27, 1.26 (m, 54H, $-t\text{Bu}$) ppm; $^{31}\text{P}\{^1\text{H}\}$ NMR (162 MHz, CDCl_3) $\delta = 115.0, 100.0$ ppm; $^{13}\text{C}\{^1\text{H}\}$ NMR (100 MHz, CDCl_3): $\delta = 1.0, 31.2, 51.3, 57.8, 60.0$ ppm. HRMS (AP^+): m/z calcd. for $[\text{C}_{36}\text{H}_{78}\text{N}_8\text{O}_6\text{P}_6]$: (902.5028) $[\text{M}+\text{H}]^+$; found: (902.5035).

1.5 Crystallographic Data

Table 1.5.1 Crystallographic data for bicyclic macrocycles 1, 2 and 4'.

Compound	1	2	4'
Chemical formula	C ₃₆ H ₇₈ P ₆ N ₈ O ₆	C ₃₆ H ₈₄ P ₆ N ₁₄	C ₃₆ H ₈₁ P ₆ N ₁₁ O ₃
molar mass	905.4592	899.5540	902.5035
Crystal system	Monoclinic	Monoclinic	Monoclinic
Space group	<i>P2₁/n</i>	<i>P2₁/c</i>	<i>P2₁/c</i>
<i>T</i> [K]	150.0(10)	200.00(10)	294.00(10)
<i>a</i> [Å]	11.3996(9)	11.4893(5)	15.4371(14)
<i>b</i> [Å]	19.0694(17)	14.8702(8)	15.4371(14)
<i>c</i> [Å]	25.219(2)	33.5049(13)	28.099(3)
<i>α</i> [°]	90	90	90.0
<i>β</i> [°]	92.051(7)	89.127(4)	90.0
<i>γ</i> [°]	90	90	120.0
<i>V</i> [Å ³]	5478.6(8)	5723.5(5)	5799(1)
<i>Z</i>	4	4	12
<i>D</i> (calcd.) [g·cm ⁻³]	1.200	1.183	1.183
<i>μ</i> (Mo-K _α) [mm ⁻¹]	0.339	2.498	2.498
Reflections collected	39787	10137	10137
Independent reflections	9713	6188	6188
Data/restraints/parameters	9713/0/550	6188/0/584	6188/0/584
<i>RI</i> , <i>wR</i> ₂ [<i>I</i> > 2σ(<i>I</i>)] ^[a]	0.0985, 0.1645	0.0663, 0.1529	0.0663, 0.1529
<i>RI</i> , <i>wR</i> ₂ (all data) ^[a]	0.1608, 0.3329	0.0934, 0.1679	0.0934, 0.1679
GOF	1.051	1.047	1.047

[a] $RI = \sum ||Fo| - |Fc|| / \sum |Fo|$. $wR2 = [\sum w(|Fo^2| - |Fc^2|)^2 / \sum w|Fo^2|^2]^{1/2}$

1.6 References

- (a) Z. Liu, S. K. M. Nalluri, and J. F. Stoddart, *Chem. Soc. Rev.*, **2017**, *46*, 2459; (b) K. Kumar, and D. Singh, *J. Serb. Chem. Soc.*, **2010**, *75*, 475; (c) B Dietrich, J-M. Lehn, and J-P. Sauvage, *Tetrahedron Lett.*, **1969**, *10*, 2889; (d) J-M. Lehn, S. H. Pine, E. Watanabe, and A. K. Willard, *J. Am. Chem. Soc.*, **1977**, *99*, 6766; (e) A. Bencini, A. Bianchi, S. Brazzini, V. Fusi, C. Giorgi, P. Paoletti, and B. Valtancoli, *Inorganica Chimica Acta*, **1998**, *273*, 326; (f) D. McDowell, and J. Nelson, *Tetrahedron Lett.*, **1988**, *28*, 385; (g) M. J. Chen, X. M. Zhuang, L. Z. Yang, L. Jiang, X. L. Feng, and T. B. Lu, *Inorg. Chem.*, **2008**, *47*, 3158; (h) D. Chen, and A. E. Martell, *Tetrahedron*, **1991**, *47*, 6895; (i) J. F. Brown, and G. M. J. Slusarczhuk, *J. Am. Chem. Soc.*, **1965**, *87*, 931; (j) D. Seyferth, C. Prudhomme, and G. H. Wiseman, *Inorg. Chem.*, **1983**, *22*, 2163; (k) C. J. Pedersen, *J. Am. Chem. Soc.*, **1967**, *89*, 7017.
- (a) M. S. Balakrishna, D. J. Eisler, and T Chivers, *Chem. Soc. Rev.*, **2007**, *36*, 650; (b) S. G. Calera, and D. S. Wright, *Dalton Trans.*, **2010**, *39*, 5055; (c) M. S. Balakrishna, *Dalton Trans.*, **2016**, *45*, 12252; (d) H. C. Niu, A. J. Plajer, R. G.-Rodriguez, S. Singh, and D. S. Wright, *Chem. Eur. J.*, **2018**, *24*, 3073; (e) S. G. Calera, D. J. Eisler, C. G. M. Benson, P. D. Matthews, A. D. Bond, S. Singh, L. H. Gade, and D. S. Wright, *Angew. Chem. Int. Ed.*, **2017**, *56*, 9242; (f) E. L. Doyle, L. Riera, and D. S. Wright, *Eur. J. Inorg. Chem.*, **2003**, 3279; (g) A. J. Plajer, R. G. Rodriguez, C. G. M. Benson, P. D. Matthews, A. D. Bond, S. Singh, L. H. Gade, and D. S. Wright, *Angew. Chem. Int. Ed.*, **2017**, *56*, 9087.
- (a) A. Bashall, E. L. Doyle, C. Tubb, S. J. Kidd, M. McPartlin, A. D. Woods, and D. S. Wright, *Chem. Commun.*, **2001**, 2542; (b) S. G. Calera, D. J. Eisler, J. M.

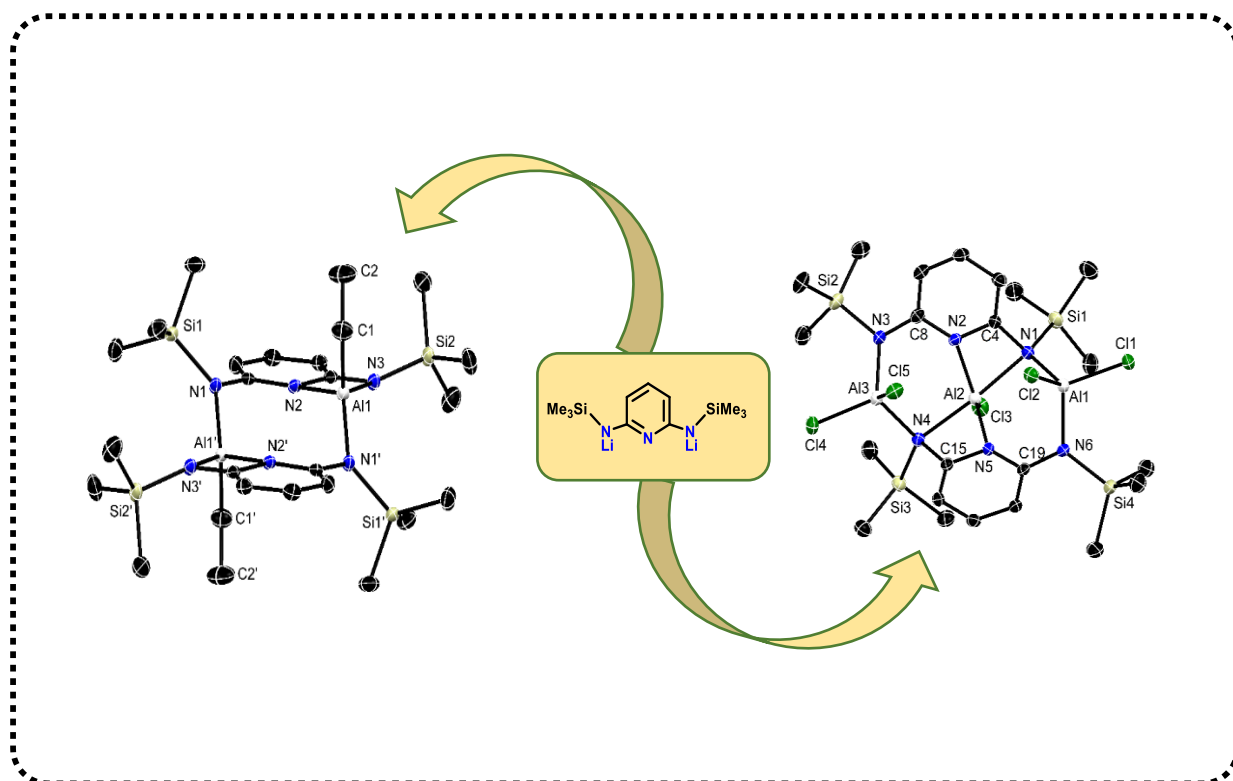
- Goodman, M. McPartlin, S. Singh, and D. S. Wright, *Dalton Trans.*, **2009**, 8, 1293; (c) S. G. Calera, D. J. Eisler, J. V. Morey, M. McPartlin, and S. Singh, *Angew. Chem. Int. Ed.*, **2008**, 47, 1111; (d) D. Bawari, B. Prashanth, S. Ravi, K. R. Shamasundar, S. Singh, and D. S. Wright, *Chem. Eur. J.*, **2016**, 22, 12027; (e) A. Bashall, A. D. Bond, E. L. Doyle, F. García, S. Kidd, G. T. Lawson, M. C. Parry, M. McPartlin, A. D. Woods, and D. S. Wright, *Chem. Eur. J.*, **2002**, 8, 3377; (f) X. Shi, F. Leon, H. C. Ong, R. Ganguly, J. Diaz, and F. Garcia, *Commun. Chem.*, **2021**, 4, 1.
4. (a) F. Garcia, J. M. Goodman, R. A. Kowenicki, I. Kuzu, M. McPartlin, M. A. Silva, L. Riera, A. D. Woods, and D. S. Wright, *Chem. Eur. J.*, **2004**, 10, 6066; (b) A. J. Plajer, H-C. Niu, F. J. Rizzuto, and D. S. Wright, *Dalton Trans.*, **2018**, 47, 6675; (c) D. Bawari, B. Prashanth, K. Jaiswal, A. R. Choudhury, and S. Singh, *Eur. J. Inorg. Chem.*, **2017**, 4123; (d) G. S. Ananthnag, S. Kuntavalli, J. T. Mague, and M. S. Balakrishna, *Inorg. Chem.*, **2012**, 51, 5919; (e) P. Kommana, and K.C. Kumaraswamy, *Inorg. Chem.*, **2000**, 39, 4384; (f) F. Dodds, *Dalton Trans.*, **2006**, 39, 4235.
5. (a) M. S. Balakrishna, *J. Organomet. Chem.*, **2010**, 695, 925; (b) M. S. Balakrishna, P. Chandrasekaran, and R. Venkateswaran, *J. Organomet. Chem.*, **2007**, 692, 2642; (c) M. K. Pandey, S. Sheokand, and M. S. Balakrishna, *Dalton Trans.*, **2023**, 52, 6420; (d) M. S. Balakrishna, *J. Organomet. Chem.*, **2010**, 695, 925; (e) D. Mondal, and M. S. Balakrishna, *Dalton trans.*, **2021**, 50, 6382.
6. (a) A. Nordheider, T. Chivers, R. Thirumoorthi, I. V-Bacac, and J. D. Woollins, *Chem. Commun.*, **2012**, 48, 6346; (b) A. Nordheider, K. Hüll, S. Kasun, A.

- Arachchige, A. M. Z. Slawin, J. D. Woollins, R. Thirumoorthib, and T. Chivers, *Dalton Trans.*, **2015**, *44*, 5338.
7. (a) A. M. Caminade, and J. P. Majoral, *Accounts*, **1996**, 1019; (b) I. Bauer, W. D. Habicher, I. S. Antipin, and O. G. Sinyashin, *Russ. Chem., Bull. Int. Ed.*, **2004**, *53*, 1402; (c) C. V. Hanisch, O. Hampe, F. Wigend, and S. Stahl, *Angew. Chem. Int. Ed.*, **2007**, *46*, 4775; (d) R. N. Naumov, A. V. Kozlov, K. B. Kanunnikov, S. Gomez-Ruiz, E. Hey-Hawkins, S. K. Latypov, A. A. Karasik, and O. G. Sinyashin, *Tetrahedron Lett.*, **2010**, *51*, 1034; (e) J. S. Ritch and T. Chivers, *Angew. Chem. Int. Ed.*, **2007**, *46*, 4610.
8. (a) J. Mitjaville, A. M. Caminade, and J. P. Majoral, *J. Chem. Soc., Chem. Commun.*, **1994**, 2161; (b) M. Stollenz, M. Barbasiewicz, A. J. N-Hultsch, T. Fiedler, R. M. Laddusaw, N. Bhuvanesh, and J. A. Gladysz, *Angew. Chem. Int. Ed.*, **2011**, *50*, 6647; (c) A. S. Baluevaa, E. I. Musinaa, Yu. A. Nikolaevaa, A. A. Karasika, and O. G. Sinyashin, *Russian Journal of Organic Chemistry*, **2019**, *55*, 1660.
9. (a) Y. Sim, F. Leon, G. Hum, S. J. I. Phang, H. C. Ong, R. Ganguly, J. Díaz, J. K. Clegg, and F. Garcia, *Commun. Chem.*, **2022**, *5*, 59; (b) V. S. Kashid, J. T. Mague, and M. S. Balakrishna, *J. Chem. Sci.*, **2017**, *129*, 1531; (c) F. Dodds, *Chem. Commun.*, **2005**, 3733.
10. (a) Y. X. Shi, K. A. Martin, R. Z. Liang, D. G. Star, Y. Li, Y. R. Ganguly, Y. Sim, D. Tan, J. Díaz, and F. García, *Inorg. Chem.*, **2018**, *57*, 10993; (b) Y. X. Shi, R. Z. Liang, K. A. Martin, D. G. Star, J. Diaz, X. Y. Li, R. Ganguly, and F. Garcia, *Chem. Commun.*, **2015**, *51*, 16468; (c) D. Tan, and F. Garcia, *Chem. Soc. Rev.*, **2019**, *48*, 2274.

11. (a) A. Mondal, K. P. Reddy, J. A. Bertke, and S. Kundu, *J. Am. Chem. Soc.*, **2020**, *142*, 1726; (b) A. Bencini, A. Bianchi, V. Fusi, C. Giorgi, P. Paoletti, and B. Valtancoli, *Tetrahedron Lett.*, **1997**, *38*, 5327.
12. P. B. Hitchcock, M. F. Lappert, L. Maron, and A. V. Protchenko, *Angew. Chem. Int. Ed.*, **2008**, *47*, 1488
13. (a) Crystal Clear 2.0; Rigaku Corporation: Tokyo, Japan, **2013**. (b) O. V. Dolomanov, L. J. Bourhis, R. J. Gildea, J. A. K. Howard, and H. J. Puschmann, *Appl. Crystallogr.*, **2009**, *42*, 339; (c) G. M. Sheldrick, *Acta Cryst. A.*, **2015**, *71*, 3; (d) G. M. Sheldrick, *Acta Cryst. A.*, **2008**, *64*, 112.

Chapter 2A

Aluminum Bridged [3.3](2,6)Pyridinophanes and Organoaluminum Complexes



C. Negi, † D. Bawari, † S. K. Thakur, A. R. Chaudhary and S. Singh*; Concise access to aluminum containing [3.3](2,6)pyridinophane and molecular bowl using 2,6-diamidopyridine modules, *J. Organomet. Chem.*, **2019**, 901, 120943-120949. (†equal contribution).

Abstract: This chapter presents the versatility of bis(trimethylsilyl)-N,N'-2,6-diaminopyridine (bap), and aluminum reagents to synthesize aluminum bridged pyridinophanes and organoaluminum complexes containing Al-N bonds. Mononuclear and dinuclear aluminum complexes (**1** and **2**) having N_{py}-Al donor-acceptor interaction have been afforded by changing the stoichiometry and reaction conditions. The 1:1 reaction of dilithiated bis(trimethylsilyl)-N,N'-2,6-diaminopyridine (bapLi₂) and EtAlCl₂ afforded [3.3](2,6) pyridinophane [$\{2,6-(\text{Me}_3\text{SiN})_2\text{C}_5\text{H}_3\text{N}\}\text{AlEt}\}_2$ (**3**) while the bowl-shaped pyridinophane [$2,6-(\text{Me}_3\text{SiN})_2\text{C}_5\text{H}_3\text{N}(\text{AlCl}_2)\}_2[\text{AlCl}]$ (**4**) was assembled with 2:3 reaction of bapLi₂ and AlCl₃. All the compounds have been characterized using multinuclear NMR, HRMS, and single crystal X-ray diffraction. The solid-state structure of **3** showed an anti-conformer with respect to the mutual orientation of two pyridine rings, and the ethyl groups in N-Al(*Et*)-N bridges are mutually trans. The pyridinophane **4** has a nice bowl-shaped structure with a diagonal -N-Al(*Cl*)-N- bridge across the ring.

2A.1 Introduction

Cyclophanes are a class of hydrocarbons consisting of an aromatic unit(s) (typically a benzene ring) bridged *via* an aliphatic unit(s) (at non-adjacent positions of the aromatic ring).^[1] More complex derivatives with multiple aromatic units and bridges forming cage-like structures are also known. The cyclophanes are widely spread in research areas such as pharmaceuticals, catalysis, supramolecular chemistry, and they are a core structural unit in various biologically active natural products such as macrocidin, nostocyclyne A, etc.^[1]

A broad categorization of cyclophanes accompanied according to the number and kind of aromatic and aliphatic moiety present in the cyclic system (Figure 2A.1). Cyclophanes consisting of two or more aromatic systems and aliphatic bridges are represented as $[n.n]$ metacyclophanes, $[n.n]$ paracyclophanes $[n.n]$ metapara or $[n.n]$ paraparacyclophanes based on the position of the attachment of the alkyl chain to the aromatic system. The prefixes (ortho, meta and para) represent the position of the attachment to an aromatic system, while $[n]$ denotes the number of methylene groups in the aliphatic bridge.^[1,2] (Figure 2A.1)

General representation of some cyclophanes and pyridinophanes

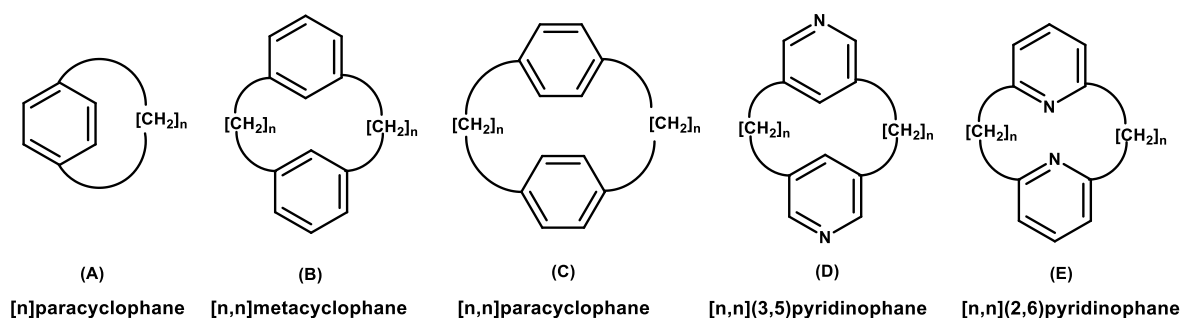


Figure 2A.1. Schematic representation of $[n]$ paracyclophane (A), $[n.n]$ metacyclophane (B), $[n.n]$ paracyclophane (C), $[n.n](3,5)$ pyridinophanes (D) and $[n.n](2,6)$ Pyridinophanes (E), $[n]$ denotes the number of $-CH_2-$ units in bridge].

If the aromatic ring in the cyclophane system is heterocyclic, then the system is called heterophane.^[2] To improve the coordination ability of cyclophanes, various research groups have made attempts to replace the benzene ring with heteroaromatic unit or introduce heteroatoms in the aliphatic side chains/bridge. The well-known cyclophane derivatives known as pyridinophanes are formed when one or more benzene rings are replaced with pyridine moiety.^[2] Pyridinophanes and their derivatives are significant for their applications as pyridoxal models, for metal complexation and in supramolecular chemistry.^[3] Among pyridinophanes, the most common are $[n.n](3,5)$ pyridinophanes (**E**) and $[n.n](2,6)$ pyridinophanes (**F**)^[2,4] (Figure 2A.1).

2A.1.1 Choice of Ligand Scaffold

The selection of suitable building blocks is a crucial step in macrocyclic syntheses and their stability depends on the binding mode and reaction conditions, as various side reactions may undergo parallelly, mainly polymerization, small ring formation (monomeric product), etc. Generally, polymers are thermodynamic products and macrocycles are kinetic products. The ligand design for the syntheses of complexes always begins with two main basic considerations, that are electronic and steric aspects. Suitable reaction conditions and an appropriate ligand framework that can provide both thermodynamic and kinetic stabilization are essential. To design a stable macrocycle, the binding groups should be appropriately positioned, i.e., preorganized and high dilution promotes the cyclic product.^[5] In this context, 2,6-N,N'-disubstituted pyridine units of the type, $[\text{ArN}(\text{NR})_2]_2^{2-}$ (ArN = pyridine) are found to be an important building block due to the desired orientation of -NR groups at 2,6 positions.

Examples of known molecules based on 2,6-substituted diaminopyridine unit

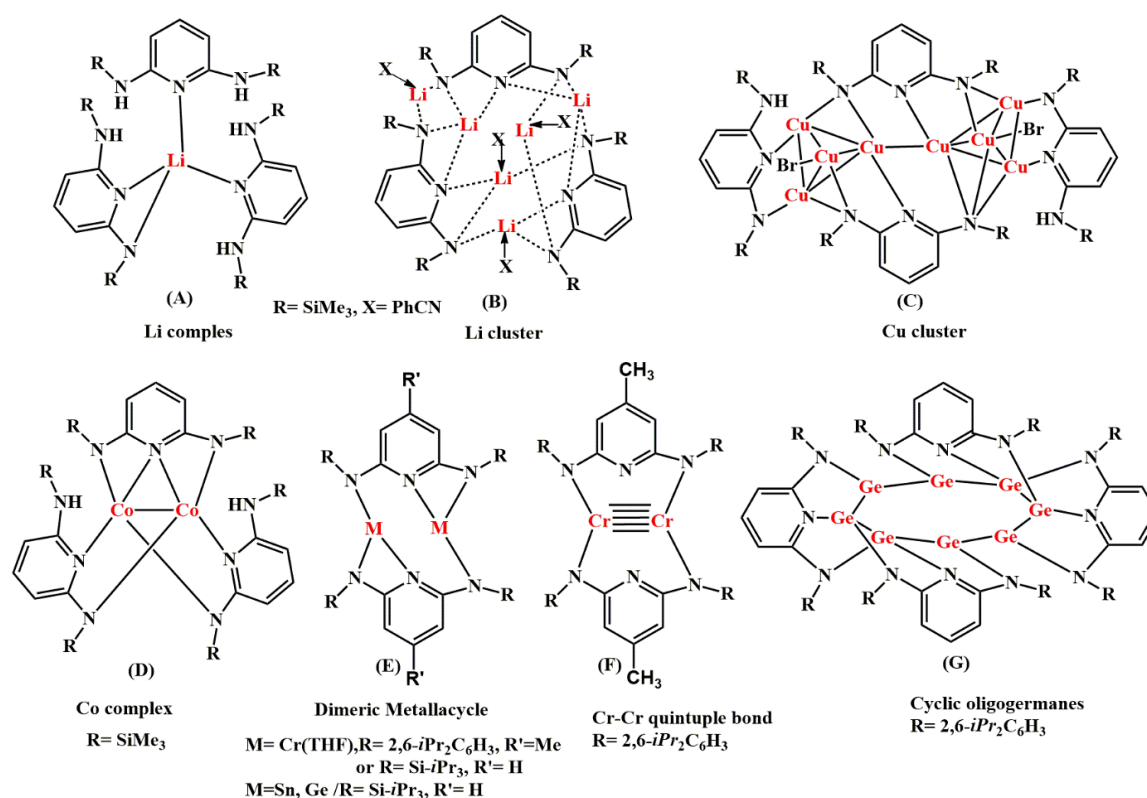


Figure 2A.2. Selected examples of some known molecules based on 2,6- diaminopyridine units.

From literature, it is found that 2,6-substituted diaminopyridine based systems have been used to stabilize multiply bonded systems^[6], metallacycles and complexes of some transition^[7], lanthanide and actinide elements^[8] where the substituents (R) on 2,6 position of nitrogen atoms were altered to modify the steric and electronic properties of the ligand. Various research groups have used N,N'-bis-(trimethylsilyl)-pyridine-2,6-diamine unit to synthesize several metal complexes of lithium, copper and cobalt (A-D) (Figure 2A.2).^[9,10] The dilithiated 2,6-diamidopyridine motif has been used by Tsai and co-workers to assemble chromium based metallacycles (E), which are very useful precursors to generate quintuple Cr-Cr bonds (F).^[11] The dilithiated 2,6-diamidopyridine units are also used to prepare cyclic oligogermanes (G).^[12] Also, 2,6-substituted pyridine units have been used to design the classical cyclic organic

molecules like crown ethers, azacalixpyridines and cryptands, which show significant applications in host-guest chemistry (Figure 2A.3).^[13,14]

Examples of [3.3](2,6)pyridinophanes containing different main group atoms in the bridges

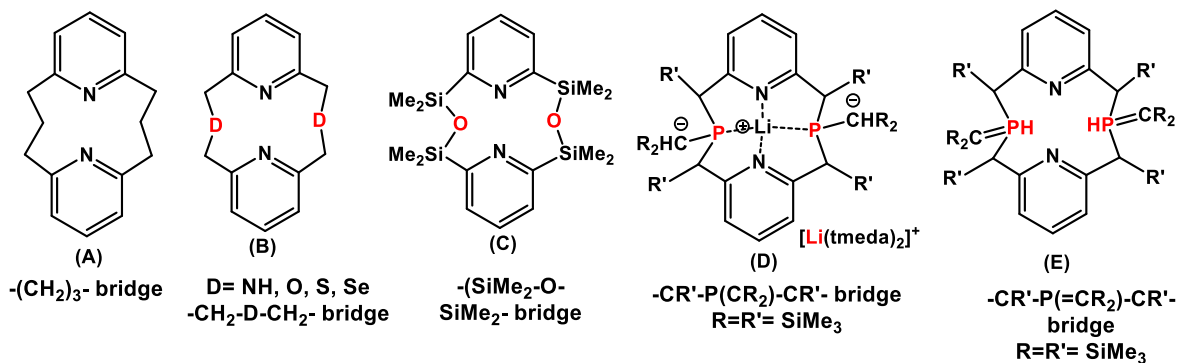


Figure 2A.3. Examples of [3.3](2,6)pyridinophanes with bridges containing trimethylene unit (A) and different main group donor atoms (B-E).

In general, cyclophanes are strained organic molecules where the aromatic rings provide rigidity, whereas the aliphatic moiety that forms the bridge between the aromatic rings provides flexibility to the overall structure^[1]. Mainly, the flexibility of the molecule depends on the aliphatic chain, as the length of aliphatic bridge increases, the molecules become more flexible and show various conformations. Pyridinophanes have advantages over conventional cyclophanes as the pyridine nitrogen (N_{py}) has additional donor sites that can form more coordinated bonds and provide tuneable conformations. The pyridinophanes containing acceptor atoms in the [3.3] bridges are less explored, some cyclophanes containing group 13 elements are depicted in Figure 2A.4.^[15-20] Paetzold and co-workers have used *para*-phenylenediamine derivative $HN(SiMe_3)C_6H_4NH(SiMe_3)$ which on lithiation and subsequent borylation followed by the hydridation yields $Li_2[(H_3B)N(SiMe_3)C_6H_4N-(SiMe_3)(BH_3)]$, which on condensation in the presence of $ZrCl_4$ give the N-B-N bridged hetero[3,3]paracyclophane $[N(SiMe_3)-p-C_6H_4-N(SiMe_3)BH]_2$ (A).^[16]

Examples of group 13 elements based macrocycles, cyclophanes and [3.3](2,6)pyridinophanes

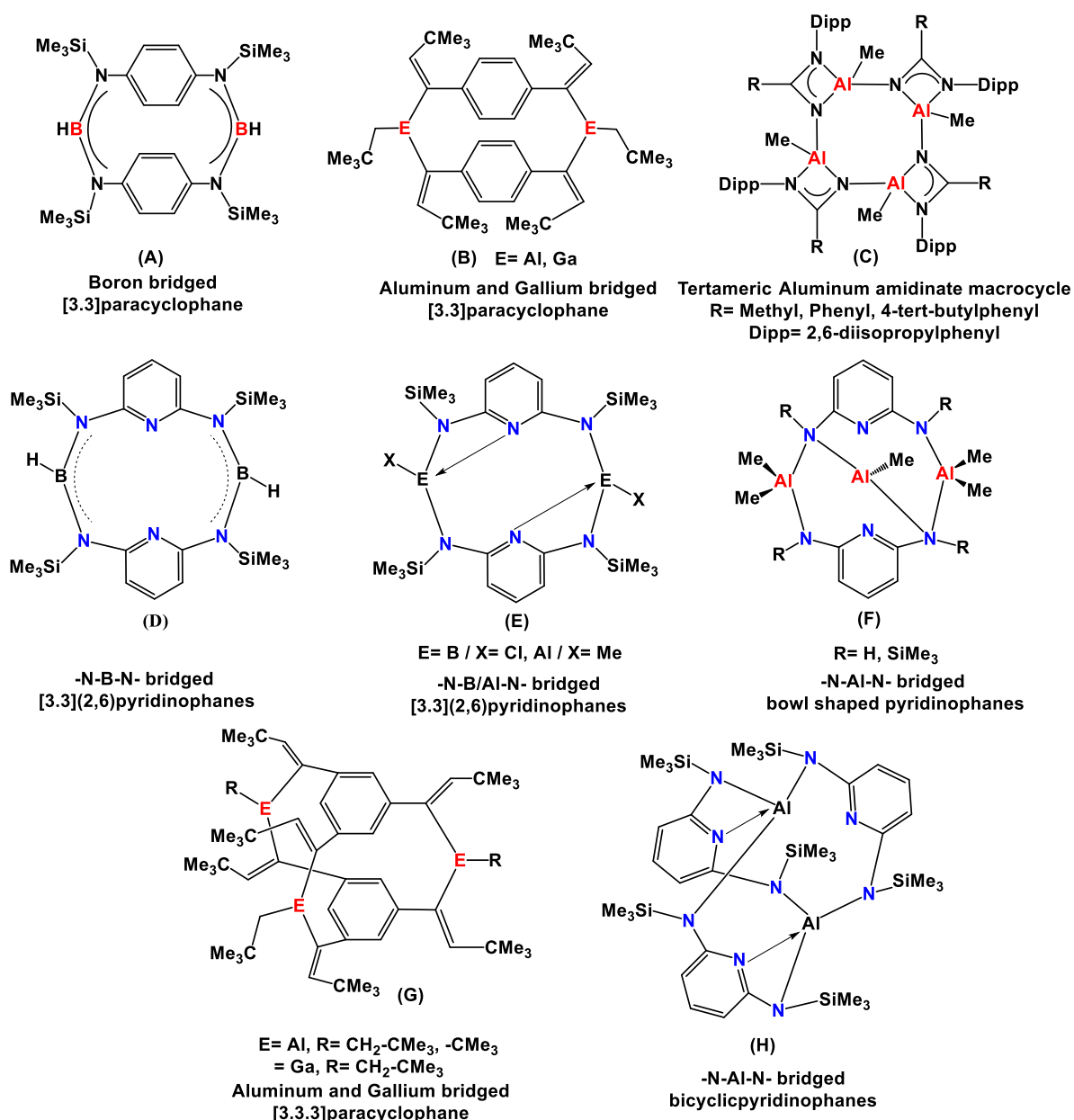


Figure 2A.4. Known examples of some group 13 based macrocycle, cyclophanes and [3.3](2,6)pyridinophanes.

Uhl and co-workers have used hydrogallation reactions which involve the addition of Ga-H bond to C≡C triple bond in the alkyl group connected with the phenyl rings to prepare a gallium bridged [3.3] and [3.3.3]cyclophanes (**B, G**).^[17] There have been very few successful attempts to prepare the aluminum-based cyclophane and pyridinophanes compared to organic macrocycles due to the lack of a general synthetic strategy in the

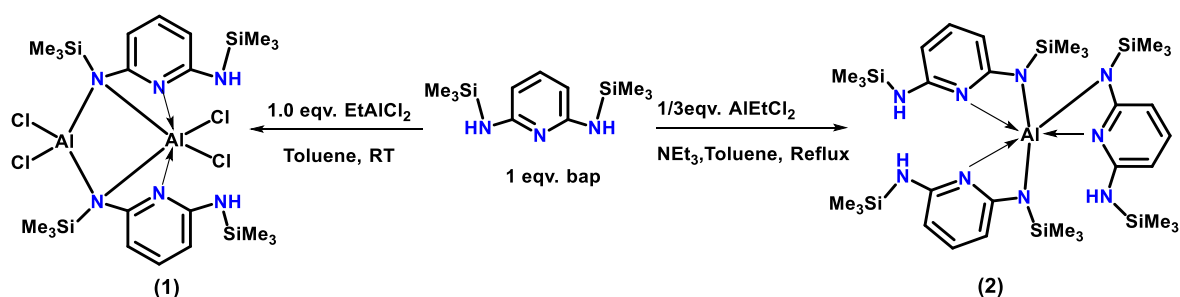
case of inorganic synthesis. In attempts to assemble macrocycles based on aluminum, Uhl and co-workers have used a hydroalumination approach to prepare aluminum bridged [3.3] and [3.3.3] cyclophanes by the reaction of 1,4-di(tert-butylalkynyl)benzene with HAlR_3 , ($\text{R} = \text{CMe}_3, \text{CH}_2\text{CMe}_3$) followed by the release of AlR_3 . The process involves the addition of Al–H bond across $\text{C}\equiv\text{C}$ triple bond in the alkyl group connected with the phenyl rings (**B**, **G**).^[17] Reddy and co-workers have assembled tetrameric macrocycles containing -N-Al-N- bonds where four aluminum are connected by four amidinate units(**C**).^[18a] Jones and co-workers have synthesized cage-type compound, $\text{AlMe}[\text{Al-Me}_2\{\text{N}(\text{H}),\text{N}(\text{H})-\text{C}_5\text{H}_3\text{N}\}]_2$ by using AlMe_3 reagent and 2,6-diaminopyridine building block (**F**).^[18b] The pyridinophanes of the type containing mainly group 13 elements as acceptor atoms in the [3.3] bridges are the area of interest. Further in this direction, we have used 2,6-diaminopyridine as a building block and analyzed the concept of whether the presence of a suitably placed acceptor atom in the bridge shows interaction with pyridine N and affects the geometry/structure of the molecule. With the successful application of this concept, in 2018, we have reported boron bridged conformationally rigid novel tetraazadibora[3.3](2,6)pyridinophanes (**D**) and their aluminum analogue (**E**) involving donor-acceptor interactions between pyridine nitrogen with group 13 acceptor atoms in the bridges.^[19] Also, assemble the -N-Al-N- bridged bowl-shaped molecule (**F**) and the bicyclic pyridinophane (**H**) having three 2,6-diamonopyridine units bonded via two Al centers.^[20]

In the extension of the above work, we have used AlEtCl_2 and AlCl_3 to assemble aluminum containing pyridinophanes. By varying stoichiometry of EtAlCl_2 and bap, different aluminum complexes were obtained, 1:1 reaction of bap and EtAlCl_2 gave the complex, $[\{2-(\text{Me}_3\text{SiN})-6-(\text{Me}_3\text{SiNH})\text{C}_5\text{H}_3\text{N}\}\text{AlCl}_2]_2$ (**1**) whereas the use of an external base Et_3N in the 3:1 reaction of bap and EtAlCl_2 afforded compound, [2-

(Me₃SiN)-6-(Me₃SiNH)C₅H₃N]₃Al (2). Dilithiated bis(trimethylsilyl)-N,N'-2,6-diamidopyridine (Li₂bap) have been used to assemble aluminum bridged pyridinophanes [{2,6-(Me₃SiN)₂C₅H₃N}AlEt]₂ (3) and the bowl-shaped pyridinophane [2,6-(Me₃SiN)₂C₅H₃N(AlCl₂)₂][AlCl] (4) with AlEtCl₂ and AlCl₃ respectively.

2A.2 Results and Discussion

Attempt to synthesise pyridinophane, the 1:1 reaction of bis(trimethylsilyl)-N,N'-2,6-diaminopyridine (bap) and EtAlCl₂ performed at room temperature rather afforded the uncyclized dimeric aluminum complex [{2-(Me₃SiN)-6-(Me₃SiNH)C₅H₃N}AlCl₂]₂ (1) with the evolution of ethane. After that we have performed a reaction in the presence of external base NEt₃ to check the possibility of elimination of HCl. The 3:1 reaction between bap and EtAlCl₂ gave a homoleptic aluminum complex [2-(Me₃SiN)-6-(Me₃SiNH)C₅H₃N]₃Al (2) *via* ethane evolution and elimination of HCl (Scheme 2A.1). The IR spectra of these complexes showed -NH stretch at 3269 (for 1) and 3356 cm⁻¹ (for 2).



Scheme 2A.1. Syntheses of aluminum complexes, [{2-(Me₃SiN)-6-(Me₃SiNH)C₅H₃N}AlCl₂]₂ (1) and [2-(Me₃SiN)-6-(Me₃SiNH)C₅H₃N]₃Al (2).

The ¹H NMR spectra of complexes 1 and 2 showed a triplet and two doublets for the pyridine hydrogens, and their corresponding carbons were observed as five signals in their ¹³C{¹H} NMR spectra. This observation indicated the chemically and magnetically non-equivalent environment around the pyridine rings. Consistent with these, the ¹H

NMR spectra of **1** (0.51 and 0.07 ppm) and **2** (0.05 and 0.27 ppm) and ^{29}Si NMR spectra (15.7 and 6.4 ppm for **1** and 3.2 and -3.2 ppm for **2**) showed different signals for a pair of SiMe_3 groups as well. The HRMS spectra of these complexes showed m/z values of 698.1058 (calcd. 698.1089 for **1**) and 783.3846 (calcd. 783.3872 for **2**) corresponding to $[\text{M}]^+$ supports the proposed compositions based on spectroscopic characterizations, and later the single crystal solid state analysis confirmed their structures.

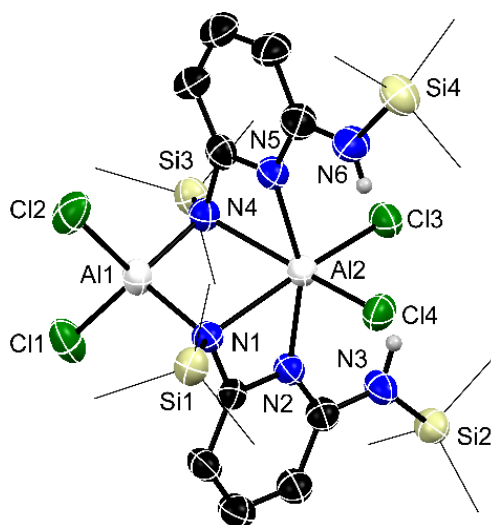


Figure 2A.5. Single crystal X-ray structure of $[\{2-(\text{Me}_3\text{SiN})-6-(\text{Me}_3\text{SiNH})\text{C}_5\text{H}_3\text{N}\}\text{AlCl}_2\}_2$ (**1**). All hydrogen atoms on carbon have been omitted for clarity. Selected bond lengths [\AA] and bond angles [$^\circ$]: Al1-Cl1 2.1183(18), Al1-Cl2 2.1336(18), Al2-Cl3 2.2305(18), Al2-Cl4 2.2262(17), Al1-N1 1.885(4), Al1-N4 1.894(4), Al2-N1 2.223(4), Al2-N2 1.982(4); Cl1-Al1-Cl2 109.64(8), N1-Al1-Cl1 111.85(13), N4-Al1-Cl1 114.13(13), N1-Al1-Cl2 113.05(12), N4-Al1-Cl2 110.53(13), Cl3-Al2-Cl4 98.16(7), N1-Al2-N2 65.69(14).

Compound **1** crystallized in the monoclinic system with $P2_1/n$ space group. The solid-state structure of $[\{2-(\text{Me}_3\text{SiN})-6-(\text{Me}_3\text{SiNH})\text{C}_5\text{H}_3\text{N}\}\text{AlCl}_2\}_2$ (**1**) (Figure 2A.5) contains two aluminum centers, one of the aluminum center Al1 is bonded to two chlorides and two amido groups [Al1-N1 1.883(3) and Al1-N4 1.895(3) \AA] in a distorted tetrahedral geometry, whereas the second aluminum center Al2 is hexacoordinated, forming a distorted octahedral geometry and is bonded to two chlorides, two pyridine N

and two amido N. The core structure of **1** contains a four-membered $[\text{Al}_2\text{N}_2]$ ring with an Al-Al separation of 2.996(3) Å (Table 2A.1).

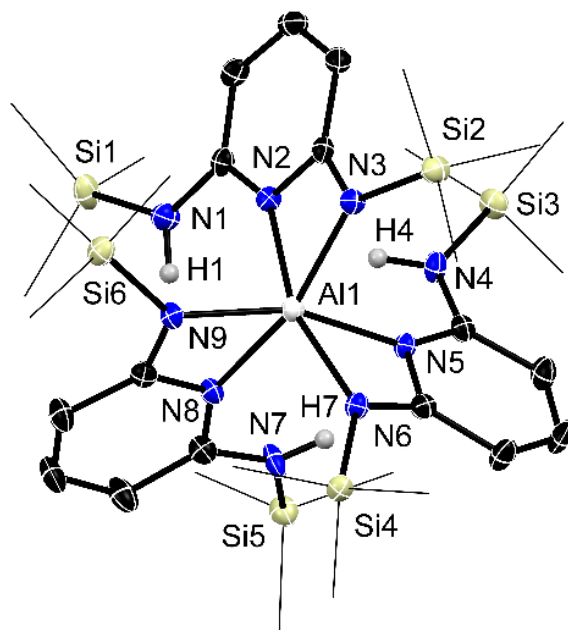
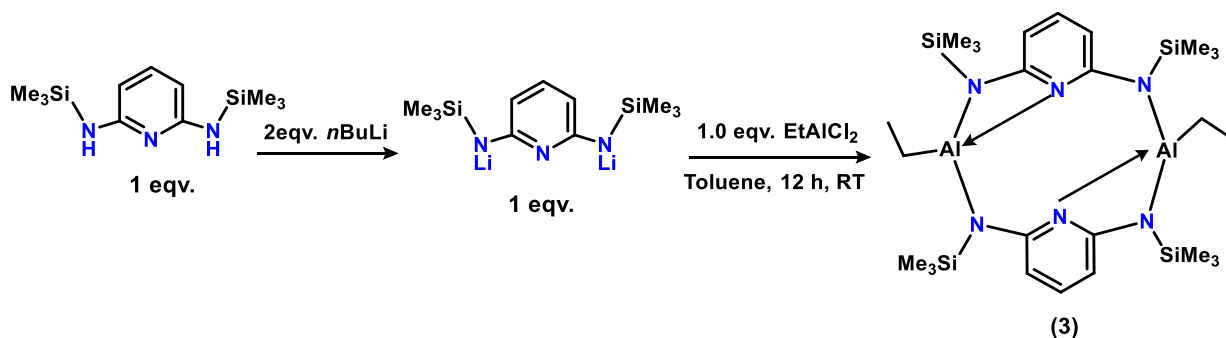


Figure 2A.6. Single crystal X-ray structure of $[\text{2}-(\text{Me}_3\text{SiN})\text{-6}-(\text{Me}_3\text{SiNH})\text{C}_5\text{H}_3\text{N}]_3\text{Al}$ (**2**). All hydrogen atoms (except N-H) have been omitted for clarity. Selected bond lengths [Å] and bond angles [°]: Al1-N2 2.0563(18), Al1-N3 1.9734(18), Al1-N5 2.0544(19), Al1-N6 1.9602(18), Al1-N8 2.0636(18), Al1-N9 1.957(2); N2-Al1-N8 94.63(7), N5-Al1-N2 94.91(8), N5-Al1-N8 93.40(7), N3-Al1-N2 66.84(7), N9-Al1-N8 67.33(7), N6-Al1-N5 67.47(8), N3-Al1-N5 91.10(8), N6-Al1-N8 95.03(7), N9-Al1-N2 94.42(8), N6-Al1-N3 103.48(8), N9-Al1-N6 105.08(8), N9-Al1-N3 109.67(8), N3-Al1-N8 161.26(8).

Compound **2** crystallized in the triclinic system with $P\bar{1}$ space group. The composition of **2** was confirmed as the mononuclear homoleptic tris-bap complex, $[\text{2}-(\text{Me}_3\text{SiN})\text{-6}-(\text{Me}_3\text{SiNH})\text{C}_5\text{H}_3\text{N}]_3\text{Al}$ in line with the observations from HRMS measurements. The Al center in **2** is hexacoordinated, bonded to one amido and one pyridine nitrogen from each of the three bap units (Figure 2A.6, Table 2A.1).

Further in order to synthesise pyridinophane, another reaction strategy has been employed. Using the reported method,^[21] the reaction of bis(trimethylsilyl)-N,N'-2,6-diaminopyridine performed with 2 equivalents of *n*BuLi in hexane gave (bapLi₂), pure

precipitate of the compound was used for further reactions. The stoichiometric reaction between Li_2bap and EtAlCl_2 gave a yellow solid, which on crystallization from hexane at $-10\text{ }^\circ\text{C}$ gave colourless square-shaped crystals of tetraazadialumino[3.3](2,6)pyridinophane, $[\{2,6-(\text{Me}_3\text{SiN})_2\text{C}_5\text{H}_3\text{N}\}\text{AlEt}]_2$ (**3**) (Scheme 2A.2).



Scheme 2A.2. Synthesis of aluminum containing [3.3](2,6)pyridinophane (**3**)

The presence of ethyl group on the aluminum center in **3** was seen as a triplet (0.78 ppm, CH_3CH_2) and a quartet (-0.21 ppm, CH_3CH_2 -) in its ^1H NMR spectrum (Figure 2A.7) and the corresponding carbon signals appeared at 8.6 and -2.1 ppm in its $^{13}\text{C}\{^1\text{H}\}$ NMR spectrum. Two equal intensity signals in ^1H NMR (0.22 and 0.11 ppm) and $^{13}\text{C}\{^1\text{H}\}$ NMR (2.3 and 0.5 ppm) spectra of **3** were attributed to four SiMe_3 groups. Only one signal at 3.15 ppm was observed in the ^{29}Si NMR spectrum of **3**. The formation of **3** as dimer was confirmed in the HRMS measurement that showed a signal at $m/z = 621.3503$ (calcd. 621.3509) for $[\text{M}+\text{H}]^+$ and the structure of dimer containing N-Al(Et)-N bridge was later confirmed by the single crystal X-ray diffraction analysis (Figure 2A.8).

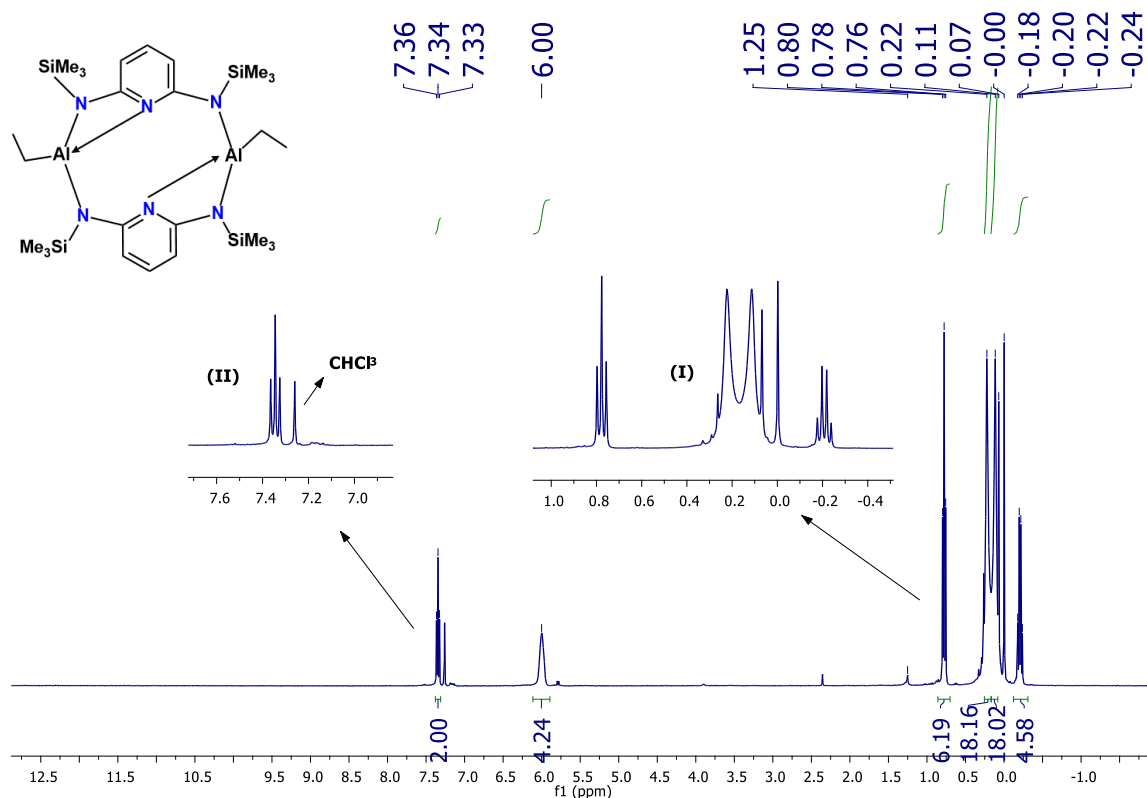


Figure 2A.7. ^1H NMR spectrum (400 MHz, CDCl_3) of $[\{2,6-(\text{Me}_3\text{SiN})_2\text{C}_5\text{H}_3\text{N}\}\text{AlEt}]_2$ (**3**). Insets **I** and **II** show expanded aliphatic and aromatic spectral regions, respectively.

Pyridinophane **3** crystallized in the orthorhombic system with $Pbca$ space group. The single crystal X-ray data for **3** showed its anti-conformer with respect to the mutual orientation of two pyridine rings, and the ethyl groups on the $\text{N-Al}(\text{Et})\text{-N}$ bridges are mutually trans. The anti-conformer of **3** is composed of a $[\text{N}_4\text{Al}_2\text{C}_2]$ eight-membered ring that acquires chair-chair conformation similar to that for cyclooctane as well as that seen in tetraazadialumino[3.3](2,6)pyridinophane.^[20] As a result of $\text{N}_{\text{py}}\text{-Al}$ (donor-acceptor) interaction, aluminum atoms are tertacoordinated, and two planar four-member $[\text{N}_2\text{AlC}]$ rings are formed. The separation between transannular Al atoms (3.725 Å) and distance between the centroids of the pyridine rings in **3** (6.043 Å) compare well with the structurally related tetraazadialumino[3.3](2,6)pyridinophane (3.732 and 6.060 Å) (E-Figure 2A.4).^[20]

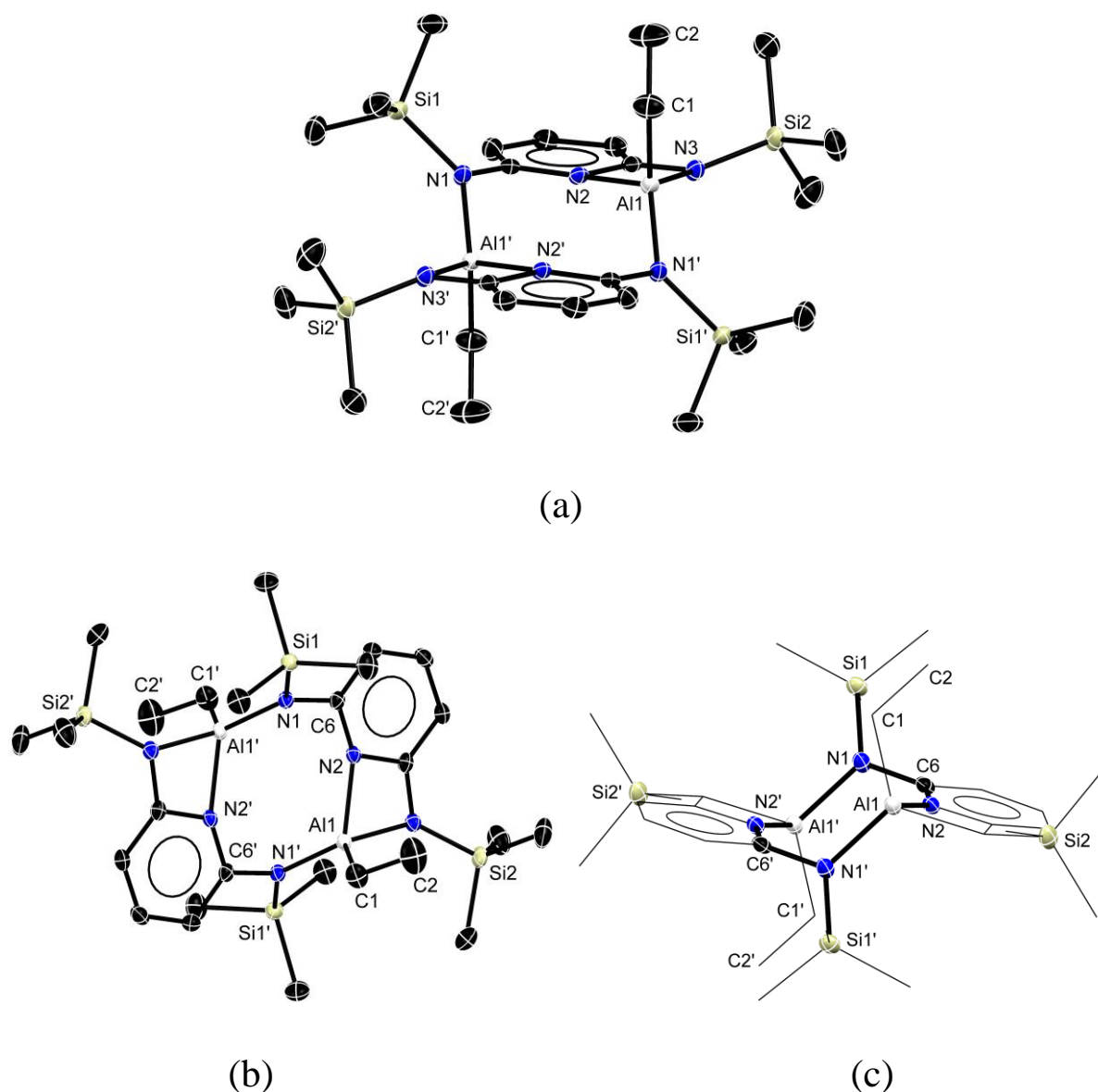
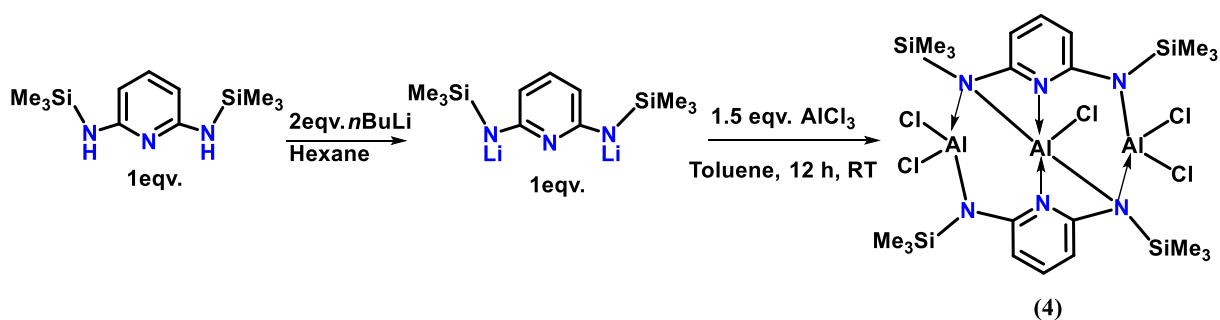


Figure 2A.8. Solid-state structure of tetraazadialumino[3.3](2,6)pyridinophane, $[\{2,6-(\text{Me}_3\text{SiN})_2\text{C}_5\text{H}_3\text{N}\}\text{AlEt}\}_2$ (**3**); *(a)* side view showing parallel orient of pyridine rings and trans Al-ethyl groups and showing $\text{N}_{\text{py}}\text{-Al}$ interaction; *(b)* top view central 8 membered $[\text{N}_4\text{Al}_2\text{C}_2]$ ring; *(c)* the chair-chair conformation of the central $[\text{N}_4\text{Al}_2\text{C}_2]$ ring and anti-arrangement of pyridine rings. All hydrogen atoms have been omitted for clarity. Selected bond lengths [\AA] and bond angles [$^\circ$]: N2-C6 1.354(2), N1-C6 1.394(2), Al1-N1' 1.8504(14), Al1-N2 1.9560(14), Al1-N3 1.8943(14), Al1-C1 1.9522(19), C1-C2 1.495(3); N1'-Al1-C1 113.85(7), N2-Al1-C1 112.62(8), N3-Al1-C1 117.20(7), N1'-Al1-N2 116.75(6), N1'-Al1-N3 118.66(6), N2-Al1-N3 70.94(6).

The 1:1 reaction of Li_2 bap and AlCl_3 at room temperature was expected to yield a pyridinophane like that of **3**, instead a mixture of products formed that could not be separated. Attempts to simplify the reaction by varying the stoichiometry of reagents gave a pyridinophane based bowl-shaped aluminum cage, $[\text{2,6-(Me}_3\text{SiN)}_2\text{C}_5\text{H}_3\text{N(AlCl}_2\text{)}]_2[\text{AlCl}]$ (**4**) in the 2:3 reaction of Li_2 bap and AlCl_3 at room temperature (Scheme 2A.3). The presence of a single resonance for SiMe_3 groups in the ^1H NMR (0.43 ppm) and $^{13}\text{C}\{^1\text{H}\}$ NMR (2.4 ppm) spectra as well as a triplet (7.64 ppm, 2H) and a doublet (6.21 ppm, 4H) in the ^1H NMR spectrum of **4** indicated its symmetrical structure in solution. Further, the signal in the HRMS spectrum of **4** at $m/z = 758.0411$ (calcd. 758.0437), for $[\text{M}]^+$ corroborated to a trinuclear aluminum containing pyridinophane. The solid-state structure of **4** confirmed its cyclic nature, containing three Al centers where two (bap AlCl_2) units are connected via a diagonal - $\text{Al}(\text{Cl})$ - bridge forming a bowl-shaped structure (Figure 2A.9), similar to Al-Me bridged bowl-shaped pyridinophane **F** (Figure 2A.4).^[19,20]



Scheme 2A.3. Synthesis of aluminum bridged bowl-shaped pyridinophane (**4**).

Compound **4** crystallized in the monoclinic system with $P2_1/c$ space group. Among three Al centers, two are tetracoordinated and form part of the main cyclic backbone, whereas the third Al center is located at the center of the molecule (in diagonal bridge) and is pentacoordinated. Each of the tetracoordinated Al centers have two Cl atoms; one Cl atom is oriented towards the cavity, whereas the other Cl is projected away from this

cavity. The N–Al distances around tetracoordinated Al centers in **4** (N1–Al1 and N6–Al1) are 1.933(2) and 1.859(2) Å and can be attributed to coordinate N→Al and covalent N–Al bonds respectively, whereas the pentacoordinated Al2 center showed Al–N distances in the range 1.906(2)-2.173(2) Å (Figure 2A.9) Table 2A.1.

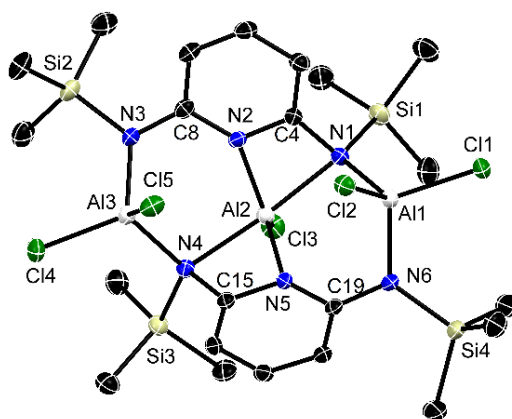


Figure 2A.9. Single crystal X-ray structure of pyridinophane based bowl shaped molecule, [2,6-(Me₃SiN)₂C₅H₃N(AlCl₂)]₂[AlCl] (**4**). All hydrogen atoms have been omitted for clarity. Selected bond lengths [Å] and bond angles [°]: Al1–Cl1 2.1205(9), Al1–Cl2 2.1482(9), Al1–N1 1.933(2), Al1–N6 1.859(2), Al2–N1 2.142(2), Al2–N2 1.913(2), Al2–N4 2.173(2), Al2–N5 1.906(2), Al2–Cl3 2.1171(9), Cl5–Al3 2.1495(9), Al3–N3 1.855(2), Al3–N4 1.925(2), N1–C4 1.439(3), N2–C4 1.364(3), N2–C8 1.365(3), N3–C8 1.380(3), N4–C15 1.445(3), N5–C15 1.369(3), N5–C19 1.370(3), N6–C19 1.371(3); N1–Al1–N6 110.32(9), N4–Al3–N3 111.16(10), N1–Al2–N2 68.09(8), N5–Al2–N4 67.43(8), N1–Al2–N5 97.43(8), N2–Al2–N4 96.38(8), N2–Al2–N5 118.58(9).

2A.3 Conclusions

We have synthesized and characterized aluminum containing pyridinophanes and a few Al complexes. Mono and dinuclear aluminum complexes containing amidinate type chelated rings have been synthesized using bis(trimethylsilyl)-N,N'-2,6-diaminopyridine (bap) and AlEtCl₂. The reactions of EtAlCl₂ and dilithium bis(trimethylsilyl)-N,N'-2,6-diamidopyridine resulted in the formation of aluminum containing [3.3](2,6)pyridinophane where the pyridine rings have anti orientation with

respect to each other. The 2:3 reaction of Li₂bap with AlCl₃ gave a bowl shaped pyridinophane. All the new molecules have [N_{py}-Al] donor-acceptor interactions. The results taken together demonstrate that the synthesis of macrocycles containing main group elements is conceivable if the building block, reaction strategy and conditions are selected carefully.

2A.4 Experimental Section

2A.4.1 General procedure

All the syntheses were carried out under an inert atmosphere of dinitrogen in oven dried glassware using standard Schlenk techniques or a glovebox where O₂ and H₂O levels were usually maintained below 0.1 ppm. All the glassware were dried at 120 °C in an oven for at least 12 h. Solvents were purified by MBRAUN solvent purification system MB SPS-800. DCM was distilled over anhydrous calcium hydride.

2A.4.2 Starting materials

All chemicals were purchased from Sigma-Aldrich and used without further purification. The starting materials bis(trimethylsilyl)-N,N'-2,6-diaminopyridine, lithium bis(trimethylsilyl)-N,N'-2,6-diamidopyridine were prepared by following the reported procedures.^[21]

2A.4.3 Physical measurements

The ¹H, ¹³C{¹H}, and ²⁹Si NMR spectra were recorded with a Bruker 400 MHz spectrometer with TMS as external references, and chemical shifts were reported in ppm. Downfield shifts relative to the reference were quoted positive, while the upfield shifts were assigned negative values. High resolution mass spectra were recorded on a Waters SYNAPT G2-S instrument. IR spectra of the complexes were recorded in the range 4000–400 cm⁻¹ using Perkin Elmer Lambda 35-spectrophotometer. The

absorptions of the characteristic functional groups were only assigned and other absorptions (moderate to very strong) were only listed. Melting points were obtained in sealed capillaries on a Büchi B-540 melting point instrument.

Single crystal X-ray diffraction data of compound **1** was collected on a Bruker *AXS KAPPA APEX-II* CCD diffractometer with MoK α radiation using omega scans. Unit cell determination, refinement, and data collection were done using the Bruker *APPEX-II* suite data reduction and integration were performed using SAINT v8.34A (Bruker, 2013) and absorption corrections and scaling were done using SADABS-2014/5 (Bruker,2014/5).^[22] Single crystal X-ray diffraction data of compounds **2**, **3** and **4** were collected using a Rigaku XtaLAB mini diffractometer equipped with Mercury375M CCD detector. The data were collected with graphite monochromatic MoK α radiation ($\lambda = 0.71073 \text{ \AA}$) at 100.0(2) K using scans. During the data collection, the detector distance was maintained at 49.5 mm and the detector was placed at $2\theta = 29.85^\circ$ (fixed) for all the data sets.^[23]

2A.4.4 Synthetic procedure

Synthesis of [$\{2-(\text{Me}_3\text{SiN})-6-(\text{Me}_3\text{SiNH})\text{C}_5\text{H}_3\text{N}\}\text{AlCl}_2\}_2$ (1**):** EtAlCl₂ (3.9 mmol, 2.2 mL, 25w% in toluene) was added slowly to a stirred solution of bis(trimethylsilyl)-N,N'-2,6-diaminopyridine (3.9 mmol, 1.0 g) in toluene (40 mL) at 0 °C. The reaction mixture was allowed to come to room temperature and stirred for 12 h. All the volatiles were removed under vacuum to give a greenish solid that afforded transparent crystals of **1** on crystallization from DCM at -30 °C. Yield: 0.7 g (51 %). Mp: 199–203 °C. IR (nujol) ν : 3269 (N-H), 2953, 2923, 2853, 1616, 1565, 1490, 1460, 1378, 1256, 1239, 1173, 1042, 846, 779, 643, 629, 522, 479, 436 cm⁻¹. ¹H NMR (400 MHz, C₆D₆): $\delta = 8.00$ (s, 2H, -NH), 6.98 (t, 2H, *p*-ArH, ³*J*_{H-H} = 8 Hz), 6.31 (d, 2H, *m*-ArH, ³*J*_{H-H} = 8 Hz),

6.01 (d, 2H, *m*-ArH, $^3J_{\text{H-H}} = 8$ Hz), 0.51 (s, 18H, SiMe₃), 0.07 (s, 18H, SiMe₃) ppm. ¹³C NMR (100 MHz, C₆D₆): $\delta = 158.3, 158.1$ (Py-C2, Py-C6), 143.0 (Py-C4), 108.7 (Py-C3), 106.5 (Py-C5),^[24] -0.9 (SiMe₃) ppm. ²⁹Si NMR (79.5 MHz, C₆D₆): $\delta = 15.7, 6.4$ (SiMe₃) ppm. HRMS (AP⁺): *m/z* calcd for C₂₂H₄₄Al₂Cl₄N₆Si₄: (698.1089) [M]⁺; found: (698.1058).

Synthesis of [2-(Me₃SiN)-6-(Me₃SiNH)C₅H₃N]₃Al (2): To a solution of bis(trimethylsilyl)-N,N'-2,6-diaminopyridine (3.9 mmol, 1.0 g) and excess NEt₃ (1.5 mL) in toluene (30 mL), EtAlCl₂ (1.3 mmol, 0.7 mL, 25w% in toluene) was added slowly at 0 °C. The reaction mixture was allowed to warm to room temperature followed by further 12 h of reflux. All the volatiles were removed under vacuum and transparent crystals of **2** were obtained from pentane at -20 °C. Yield: 0.5 g (48 %). Mp: 134–137 °C. IR (nujol) ν : 3356 (N-H), 2954, 2924, 2854, 1599, 1564, 1464, 1377, 1326, 1296, 1258, 1246, 1159, 1093, 1071, 884, 722, 632, 594, 490, 426 cm⁻¹. ¹H NMR (400 MHz, CDCl₃): $\delta = 7.13$ (t, 3H, *p*-ArH, $^3J_{\text{H-H}} = 8$ Hz), 5.83 (d, 3H, *m*-ArH, $^3J_{\text{H-H}} = 8$ Hz), 5.49 (d, 3H, *m*-ArH, $^3J_{\text{H-H}} = 8$ Hz), 0.05 (s, 27H, SiMe₃), 0.00 (s, 27H, SiMe₃) ppm. ¹³C NMR (100 MHz, CDCl₃): $\delta = 165.6$ (Py-C2), 155.2 (Py-C6), 141.0 (Py-C4), 99.00 (Py-C3), 93.4(Py-C5),^[24] 0.9 (SiMe₃), -0.3 (SiMe₃) ppm. ²⁹Si NMR (79.5 MHz, CDCl₃): $\delta = 3.2, -3.2$ (SiMe₃) ppm. HRMS (AP⁺): *m/z* calcd. for C₃₃H₆₆AlN₉Si₆: (783.3872) [M]⁺; found: (783.3846).

Synthesis of [{2,6-(Me₃SiN)₂C₅H₃N}AlEt]₂ (3): EtAlCl₂ (3.8 mmol, 2.1 mL, 25w% in toluene) was added slowly to a stirred solution of dilithium bis(trimethylsilyl)-N,N'-2,6-diamidopyridine (3.8 mmol, 1.0 g) in hexane (30 mL), at 0 °C. The reaction mixture was allowed to warm to room temperature and stirred for another 12 hours. The mixture was then filtered to remove LiCl and the volume of the filtrate was reduced to 10 mL and stored at -20 °C to afford transparent crystals of **3**. Yield: 0.40 g (34 %). Mp: 196–

199 °C. IR (nujol) ν : 2954, 2924, 2855, 1584, 1549, 1456, 1378, 1341, 1262, 1249, 1162, 1103, 1074, 842, 734, 686, 656, 616, 518, 496 cm^{-1} . ^1H NMR (400 MHz, CDCl_3): δ = 7.34 (t, 2H, *p*-ArH, $^3J_{\text{H-H}} = 8$ Hz), 6.0 (broad, 4H, *m*-ArH), 0.78 (t, 6H, $-\text{CH}_2\text{-CH}_3$, $^3J_{\text{H-H}} = 8$ Hz), 0.22 (s, 18H, SiMe₃), 0.11 (s, 18H, SiMe₃), -0.21 (q, 4H, $-\text{CH}_2\text{-CH}_3$, $^3J_{\text{H-H}} = 8$ Hz) ppm; ^{13}C NMR (100 MHz, CDCl_3): δ = 166.2 (Py-C2), 143.4 (Py-C4), 129.0 (Py-C6), 108.2, 101.4 (Py-C3, Py-C5),^[24] 8.6 ($-\text{CH}_2\text{-CH}_3$), 2.3 (SiMe₃), 0.5 (SiMe₃), -2.1 ($-\text{CH}_2\text{-CH}_3$) ppm; ^{29}Si NMR (79.5 MHz, CDCl_3): δ = 3.2 (SiMe₃) ppm. HRMS (AP⁺): *m/z* calcd for C₂₆H₅₉Al₂N₆Si₄: (621.3509) [M+H]⁺; found: (621.3503).

Synthesis of {[2,6-(Me₃SiN)₂C₅H₃N(AlCl₂)₂(AlCl)]₂(AlCl)} (4): A solution of dilithium bis(trimethylsilyl)-N,N'-2,6-diamidopyridine (3.8 mmol, 1.0 g) in toluene (30 mL) was added slowly to a solution of AlCl₃ (5.7 mmol, 0.76 g) in toluene (30 mL) at 0 °C. The reaction mixture was allowed to warm to room temperature and stirred for another 12 h. The mixture was then filtered to remove LiCl and the volume of the filtrate was reduced to 10 mL and stored at -20 °C to afford transparent crystals of **4**. Yield: 0.35 g (24 %). Mp: 276–280 °C (decomposition). IR (nujol) ν : 2956, 2924, 2855, 1646, 1607, 1547, 1457, 1378, 1259, 1173, 1088, 1044, 1028, 846, 801 cm^{-1} . ^1H NMR (400 MHz, CDCl_3): δ = 7.64(t, 2H, *p*-ArH, $^3J_{\text{H-H}} = 8$ Hz), 6.62 (d, 4H, *m*-ArH), 0.43 (s, 36H, SiMe₃) ppm; ^{13}C NMR (100 MHz, CDCl_3): δ = 160.9 (Py-C2, Py-C6), 144.4 (Py-C4), 113.0 (Py-C3, Py-C5),^[24] 2.4 (SiMe₃) ppm. HRMS (AP⁺): *m/z* calcd for C₂₂H₄₂Al₃Cl₅N₆Si₄: (758.0437) [M]⁺; found: (758.0411).

2A.5 Crystallographic Data

Table 2A.5.1. Crystallographic data for compounds 1-4.

Compound	1	2	3	4
Chemical formula	C ₁₃ H ₂₆ AlN ₃ Si ₂	C ₂₂ H ₄₂ Al ₃ Cl ₅ N ₆ Si ₄	C ₂₃ H ₄₆ Al ₂ Cl ₆ N ₆ Si ₄	C ₃₃ H ₆₆ AlN ₉ Si ₆
molar mass	307.53	761.17	785.68	784.46
Crystal system	orthorhombic	monoclinic	monoclinic	triclinic
Space group	<i>Pbca</i>	<i>P2₁/c</i>	<i>P2₁/n</i>	<i>P-1</i>
<i>T</i> [K]	100.0(2)	100.0(2)	200.0(2)	100.0(2)
<i>a</i> [Å]	12.8039(6)	15.6517(4)	16.3788(9)	11.6886(9)
<i>b</i> [Å]	12.9957(6)	18.5868(5)	12.9957(6)	12.5920(9)
<i>c</i> [Å]	21.3377(11)	13.5246(4)	19.5971(10)	17.9012(13)
α [°]	90	90	90	99.173(2)
β [°]	90	103.783(3)	90.720(5)	96.039(2)
γ [°]	90	90	90	115.0130(10)
<i>V</i> [Å ³]	3550.5(3)	3821.22(19)	4171.0(4)	2312.8(3)
<i>Z</i>	8	4	4	2
<i>D</i> (calcd.) [g·cm ⁻³]	1.151	1.3230	1.251	1.126
μ (Mo-K α) [mm ⁻¹]	0.242	0.598	0.592	0.232
Reflections collected	18923	43581	30360	30582
Independent reflections	3136	13454	7384	10037
Data/restraints/parameters	3136/0/179	13454/0/373	7384/0/399	10037/0/460
<i>RI</i> , <i>wR</i> ₂ [<i>I</i> > 2 σ (<i>I</i>)] ^[a]	0.0310, 0.0785	0.0559, 0.1335	0.0655, 0.1546	0.0466, 0.0972
<i>RI</i> , <i>wR</i> ₂ (all data) ^[a]	0.0371, 0.0822	0.0946, 0.1746	0.1078, 0.1921	0.0804, 0.1098
GOF	1.070	1.0118	1.042	1.023
CCDC	1946689	1946690	1946691	1946693

$$[a] \text{ } RI = \frac{\sum ||Fo| - |Fc||}{\sum |Fo|}, wR2 = \frac{[\sum w(|Fo^2| - |Fc^2|)^2 / \sum w|Fo^2|^2]}{I^{1/2}}$$

2A.6. References

1. S. Kotha, M. E. Shirbhate, and G. T. Waghule, *Beilstein J. Org. Chem.*, **2015**, *11*, 1274.
2. (a) G. P. Shkil, and R. S. Sagitnllin, *Chem. Heterocycl. Compd.*, **1998**, *34*, 507; (b) P. G. Ghasemabadi, T. Yao, and G. J. Bodwell, *Chem. Soc. Rev.*, **2015**, *44*, 6494; (c) Z. Hassan, E. Spuling, D. M. Knoll, J. Lahann, and S. Bräse, *Chem. Soc. Rev.*, **2018**, *47*, 6947.
3. (a) A. R. Sabio, C. S. Bonnet, M. M. Iglesias, D. E. Gómez, É. Tóth, A. de Blas, T. R. Blas, and C. P. Iglesias, *Inorg. Chem.*, **2012**, *51*, 10893; (b) F. Tang, N.P. Rath, and L. M. Mirica, *Chem. Commun.*, **2015**, *51*, 3113; (c) G. Castro, R. Bastida, A. Macías, P. P. Lourido, C. P. Iglesias, and L. Valencia, *Inorg. Chem.*, **2015**, *54*, 1671; (d) H. Kuzuhara, N. Watanabe, and M. Ando, *Chem. Commun.*, **1987**, 95; (e) K. Fuchigami, N. P. Rath, and L. M. Mirica, *Inorg. Chem.*, **2017**, *56*, 9404; (f) H. Kuzuhara, M. Iwata, and S. Emoto, *J. Am. Chem. Soc.*, **1977**, *99*, 4173.
4. (a) H. Kawai, T. Suzuki, M. Ohkita, and T. Tsuji, *Angew. Chem. Int. Ed.*, **1998**, *37*, 817; (b) W. Jenny, and H. Holzrichter, *Chimia*, **1967**, *21*, 509; (c) H. J. J. B. Martel, S. McMahon, and M. Rasmussen, *Aust. J. Chem.*, **1979**, *32*, 1241; (d) N. B. Pahor, M. Calligaris, and L. Randaccio, *J. Chem. Soc. Perkin Trans. II*, **1978**, 38; (e) D. J. Cram, and H. Steinbrg, *J. Am. Chem. Soc.*, **1951**, *73*, 5691.
5. P. Kumar, and R. Gupta, *Dalton Trans.*, **2016**, *45*, 18769.
6. (a) N. V. S. Harisomayajula, A. K. Nair, and Y. C. Tsai, *Chem. Commun.*, **2014**, *50*, 3391; (b) A. Noor, E. S. Tamne, B. Oelkers, T. Bauer, S. Demeshko, F. Meyer, F. W. Heinemann, and R. Kempe, *Inorg. Chem.*, **2014**, *53*, 12283; (c) A.

- Falceto, K. H. Theopold, and S. Alvarez, *Inorg. Chem.*, **2015**, *54*, 10966; (d) N. Curado, M. Carrasco, E. Álvarez, C. Maya, R. Peloso, A. Rodríguez, J. L. Serrano, and E. Carmona, *J. Am. Chem. Soc.*, **2015**, *137*, 12378; (e) A. Noor, S. Schwarz, and R. Kempe, *Organometallics*, **2015**, *34*, 2122.
7. (a) Y. Fedorova, O. Fedorova, A. Peregudov, S. Kalmykov, B. Egorova, D. Arkhipov, A. Zubenko, and M. Oshchepkov, *J. Phys. Org. Chem.*, **2016**, *29*, 244; (b) K. M. Lincoln, M. E. Offutt, T. D. Hayden, R. E. Saunders, and K. N. Green, *Inorg. Chem.*, **2014**, *53*, 1406; (c) J. Casabb, L. Escriche, S. Alegret, C. Jaime, C. P. Crez-Jim Cnez, L. Mestres, J. Rius, E. Molins, C. Miravittles, and F. Teixidor, *Inorg. Chem.*, **1991**, *30*, 1893; (d) S. A. Al-Jibori, S. A. O. Ahmed, C. Wagner, H. Schmidt, and G. Hogarth, *Inorg. Chim. Acta*, **2014**, *410*, 118; (e) T. Sciarone, J. Hoogboom, P. P. J. Schlebos, P. H. M. Budzelaar, R. de Gelder, J. M. M. Smits, and A. Ga, *Eur. J. Inorg. Chem.*, **2002**, 457; (f) F. Tang, F. Qu, J. R. Khusnutdinova, N. P. Rath and L. M. Mirica, *Dalton Trans.*, **2012**, *41*, 1404; (g) J. R. Khusnutdinova, J. Luo, N. P. Rath, and L. M. Mirica, *Inorg. Chem.*, **2013**, *52*, 3920; (h) H. Kelm, and H. J. Krüger, *Inorg. Chem.*, **1996**, *35*, 3533; (i) S. P. Meneghetti, P. J. Lutz, and J. Kress, *Organometallics*, **2001**, *20*, 5050; (j) S. P. Meneghetti, P. J. Lutz, J. Fischer, and J. Kress, *Polyhedron*, **2001**, *20*, 2705; (k) Y. Meng, Y. R. Gui, P. C. Wu, N. N. Li, and M. Zhou, *Russian J. Coord. Chem.*, **2011**, *37*, 294.
8. (a) A. Gerus, K. Slepokura, and J. Lisowski, *Inorg. Chem.*, **2013**, *52*, 12450; (b) V. Alexander, *Chem. Rev.*, **1995**, *95*, 273; (c) C. Galaup, J. M. Couchet, C. Picard, and P. Tisnes, *Tetrahedron Lett.*, **2001**, *42*, 6275; (d) C. Galaup, M. C. Carrie, J. Azma, and C. Picard, *Tetrahedron Lett.*, **1998**, *39*, 1573; (e) A. de Bettencourt-Dias, P. S. Barber, and S. Viswanathan, *Coord. Chem. Rev.*, **2014**,

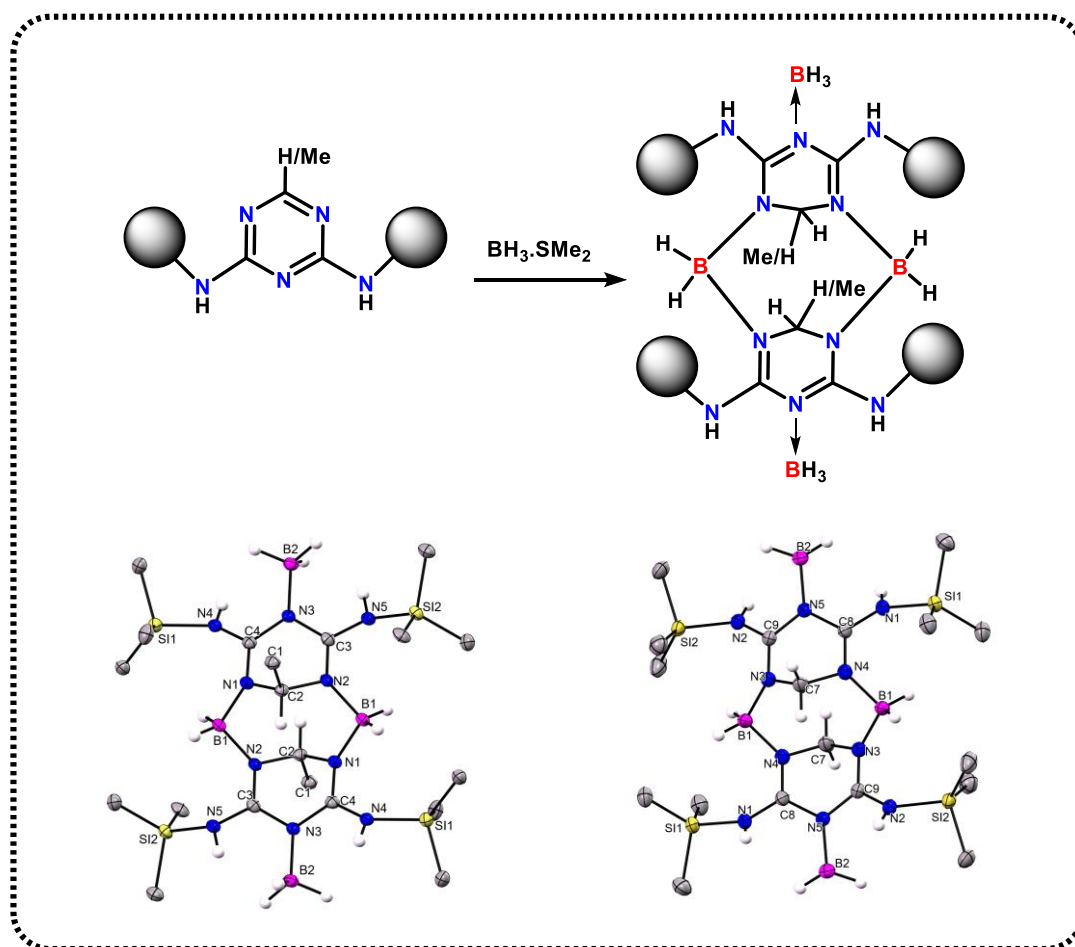
- 273; (f) A. Roca-Sabio, C. S. Bonnet, M. M. Iglesias, D. E. Gómez, É. Tóth, A. de Blas, T. R. Blas, and C. P. Iglesias, *Inorg. Chem.*, **2012**, *51*, 1089; (g) W. P. To, T. W. S. Chow, C. W. Tse, X. Guan, J. S. Huanga, and C. M. Che, *Chem. Sci.*, **2015**, *6*, 5891.
9. (a) G. G. Skvortsov, G. K. Fukin, S. Y. Ketkov, A. V. Cherkasov, K. A. Lyssenko, and A. A. Trifonov, *Eur. J. Inorg. Chem.*, **2013**, 4173; (b) G. Glatz, and R. Kempe, *Z. Kristallogr. NCS*, **2008**, *223*, 307; (c) G. Glatz and R. Kempe, *Z. Kristallogr. NCS*, **2008**, *223*, 309; (d) G. Glatz and R. Kempe, *Z. Kristallogr. NCS*, **2008**, *223*, 313.
10. Y. L. Huang, D. Y. Lu, H. C. Yu, J. S. K. Yu, C. W. Hsu, T. S. Kuo, G. H. Lee, Y. Wang, and Y. C. Tsai, *Angew. Chem. Int. Ed.*, **2012**, *51*, 7781.
11. Y. T. Wey, F. S. Yang, H. C. Yu, T. S. Kuo, and Y. C. Tsai, *Angew. Chem. Int. Ed.*, **2017**, *56*, 15108.
12. (a) M. Shibahara, M. Watanabe, M. Suenaga, K. Ideta, T. Matsumoto, and T. Shinmyozu, *Tetrahedron Lett.*, **2009**, *50*, 1340; (b) T. Satou, and T. Shinmyozu, *J. Chem. Soc., Perkin Trans.*, **2002**, *2*, 393.
13. (a) A. T. Le, and A. T. Soldatenkov, *Chem. Heterocycl. Compd.*, **2016**, *52*, 152; (b) M. X. Wang, *Acc. Chem. Res.*, **2012**, *45*, 182.
14. (a) S. O. Kang, J. M. Llinares, V. W. Day, and K. B. James, *Chem. Soc. Rev.*, **2010**, *39*, 3980; (b) S. O. Kang, V. W. Day, and K. B. James, *Inorg. Chem.*, **2010**, *49*, 8629; (c) B. A. Moyer, R. Custelcean, B. P. Hay, J. L. Sessler, K. B. James, V. W. Day, and S. O. Kang, *Inorg. Chem.*, **2013**, *52*, 3473.
15. (a) K. Reuter, R. G. M. Maas, A. Reuter, F. Kilgenstein, Y. Asfaha, and C. von Hänisch, *Dalton Trans.*, **2017**, *46*, 4530; (b) M. Newcomb, J. M. Timko, D. M.

- Walba, and D. J. Cram, *J. Am. Chem. Soc.*, **1977**, 6392; (c) G. R. Newkome, S. Pappalardo, and F. R. Fronczek, *J. Am. Chem. Soc.*, **1983**, *105*, 5152; (d) H. Higuchi and S. Misumi, *Tetrahedron Lett.*, **1982**, *23*, 5571; (e) S. Muralidharan, M. Hojjatie, M. Firestone, and H. Freiser, *J. Org. Chem.*, **1989**, *54*, 393; (f) S. Ekici, D. Gudat, M. Nieger, L. Nyulaszi, and E. Niecke, *Angew. Chem., Int. Ed.*, **2002**, *41*, 3367.
16. P. Paetzold, U. W. Osterloh, and U. Englert, *Z. Anorg. Allg. Chem.*, **2004**, *630*, 2569.
17. (a) W. Uhl, F. Breher, S. Haddadpour, and F. Rogel, *Organometallics*, **2005**, *24*, 2210; (b) W. Uhl, M. Claesener, S. Haddadpour, B. Jasper, and A. Hepp, *Dalton Trans.*, **2007**, 417; (c) W. Uhl, M. Claesener, A. Hepp, B. Jasper, A. Vinogradov, L. van Wüllen, and T. K.-J. Köster, *Dalton Trans.*, **2009**, 10550; (d) W. Uhl, A. Hepp, M. Matar, and A. Vinogradov, *Eur. J. Inorg. Chem.*, **2007**, 4133; (e) W. Uhl, S. Haddadpour, and M. Matar, *Organometallics*, **2006**, *25*, 159; (f) F. P. Gabbaï, *Angew. Chem., Int. Ed.*, **2012**, *51*, 6316.
18. (a) K. Maheswari, and N. D. Reddy, *Organometallics*, **2012**, *31*, 197; (b) P. Shukla, J. C. Gordon, A. H. Cowley, and J. N. Jones, *Inorg. Chim. Acta*, **2005**, *358*, 4407.
19. D. Bawari, C. Negi, K. Jaiswal, B. Prashanth, A. R. Choudhury, and S. Singh, *Chem. Commun.*, **2018**, *54*, 8857.
20. D. Bawari, C. Negi, V. K. Porwal, S. Ravi, K. R. Shamasundar, and S. Singh, *Dalton Trans.*, **2019**, *48*, 7442.

21. L. Beer, J. F. Britten, J. L. Brusso, A. W. Cordes, R. C. Haddon, M. E. Itkis, D. S. MacGregor, R. T. Oakley, R. W. Reed, and C. M. Robertson *J. Am. Chem. Soc.*, **2003**, *125*, 14394.
22. (a) Bruker (2012). Apex-II. Bruker AXS Inc., Madison, Wisconsin, USA; (b) Bruker (2013). SAINT v8.34A. Bruker AXS Inc., Madison, Wisconsin, USA; (c) Bruker (2014/5). Sadabs, 2014/5. Bruker AXS Inc., Madison, Wisconsin, USA.
23. (a) CrystalClear 2.0; Rigaku Corporation: Tokyo, Japan, **2013**; (b) O. V. Dolomanov, L. J. Bourhis, R. J. Gildea, J. A. K. Howard, H. Puschmann, *J. Appl. Crystallogr.*, **2009**, *42*, 339; (c) G. M. Sheldrick, *Acta Cryst. A*, **2015**, *71*, 3.
24. (a) A. K. El-Qisairia, H.A. Qaseera, M. H. Zaghaleb, S. Magairehb, R. Saymehb, and Y. A. Yousef, *Jordan J. Chem.*, **2007**, *2*, 255; (b) C. S-Holzhaecker, B. Stoger, E. Pittenauer, G. Allmaier, L. F. Veiros, and K. Kirchner, *Monatsh. Chem.*, **2016**, *147*, 1; (c) N. Farfan, H. Hopfl, V. Barba, M. E. Ochoa, R. Santillan, E. Gomez, and A. Gutierrez, *J. Organomet. Chem.*, **1999**, *581*, 70; (d) B. Wrackmeyer, G. Kehr, H. Zhou, and S. Alif, *Magn. Reson. Chem.*, **1996**, *34*, 921.

Chapter 2B

Macrocycles Assembled *via* Hydroborative Dearomatization and Self-sorting of Triazine Rings



D. Bawari, C. Negi, V. K. Porwal, A. Saha, and S. Singh,* Catalyst free dearomative hydroboration of triazine: Unprecedented synthesis of $-\text{BH}_2-$ bridged macrocycles. *Unpublished results*.

Abstract: This chapter presents a modular approach for the synthesis of boron containing macrocycles. The reaction of *bis*(trimethylsilyl)-N,N'-2,4-diamino-6-(Me)-triazine (BDMT) with borane was expected to give a cyclic structure with the evolution of H₂ gas. Instead, the Markonikov addition of B-H bond across the -C=N- bond at 5,6-position of the triazine ring occurred which results in the dearomatization of the triazine ring. The dearomatized triazine rings self-assembled in the solution to afford an unprecedented trimeric macrocycle, [N,N'-2,4-(SiMe₃)₂{CH(Me)C₂N₃}(μ-BH₂)]₃ (**1**) where three dearomatized triazine rings connected through three -BH₂- units. Further, by varying the stoichiometry of reagents (BH₃ and BH₂Cl), the dimeric structures [2,4-(NHSiMe₃)₂{CH(Me)C₂N₃}(μ-BH₂)]₂·(BH₃)₂ (**2**) and [N,N'-2,4-(SiMe₃)₂{CH(Me)C₂N₃}(μ-BH₂)]₂(BH₂Cl)₂ (**5**) were obtained by self-assembling of the reduced triazine rings. Another derivative bis(trimethylsilyl)-N,N'-2,4-diamino-1,3,5-triazine (**3**), has also been used to check the feasibility of the reaction and a similar dearomatized product was obtained which also self-assembled to give dimeric [N,N'-2,4-(SiMe₃)₂{C₃N₃H₂}(μ-BH₂)]₂·(BH₃)₂ (**4**) macrocycle. This work is the first example of hydroboration of triazine ring without use of any external catalysts.

2B.1 Introduction

N-heterocycles and their reduced products are important structural skeletons in natural products and biologically active molecules as well as cover the broad area of synthetic organic and material chemistry.^[1] Initially, a stoichiometric amount of metal hydrides (NaBH_4 or LiAlH_4) or reactive alkali metals have been used for dearomatization of heteroarenes. After that, hydrogenation procedures were employed based on the fact that it is a straightforward and atom-efficient technique for the reduction of N-heteroaromatic compounds. However, these are generally operative under elevated temperatures, high pressures (H_2) and usually require N-activated pyridinium species as the starting materials.^[2] Also, the tendency of H_2 towards the complete reduction of N-heteroaromatic compounds certainly limits the opportunity for the syntheses of various alkaloids and natural products. In terms of molecular diversity, selective partial reduction is highly desired. The dearomatization of N-heteroarenes is a kinetically and thermodynamically unfavourable process because of the resonance stabilization of the N-aromatic core,^[3] as the resultant hydroarenes often undergo rearomatization. To overcome the above-mentioned obstacles in accomplishing the controlled reduction process, hydrosilanes and hydroboranes have been utilized as competent alternatives to H_2 . In this regard, hydrosilylation and hydroboration approaches have various advantages over hydrogenation as they offer steric and electronic variables, also silicon and boron moieties can be transformed into a range of functional groups, which opens the opportunity for the syntheses of diverse azacyclic compounds.^[4] Organoboranes are important intermediates in many organic transformations and can be prepared by the direct addition of B–H across unsaturated bonds known as hydroboration, which was initially observed by H. C. Brown et al. in 1956.^[5] The strong affinity between nitrogen and boron can be beneficial in activating N-aromatic ring. Dearomative hydroboration

of N-heteroarenes offers an alternative route to hydrogenation, and the partially reduced azacyclic compounds such as piperidines, dihydropyridines serve as important building blocks for the syntheses of many bioactive alkaloids, natural products, and commercial drugs.^[1,4] Since Hill reported the first example of hydroboration of pyridines using an alkyl magnesium as a precatalyst, intensive studies on the hydroboration of N-heteroarenes are being performed by many research groups,^[6] catalytic systems ranging from main-group element P or Mg based-catalysts, transition metal catalysts including Fe, Zn, Ni, La, Zr, Hf, Ce, Th, Rh and Ru^[7] as well as metal-free catalytic systems^[8] have been explored. The only case without a catalyst involves the reaction of pyrazine with pinacolborane (HBpin) that afforded its corresponding diboration product.^[9] A series of reviews were published that highlight the synthetic utility of dihydropyridines, tetrahydropyridine, piperidines, and partially reduced azacyclic compounds.^[2,4] Despite numerous examples of reduction of N-heteroarenes such as pyridine and pyrazine, the dearomative hydroboration of triazine systems remained unexplored, and the only report on the hydroboration of 1,3,5-triazine with pinacolborane (HBpin) used a thorium hydride based catalyst.^[10] The reduced derivatives of 1,3,5-triazine such as cycloguanil, chlorcycloguanil, clociguanil, and WR99210 have been known as potent antimalarial agents.^[11]

Due to the lack of general and well-defined routes to prepare the main group containing inorganic-organic hybrid macrocycles, the dearomative hydroboration approach proves to be an important alternative synthetic strategy. The interaction of a Lewis-acidic boron center with the N-donor atom by strong (N→B) coordination promotes the self-assembly of monomeric units in a variety of molecular motifs such as imine,^[12] pyridine,^[13] pyrazole and imidazole^[14] derivatives. With the successful application of this donor-acceptor interaction concept, we have reported boron and

aluminum bridged conformationally rigid [3.3](2,6)pyridinophanes and aluminum complexes (Chapter 2A).^[15] The present work is inspired by our earlier report on the synthesis of tetraazadibora[3.3](2,6)pyridinophane derived from the reaction of *bis*(trimethylsilyl)-*N,N'*-2,6-diaminopyridine (bap) with $\text{BH}_3\cdot\text{SMe}_2$ and bapLi_2 with BCl_3 .^[15c]

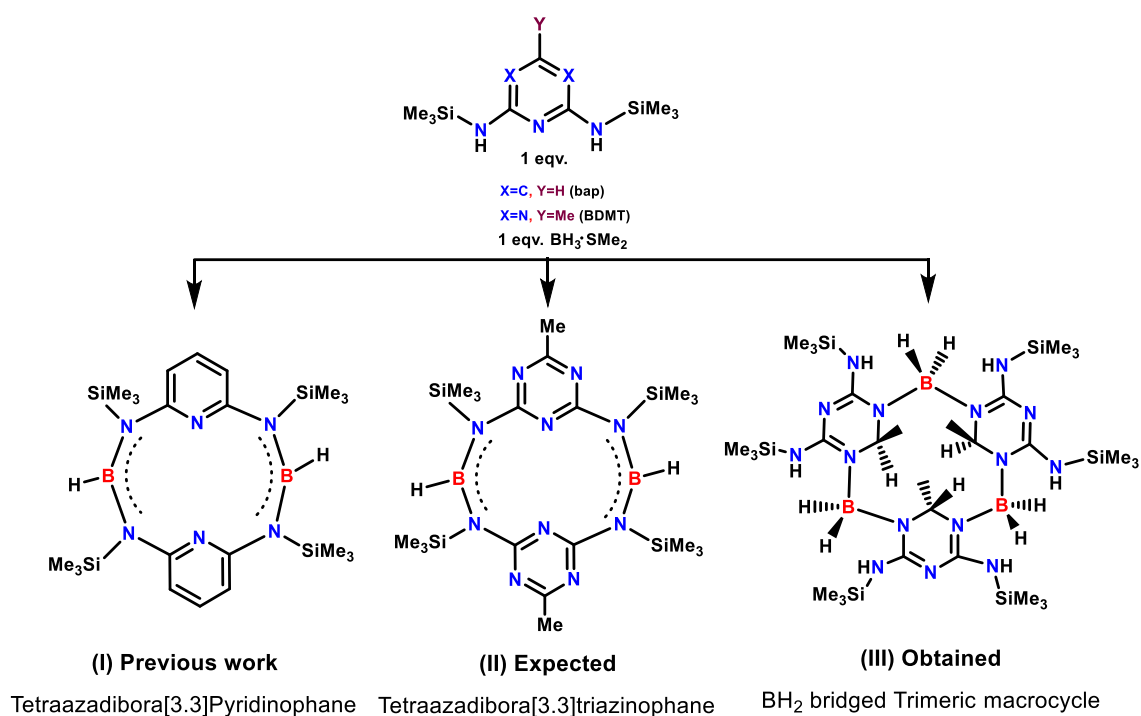


Figure 2B.1. Tetraazadibora[3.3](2,6)pyridinophane (**I**); triazinophane (**II**) analogous to (**I**) that was expected to form and the actually obtained trimeric macrocycle $[\text{N},\text{N}'\text{-}2,4\text{-}(\text{SiMe}_3)_2\{\text{CH}(\text{Me})\text{C}_2\text{N}_3\}(\mu\text{-BH}_2)]_3$ (**III**).

To synthesize an analogous triazine based macrocycle, we employed a similar approach using 6-methyltriazine derivative as a building block. The reaction of *bis*(trimethylsilyl)-*N,N'*-2,4-diamino-6-methyl-1,3,5-triazine (BDMT) with borane was expected to give a cyclic structure (*say* triazinophane) like pyridinophane (Figure 2B.1) with the evolution of H_2 gas, however no gas evolution observed in this case. ^1H NMR observations ruled out the formation of triazinophane. Interestingly, the addition of B–H across the -C=N- bond at 5,6-positions of triazine ring results in the dearomatization of

triazine ring which cyclize to give boron bridged trimeric macrocycle, $[\text{N},\text{N}'\text{-}2,4\text{-}(\text{SiMe}_3)_2\{\text{CH}(\text{Me})\text{C}_2\text{N}_3\}(\mu\text{-BH}_2)]_3$ (**1**) where three dearomatized triazine moieties were connected by three $\text{-BH}_2\text{-}$ units through coordinative ($\text{N}\rightarrow\text{B}$) bonds (Figure 2B.1).^[15] Prior to our work, there have been some reports (**A-F**) in the last few years on boron-based macrocycles containing $\text{-BH}_2\text{-}$ bridges. S. Trofimenko in 1967, reported the first pyrazole based BH_2 bridged dimeric cyclic molecule with various R/R' groups (**A**) (Figure 2B.2). Later in 2014, group of Blanchard and Lalevee also assembled some more derivatives of dimeric pyrazoles and similar $\text{-BH}_2\text{-}$ bridged trimeric macrocyclic pyrazaboles (**B**).^[16]

Known examples of BH_2 bridged macrocycles of pyrazole and imidazole derivatives

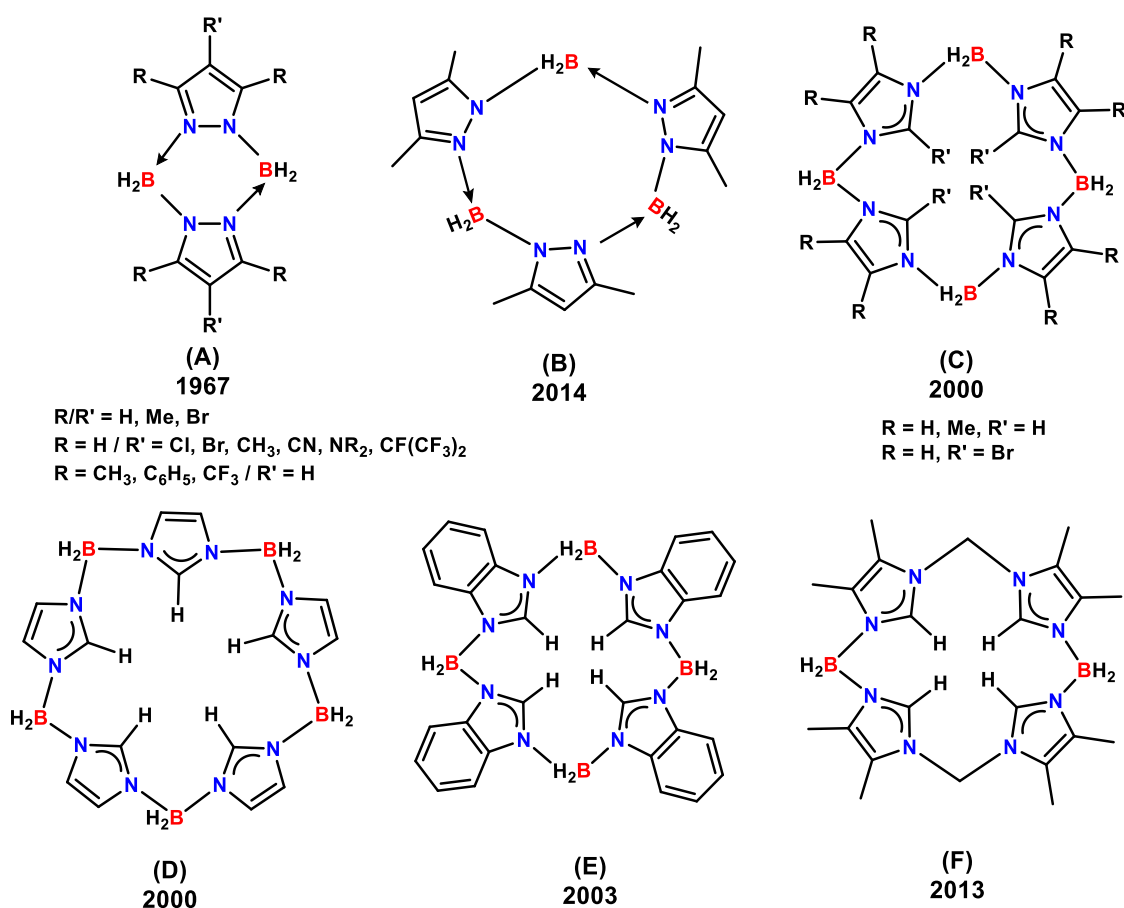


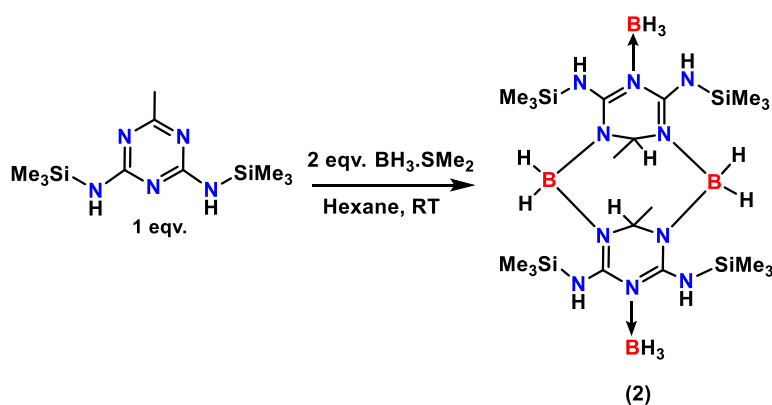
Figure 2B.2. Known $\text{-BH}_2\text{-}$ bridged macrocycles of pyrazole (**A, B**) and imidazole derivatives (**C-F**).

Siebert and coworkers reported imidazole based $\text{-BH}_2\text{-}$ bridged tetrameric and pentameric macrocycles (**C-E**).^[17] Jenkins and co-workers in 2013, reported $\text{-BH}_2\text{-}$ and $\text{-CH}_2\text{-}$ bridge imidazole based tetrameric cyclic molecule (**F**).^[17] The syntheses of these macrocycles proceeds through the elimination of molecules such as H_2 , Me_3SiCl . Whereas there are no reports available that proceed with the dearomative hydroboration of heterocyclic rings followed by self-assembling to construct boron based macrocyclic structures. Our work not only represents a novel path to assemble boron based macrocycles but also presents the first example of partial dearomative hydroboration of triazine systems without use of any external catalyst. Catalyst-free partial hydroboration of triazine rings has been observed for BDMT, and the dearomatized units further self-assembled to produce $\text{-BH}_2\text{-}$ bridged trimeric macrocycle $[\text{N},\text{N}'\text{-}2,4\text{-}(\text{SiMe}_3)_2\{\text{CH}(\text{Me})\text{C}_2\text{N}_3\}(\mu\text{-BH}_2)]_3$ (**1**).^[15c] Further attempts to reduce all the bonds with stoichiometric and excess borane were unsuccessful, rather similar $\text{-BH}_2\text{-}$ bridged dimeric macrocycles $[2,4\text{-}(\text{NHSiMe}_3)_2\{\text{CH}(\text{Me})\text{C}_2\text{N}_3\}(\mu\text{-BH}_2)]_2\cdot(\text{BH}_3)_2$ (**2**) and $[\text{N},\text{N}'\text{-}2,4\text{-}(\text{SiMe}_3)_2\{\text{CH}(\text{Me})\text{C}_2\text{N}_3\}(\mu\text{-BH}_2)]_2\cdot(\text{BH}_2\text{Cl})_2$ (**5**) afforded with BH_3 and BH_2Cl respectively. Another triazine derivative, bis(trimethylsilyl)- $\text{N},\text{N}'\text{-}2,4\text{-}$ diamino-1,3,5-triazine (BDT) (**3**) with borane gives similar dearomatized product by addition of B-H unit across the -C=N- bond which cyclizes to afford dimeric macrocycle $[2,4\text{-}(\text{NHSiMe}_3)_2\{\text{C}_3\text{N}_3\text{H}_2\}(\mu\text{-BH}_2)]_2\cdot(\text{BH}_3)_2$ (**4**).

2B.2 Results and Discussion

The key building block, *bis*(trimethylsilyl)- $\text{N},\text{N}'\text{-}2,4\text{-}$ diamino-6-(Me)-triazine (BDMT), has been synthesized by the reported procedure.^[18] The stoichiometric reaction of BDMT with $\text{BH}_3\cdot\text{SMe}_2$ at room temperature afforded a $\text{-BH}_2\text{-}$ bridged trimeric macrocycle $[\text{N},\text{N}'\text{-}2,4\text{-}(\text{SiMe}_3)_2\{\text{CH}(\text{Me})\text{C}_2\text{N}_3\}(\mu\text{-BH}_2)]_3$ (**1**) as a result of

dearomatization of triazine ring followed by self-assembly of partially reduced triazine rings (structure **III** in Figure 2B.1). Further, for complete dearomatization of triazine ring, 3 equivalents as well as excess of $\text{BH}_3 \cdot \text{SMe}_2$ was added in the reaction however, no further reduction of $\text{C}=\text{N}$ bonds of the triazine was observed. The ^1H NMR spectrum of the crude reaction mixture showed signals for trimer **1** (major) along with a new dimeric product $[\text{2,4-(NHSiMe}_3)_2\{\text{CH(Me)C}_2\text{N}_3\}(\mu\text{-BH}_2)]_2 \cdot (\text{BH}_3)_2$ (**2**) and an unidentified compound. To synthesise dimer **2** as an exclusively major product, 1:2 stoichiometric reaction of BDMT and $\text{BH}_3 \cdot \text{SMe}_2$ have also performed, the ^1H NMR spectrum of the crude compound obtained from 1:2 reaction of BDMT and $\text{BH}_3 \cdot \text{SMe}_2$ showed similar mixture of products (Scheme 2B.1).



Scheme 2B.1. Synthesis of dimeric macrocycle, $[\text{2,4-(NHSiMe}_3)_2\{\text{CH(Me)C}_2\text{N}_3\}(\mu\text{-BH}_2)]_2 \cdot (\text{BH}_3)_2$ (**2**).

Various attempts to obtain **2** as major/exclusive product were unsuccessful. Compound **2** could not be separated from this mixture; however, the NMR spectrum of the material obtained after crystallization turned out to be the mixture of **1** (50%) and **2** (50%) (Figure 2B.3). Similar to **1**, the ^1H NMR spectrum of **2** also included a set of singlets (5.82 ppm $-\text{NH}$), quartet (4.33 ppm), doublet (1.15 ppm, merged with the signal of **1**) and singlets (0.35 ppm, $-\text{SiMe}_3$). The signal at 63.29 ppm in $^{13}\text{C}\{^1\text{H}\}$ NMR spectrum is also attributed to the reduced carbon (H-C-Me) of the triazine ring. The ^{11}B NMR

spectrum showed the resonances at -6.87 and -23.47 ppm, where the former signal corresponds to the $-BH_2-$ bridge in dimer while the latter signal was attributed to the tetra-coordinated boron of $-BH_3$ unit to the nitrogen atom of reduced triazine ring.

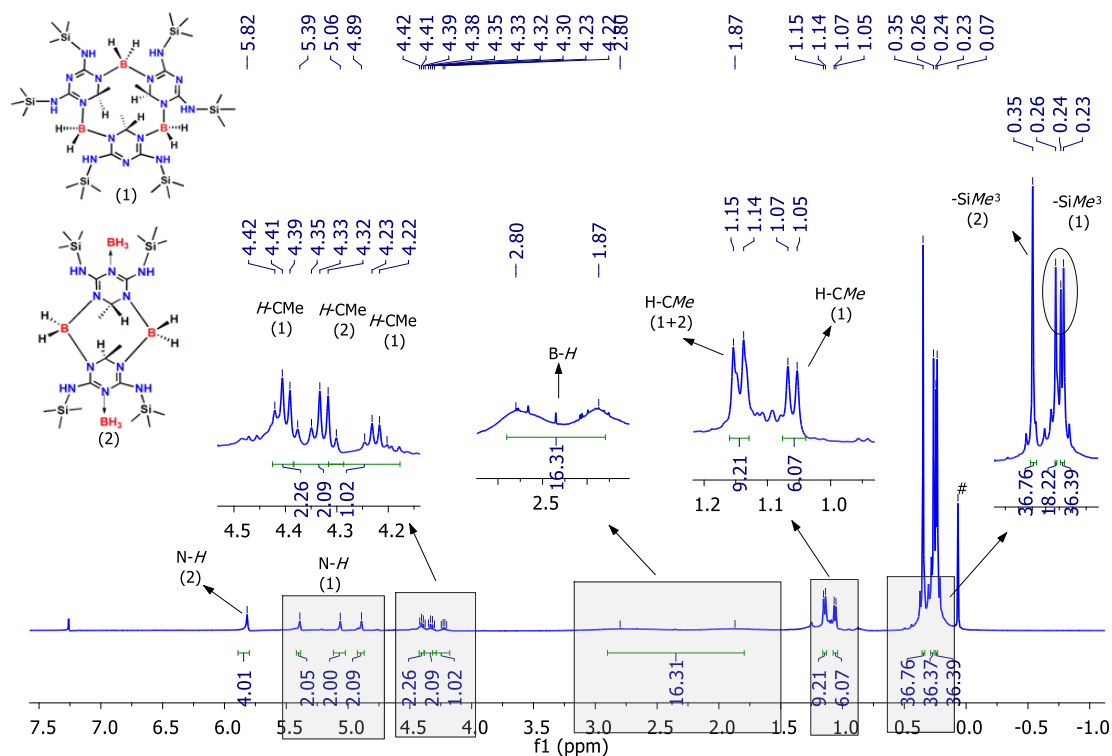


Figure 2B.3. 1H NMR (400 MHz, $CDCl_3$) spectrum attributing 1:1 mixture of trimeric (1) and dimeric (2) macrocycles. # = silicon grease.

The presence of BH_3 units coordinated to the dimer **2** could also be seen from its HRMS spectrum that showed signals at m/z 594.4339 (calcd. 594.4313), for $[M^+]$ and also observed m/z 567.3702 (calcd. 567.3727), for $[M-(2BH_3)+H]^+$. Further, the dimeric nature of **2** was confirmed using single crystal X-ray structure analysis. The single crystals of the dimer suitable for X-ray diffraction were obtained from hexane at -10 °C. This result assured the dearomative hydroboration of the triazine ring and also confirmed the presence of two additional BH_3 units coordinated with the dearomatized C_3N_3 ring nitrogen. Thus, all these features attributed that the formation of **2** also involved the dearomative hydroboration of the triazine units.

Compound **2** crystallized in the monoclinic system with $P2_1/c$ space group. The solid-state structure of **2** consists of eight-membered cyclic core containing boraamidinate (-N-B-N-) bridge, where two -BH₂- units connect the two partially reduced triazine moieties by coordinative N→B bonds. The reduction across 5,6-position of triazine ring can be seen by the average bond lengths and tetrahedral geometry around ring carbon (C2) (Figure 2B.4).

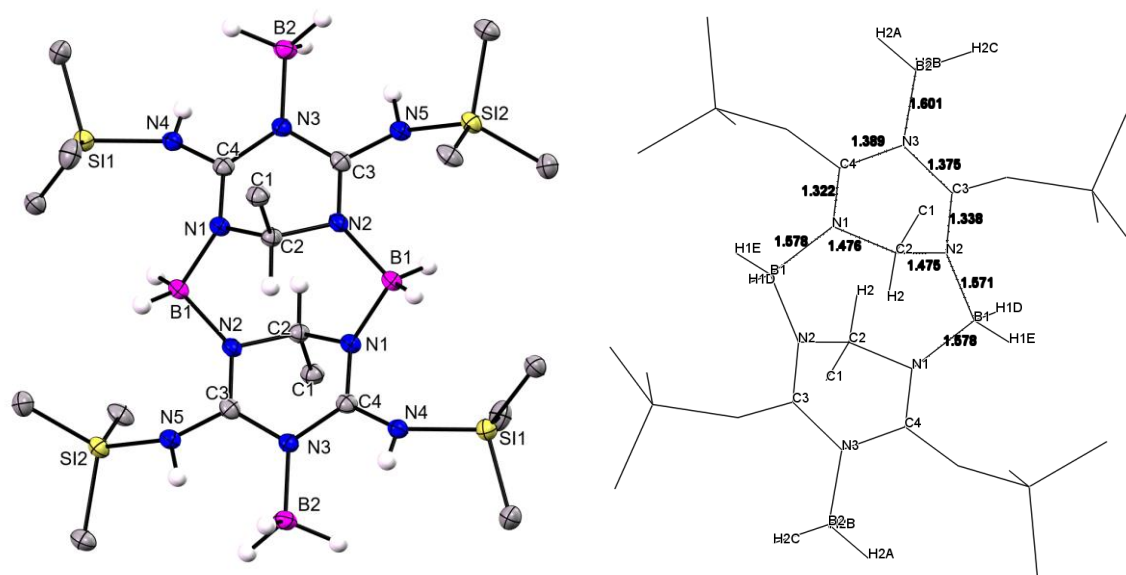
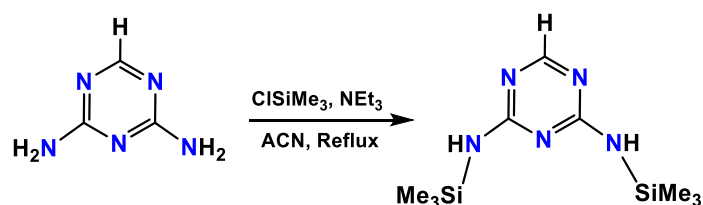


Figure 2B.4. Single crystal X-ray structure of dimer, [2,4-(NHSiMe₃)₂{CH(Me)C₂N₃}(μ-BH₂)]₂·(BH₃)₂ (**2**) (left) and wireframe (right) with bond lengths; All hydrogen atoms except that on relevant C, N and B atoms have been omitted for clarity. Selected bond distances (Å) and angles (°): N3-C4 1.389(4), N3-C3 1.375(4), N3-B2 1.601(5), N2-C3 1.338(4), N2-C2 1.475(4), N2-B1 1.571(5), N1-C4 1.322(4), N1-C2 1.476(4), N1-B1 1.578(5), N4-C4 1.345(4), N5-C3-1.350(4), C1 C2 1.520(5); N2-C2-N1 107.6(3), N2-C2-C1 112.9(3), N1-C2-C1 112.7(3), N2-B1-N1 106.0(3).

The C-N bond lengths in triazine ring of **2** N2-C2 1.475(4) and N1-C2 1.476(4) Å show single bond character whereas, the rest of the ring still contains the short -C=N- bonds with the bond lengths in the double bond range 1.322-1.389 Å indicates the partial

dearomatization of triazine ring. The transannular B1-B1 and C2-C2 separations are 4.276 and 3.100 Å.

In order to extend this strategy, more triazine substrates were explored, *tris*(trimethylsilyl)-*N,N',N'*-2,4,6-triamino-triazine (TTT), *bis*(trimethylsilyl)-*N,N'*-2,4-diamino-6-(Phenyl)-triazine (BDPT) and *bis*(trimethylsilyl)-*N,N'*-2,4-diamino-1,3,5-triazine (BDT). The reactions of these triazines were performed with $\text{BH}_3 \cdot \text{SMe}_2$ that resulted in the formation of simple adducts $\text{TTT} \cdot \text{BH}_3$ and $\text{BDPT} \cdot \text{BH}_3$ while in the case of BDT, partial dearomatization of triazine ring was observed. *N,N'*-2,4-diamino-1,3,5-triazine have been synthesized in steps by following the reported procedure, and further selective silylation of BDT (**3**) was done following the procedure used for silylation of other triazine derivatives^[18] but in this case the yield was comparatively low (10%) (Scheme 2B.2). Crude BDT (**3**) contains impurity, washing with hexane and pentane gave pure compound.



Scheme 2B.2. Synthesis of *bis*(trimethylsilyl)-*N,N'*-2,4-diamino-1,3,5-triazine (BDT) (**3**).

The ^1H NMR measurement of **3** showed a signal at 8.11 ppm for the single proton of the aromatic triazine ring and a signal for N-H (2H) at 4.93 ppm. The signal for SiMe_3 groups appeared at 0.28 ppm in ^1H NMR spectrum, at 6.16 ppm in ^{29}Si NMR spectrum and the corresponding carbon signal in $^{13}\text{C}\{^1\text{H}\}$ NMR spectrum appeared at -0.31 ppm. The HRMS data of the product showed peak at $m/z = 256.1422$ (calcd: 256.1414) for $[\text{M}+\text{H}]^+$ $\text{C}_9\text{H}_{22}\text{N}_2\text{Si}_2$. The single crystals suitable for X-ray diffraction were obtained in

pentane at -10 °C. Compound **3** crystallized in the tetragonal system with *I*-42d space group.

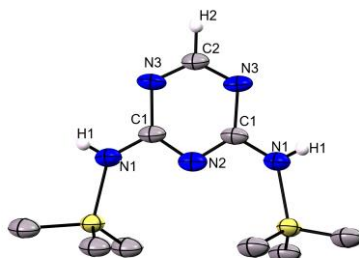
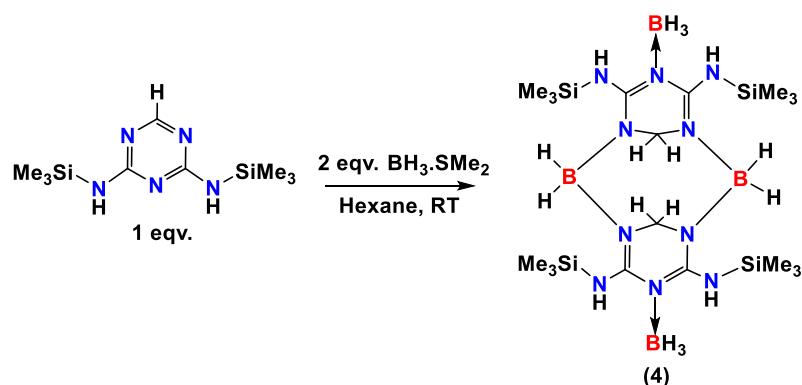


Figure. 2B.5. Single crystal X-ray structure of *bis*(trimethylsilyl)-*N,N'*-2,4-diamino-1,3,5-triazine (**3**). Hydrogen atoms of SiMe₃ have been omitted for clarity. Selected bond distances (Å) and angles (°): N2-C1 1.329(6), N2-C1 1.329(6), N3-C1 1.384(5), N3-C2 1.313(5), N1-C1 1.344(7), N1-Si1 1.757(11); C1-N2-C1 116.1(5), C2-N3-C1 113.2(5), C1-N1-Si1 121.4(4), C1-N1-H1 122(4), N2-C1-N3 124.3(5), N2-C1-N1 119.5(4).

The equimolar reaction of BDT (**3**) and BH₃·SMe₂ was not selective and gave a mixture of products that could not be separated for further characterization. The 1:2 reaction of *bis*(trimethylsilyl)-*N,N'*-2,4-diamino-1,3,5-triazine and BH₃·SMe₂ in hexane afforded a white solid which on crystallization from pentane at -10 °C gave colourless crystals of [2,4-(SiMe₃)₂{C₃N₃H₂}(μ-BH₂)₂·(BH₃)₂ (**4**) (Scheme 2B.3).



Scheme 2B.3. Synthesis of dimeric macrocycle [2,4-(NHSiMe₃)₂{C₂N₃H₂}(μ-BH₂)₂·(BH₃)₂ (**4**).

The IR spectrum of **4** showed the N-H stretching bands at 3484 and 3371 cm^{-1} and the B-H stretching at 2369 and 2248 cm^{-1} . Also, the ^1H NMR spectrum of the product **4** shows the signal at 5.81 ppm for 4H indicating the presence of N-H. Also, two separate doublets (at 4.01 and 3.92 ppm, $^2J_{\text{H-H}} = 12$ Hz) in 1:1 ratio indicate the presence of two types of protons indicative of additional hydrogen and these signals were attributed to the geminal $-\text{CH}_2$ moiety that could form due to addition of $-\text{B-H}-$ across the $-\text{C}=\text{N}-$ double bond at 5,6-position of the triazine ring that leads to dearomative hydroboration. Additionally, two broad signals at 2.80 and 1.85 ppm for ten protons were attributed to the $-\text{BH}_2$ and $-\text{BH}_3$ moieties (Figure 2B.6). Two broad signals at -8.5 for $-\text{BH}_2-$ and -24.2 ppm for $-\text{BH}_3$ in the ^{11}B NMR spectrum of **4** were assigned to tetra-coordinated boron centers (Figure 2B.7).

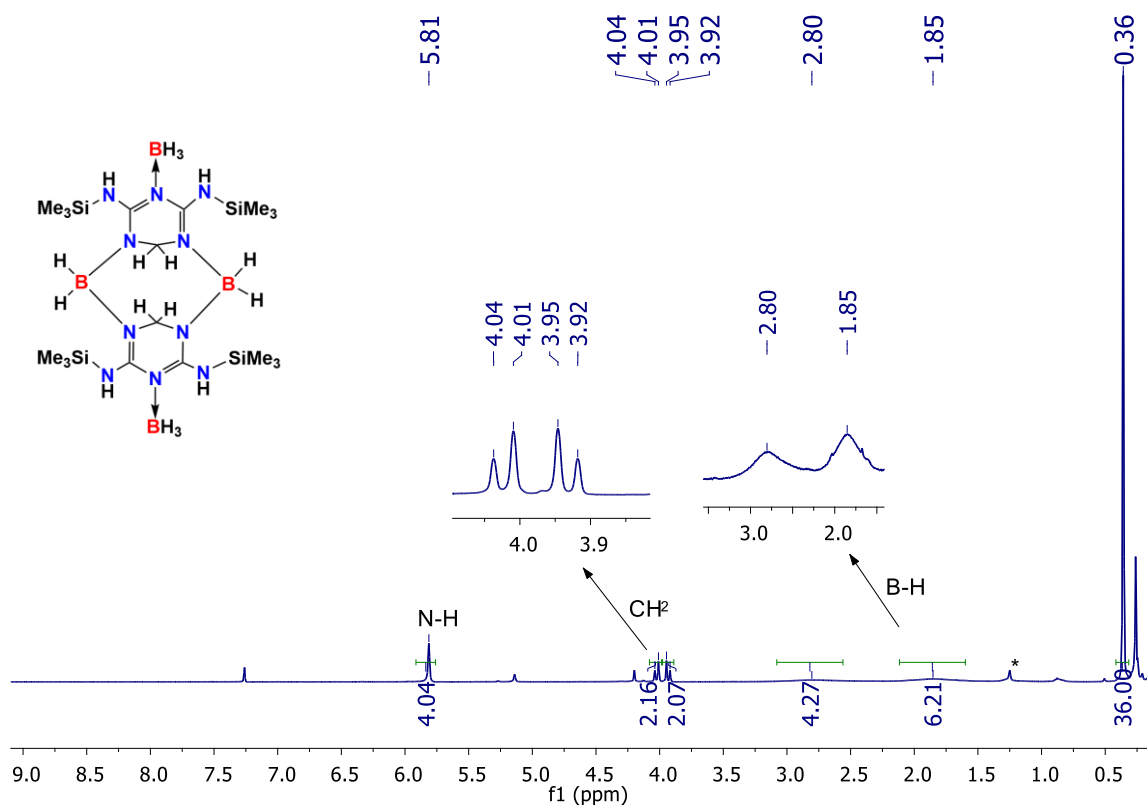


Figure. 2B.6. ^1H NMR (400 MHz, CDCl_3) spectrum of dimeric macrocycle (**4**). * = hexane, # = silicon grease, ^ = trace amounts of unknown compound.

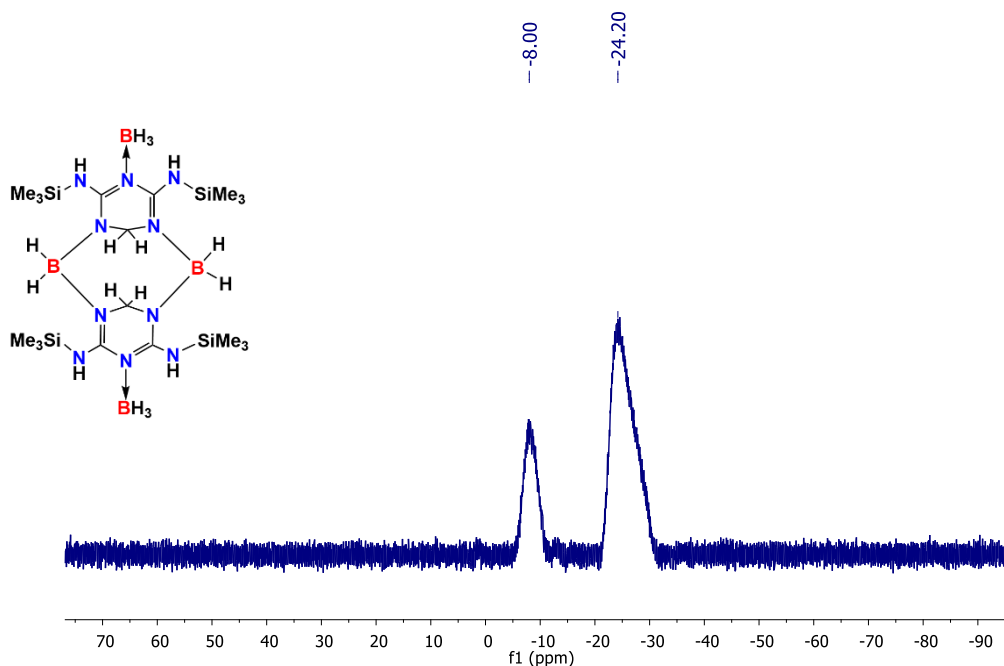


Figure. 2B.7. ^{11}B NMR (128 MHz, CDCl_3) spectrum of the dimeric macrocycle **4**.

The presence of coordinated $-\text{BH}_3$ adduct in **4** was also confirmed from the HRMS spectrum that showed molecular ion peak at $m/z = 566.4026$ (calcd. 566.4000), for $[\text{M}]^+$ and also observed m/z 539.3414 (calcd. 539.3437), for $[\text{M}-2\text{BH}_3]^+$. The structure of **4** as the dimer was later confirmed from single crystal X-ray diffraction that also revealed the BH_3 adducts in addition to the $-\text{BH}_2-$ bridged dimer (Figure 2B.8). The single crystals suitable for X-ray were obtained in pentane at $-10\text{ }^\circ\text{C}$

Compound **4** crystallized in the monoclinic ($\beta = 99.246(4)$) system with $P2_1/c$ space group. The cyclic core of $[2,4-(\text{NHSiMe}_3)_2\{\text{C}_3\text{N}_3\text{H}_2\}(\mu\text{-BH}_2)]_2\cdot(\text{BH}_3)_2$ (**4**) contains 8 atoms $\text{C}_2\text{B}_2\text{N}_4$ involving boraamidinate ($\text{N}-\text{B}-\text{N}$) bridge where two $-\text{BH}_2-$ units connect the reduced triazine rings by coordinative $\text{N}\rightarrow\text{B}$ bonds. The $\text{C}-\text{N}$ bond lengths in the triazine ring ($\text{N}4-\text{C}7$ 1.456(2) Å and $\text{N}3-\text{C}7$ 1.460(3) Å) are attributed to $\text{C}-\text{N}$ single bond character due to hydroboration, whereas the rest of the triazine backbone still contains a double bond character with the shorter bond lengths in the

range of 1.33–1.38 Å. The transannular B1–B1' and C2–C2' separations are 4.252 and 3.132 Å in **4**, which is similar to the cavity size of **2** (Figure 2B.8).

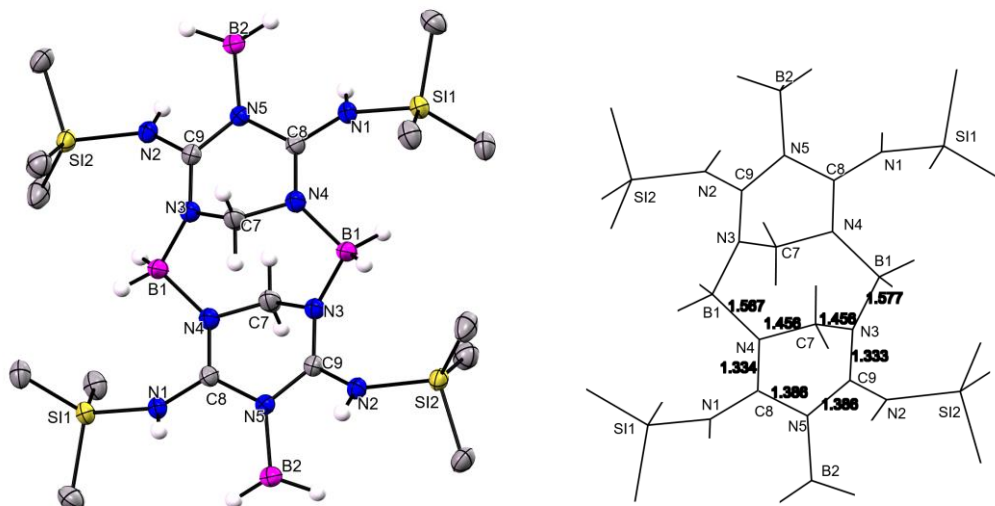
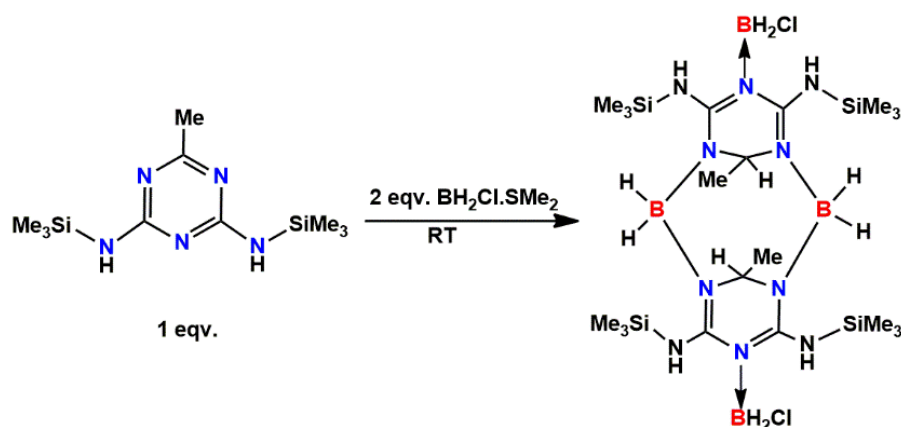


Figure 2B.8. Single crystal X-ray structure of dimer, $[2,4\text{-}(\text{NHSiMe}_3)_2\{\text{C}_3\text{N}_3\text{H}_2\}(\mu\text{-BH}_2)]_2(\text{BH}_3)_2$ (**4**) (left) and wireframe (right) with bond lengths; all hydrogen atoms except that on relevant C, N and B atoms have been omitted for clarity. Selected bond distances (Å) and angles ($^\circ$): N1–H1 0.8800, N1–C8 1.3439(18), N2–H2 0.8800, N2–C9 1.3353(18), N3–C7 1.4596(19), N3–C9 1.3330(18), N3–B1 1.577(2), N4–C7 1.4562(19), N4–C8 1.3337(19), N4–B1 1.567(2), N5–C8 1.3860(18), N5–C9 1.3864(18), N5–B2 1.606(2), B1–N4 1.567(2); N4–B1–N3 106.87(12), N4–C7–N3 109.28(12), C8–N5–C9 116.14(12).

Further, on varying the borane reagent from BH_3 to BH_2Cl , the 1:2 reaction of *bis*(trimethylsilyl)-*N,N'*-2,4-diamino-6-(Me)-triazine (BDMT) and $\text{H}_2\text{BCl}\cdot\text{SMe}_2$ in hexane/toluene at room temperature successfully afforded a dimeric structure, $[\text{N},\text{N}'\text{-}2,4\text{-}(\text{SiMe}_3)_2\{\text{CH}(\text{Me})\text{C}_2\text{N}_3\}(\mu\text{-BH}_2)]_2[\text{BH}_2\text{Cl}]_2$ (**5**) (Scheme 2B.4). The ^1H NMR spectrum of **5** showed a signal at 5.89 ppm indicates the presence of unreacted *N-H*, additionally a quartet (4.32 ppm, *H-C-Me*, $^2J_{\text{H-H}} = 8$ Hz) and a doublet (1.19 ppm, *H-C-Me*, $^2J_{\text{H-H}} = 8$ Hz) were attributed to *H-C-Me* moiety formed due to addition of -B-H across the $\text{C}=\text{N}$ double bond at 5,6-position of the triazine ring. The $^{13}\text{C}\{^1\text{H}\}$ NMR spectrum also corroborated the hydroboration due to the presence of a signal at 63.80

ppm. The signal in ^{11}B NMR at 7.5 ppm and 3.0 ppm in the ^1H NMR spectrum for eight hydrogens indicates the presence of $-\text{BH}_2-$ bridges. The HRMS data of the product showed a peak at $m/z = 565.3542$. (calcd. 565.3571) for $\text{C}_{20}\text{H}_{51}\text{B}_2\text{N}_{10}\text{Si}_4$ also indicates the formation of a dimeric macrocycle. Later, the structure of **5** was confirmed from single crystal X-ray diffraction analysis as the dimer where two units of reduced triazine rings were connected via $-\text{BH}_2-$ bridged (Figure 2B.9). The solid-state structure shows the presence of BHCIME adduct (could not be seen in NMR) along with BH_2Cl adduct over triazine ring nitrogen. The dimeric molecule contains BH_2 bridges which could form either by $-\text{Cl}$ exchange with $-\text{H}$ in the reaction or the dearomatization proceeding from the residual BH_3 proportion in the solution of commercial $\text{BH}_2\text{Cl}\cdot\text{SMe}_2$ reagent.^{19]}



Scheme 2B.4. Synthesis of the dimeric macrocycle, $[\text{2,4-(NHSiMe}_3)_2\{\text{CH(Me)C}_2\text{N}_3\}(\mu\text{-BH}_2)]_2(\text{BH}_2\text{Cl})_2$ (**5**).

The crystals of **5** were grown at $-20\text{ }^\circ\text{C}$ from a solution in hexane/pentane by slow evaporation. The structure was solved in monoclinic crystal system with $P2_1/c$ space group. Two molecules of **5** were seen in the asymmetric unit that have the same core but are different in composition in terms of BH_2Cl and BHCIME adducts at triazine ring nitrogen (N3 and N8). It was found that one molecule of the asymmetric unit contains 80% $[\text{2,4-(NHSiMe}_3)_2\{\text{CH(Me)C}_2\text{N}_3\}(\mu\text{-BH}_2)]_2(\text{BH}_2\text{Cl})_2$ (**5a**) and 20% $[\text{N,N}'\text{-2,4-}$

(SiMe₃)₂{CH(Me)C₂N₃}(μ-BH₂)₂·(BHClMe)₂ (**5b**), while another contains 55% **5a** and 45% **5b** (occupancies were refined using PART command).

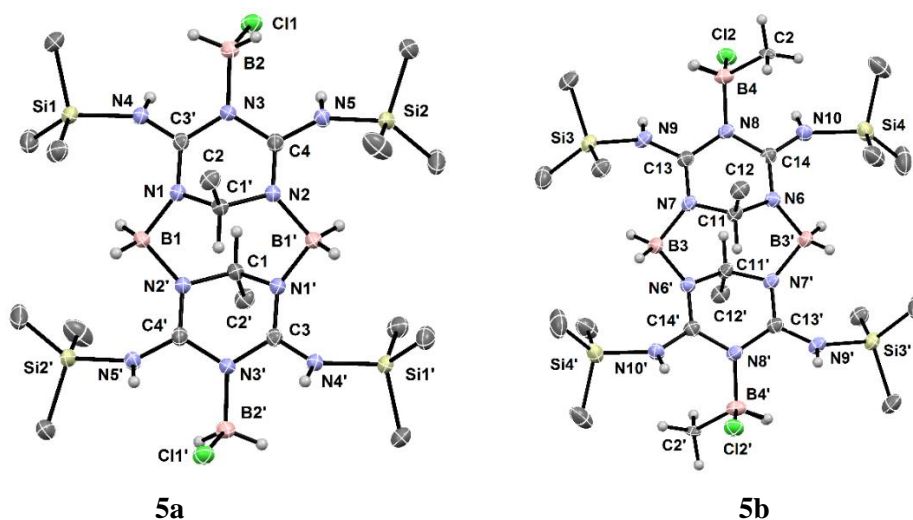


Figure. 2B.9. Single crystal X-ray structure of dimer (**5**), exhibiting both the molecules present in the asymmetric unit as [2,4-(NHSiMe₃)₂{CH(Me)C₂N₃}(μ-BH₂)₂·(BH₂Cl)₂ (**5a**) and [N,N'-2,4-(SiMe₃)₂{CH(Me)C₂N₃}(μ-BH₂)₂·(BHCIMe)₂ (**5b**); all hydrogen atoms except that on relevant C, N and B atoms have been omitted for clarity. Selected bond distances (Å) and angles (°): (**5a**) N1-C1 1.479(2), N2-C1 1.473(2), N1-C3 1.328(2), N2-C4 1.325(2), N1-B1 1.575(2), N2-B1 1.592(2), N3-C3 1.385(2), N3-C4 1.391(2), N3-B2 1.568(2), N4-C3 1.347(2), C1-C2 1.526(3), B2-C11 1.924(2); (**5b**) N6-C11 1.473(2), N7-C11 1.471(2), N6-C14 1.323(2), N7-C13 1.329(2), N6-B3 1.579(2), N7-B3 1.576(3), N8-C13 1.391(2), N8-C14 1.393(2), N8-B4 1.561(3), N9-C13 1.341(2), N10-C14 1.334(2); (**5a**) N1-C1-C2 112.24(14), N2-C1-N1 107.32(13), N2-C1-C2 113.33(14), C1-N1-B1 118.94(14), C3-N1-C1 113.02(14), C3-N1-B1 127.12(15), C1-N2-B1 121.03(14), C4-N2-C1 112.78(14), C4-N2-B1 123.95(15), N1-B1-N2 106.30(14), C3-N3-C4 116.87(14), C3-N3-B2 122.86(14); (**5b**) C11-N6-B3 119.84(14), C14-N6-C11 113.50(14), C14-N6-B3 124.86(16), C11-N7-B3 119.41(14), C13-N7-C11 113.68(15), C13-N7-B3 125.45(16), C13-N8-C14 116.80(14), C13-N8-B4 122.17(15).

All the boron centers are tetracoordinated, having distorted tetrahedral geometry. The reduction of the triazine ring was evident by the presence of tetracoordinated carbon centers (C1 and C11), where carbons attached with two N, H and methyl. The tetrahedral geometry and bond lengths 1.473(2), 1.471(2) Å for (N6-C11, N7-C11) and 1.479(2),

1.473(2) Å for (N1-C1, N2-C1) of the triazine ring have single bond character while the other bonds of triazine ring have bond lengths in the range of double bond 1.323(2)-1.391(2) Å, which confirms the partial reduction of triazine ring. The B–N bond lengths in the core are 1.575(2), 1.592(2), 1.579(2) and 1.576(3) Å for B1-N1, B1-N2, B3-N6, B3-N7). The B1-B1', C1-C1' distances are 4.273Å, 3.134 Å, similarly B3-B3', C11-C11' separation are 4.916Å, 3.097 Å.

2B.2.1 Computational study to understand the mechanism of dearomative hydroboration pathway

To understand the process during the dearomative hydroboration of triazine ring in **1** and **2**, the geometries of different intermediate steps during cyclization and the final trimers and dimers have been optimized, and their interaction energies have been calculated.. In order to comprehend the reaction mechanism further, detailed DFT calculations were performed using B3LYP (TZVP) functional with CPCM solvent model (toluene as solvent).^[23]

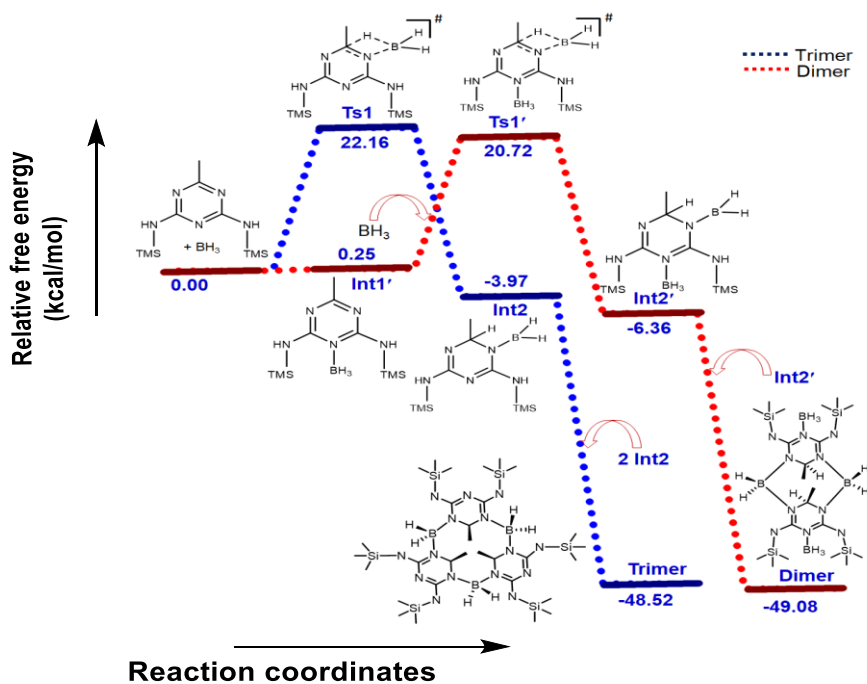


Figure. 2B.10. Energy profile diagram for the formation of trimer (**1**) and dimer (**2**) from BDMT.

The reaction has been initiated via direct hydroboration of BDMT with BH_3 through **TS1** with an activation energy barrier of 22.16 kcal/mol (Figure 2B.10). This energy value supports the spontaneity of the above reaction at room temperature only.^[20] In the next step, dearomatized **Int2** has formed via hydroboration of the triazine ring, which is found to be exergonic by 3.97 kcal/mol with respect to starting BDMT and BH_3 . Now via self-sorting of three molecules of **Int2** forms highly stable - BH_2 - bridged trimeric macrocycle **1** ($\Delta G = -48.52$ kcal/mol). While in the presence of two equivalents of borane, **Int1'** formed first, and then this intermediate underwent dearomative hydroboration reaction across the $\text{C}=\text{N}$ bond at 5,6 position of the triazine ring via **TS1'** with an activation energy barrier of 20.72 kcal/mol to give **Int2'** ($\Delta G = -6.36$ kcal/mol). In the next step, this dearomatized hydroborated **Int2'** ($\Delta G = -6.36$ kcal/mol) affords stable dimeric structure **2** via self-assembling of two units ($\Delta G = -49.08$ kcal/mol) having comparable energy as of trimer **1**. Hence, all these computationally derived results infer that the addition of B-H across the $\text{C}(6) = \text{N}(5)$ bond occurs in a concerted manner, which is analogous to B-C bond forming step in the hydroboration of alkene.^[20] Comparable energy of both the dimeric and trimeric units as well as their corresponding comparable activation energy barrier in rate determining steps support the experimentally obtained 1:1 product distribution.

2B.3 Conclusions

The work presents a modular approach for synthesizing boron containing macrocycles via self-sorting of reduced triazine ring at room temperature. Also, without any external catalyst, the dearomative hydroboration of a substituted triazine molecule was demonstrated for the first time. In this approach, the intermolecular $\text{N} \rightarrow \text{B}$ coordination was followed by the addition of B-H across the $-\text{C}=\text{N}-$ double bond at the 5,6 positions of the triazine ring leads to the dearomatization of the triazine ring and the reduced

triazine moieties were self-assembled to form the BH₂ bridged dimeric macrocycle. The 1:2 reaction of building block (triazine moiety) and reagent (borane) afforded a stable -BH₂- bridged dimeric macrocycle using this approach. The pathways involved in the dearomatization of triazine ring with BH₃ and different product distribution have also been supported by the DFT calculations.

2B.4 Experimental Section

2B.4.1 General procedure

All syntheses were carried out under an inert atmosphere of dinitrogen using standard Schlenk techniques or a glovebox where O₂ and H₂O levels were maintained usually below 0.1 ppm. All the glassware were dried at 150 °C in an oven for at least 12 h. Solvents were purified by MBRAUN solvent purification system MB SPS-800.

2B.4.2 Starting materials

All chemicals were purchased from Sigma-Aldrich and used without further purification. The starting materials, *bis*(trimethylsilyl)-N,N'-2,4-diamino-6-(Me)-triazine and *bis*(trimethylsilyl)-N,N'-2,4-diamino-triazine^[18] were prepared by following the reported procedures.

2B.4.3 Physical measurements

The ¹H, ¹³C{¹H}, and ¹¹B NMR spectra were recorded with a Bruker 400 MHz spectrometer with TMS and BF₃·OEt₂ respectively, as external references and chemical shifts were reported in ppm. High resolution mass spectra were recorded on a Waters SYNAPT G2-S instrument. IR spectra of the complexes were recorded in the range 4000–400 cm⁻¹ using a Perkin Elmer Lambda 35-spectrophotometer. The absorptions of the characteristic functional groups were only assigned and other absorptions

(moderate to very strong) were listed. Melting points were obtained in sealed capillaries on a Büchi B-540 melting point instrument.

Single crystal X-ray diffraction data of compounds **2-5** were collected using a Rigaku XtaLAB mini diffractometer equipped with Mercury 375M CCD detector. The data were collected with MoK α radiation ($\lambda = 0.71073 \text{ \AA}$) using omega scans. During the data collection, the detector distance was 49.9 mm (constant), and the detector was placed at $2\theta = 29.85^\circ$ (fixed) for all the data sets. The data collection and data reduction were done using Crystal Clear suite.^[21] All the crystal structures were solved through OLEX2 package using XT, and the structures were refined using XL. All non-hydrogen atoms were refined anisotropically. All figures were generated using Mercury 3.2.

2B.4.4 Synthetic procedure

Synthesis of the dimer, [2,4-(NHSiMe₃)₂{CH(Me)C₂N₃}(μ -BH₂)₂·(BH₃)₂ (2**):** BH₃·SMe₂ (0.8 mL, 7.44 mmol,) was added slowly to a stirred solution of BDMT (1.0 g, 3.72 mmol) in toluene (30 mL) at 0 °C. The reaction mixture was allowed to come to room temperature and stirred for 3 h. All volatiles were removed under vacuum to give a white solid. This solid was crystallized at -10 °C from pentane that afforded a mixture of **1** (50%) and **2** (50%). **NMR of 2:** ¹H NMR (400 MHz, CDCl₃): $\delta = 5.82$ (s, 4H, -NH), 4.33 (q, 2H, H-C(CH₃), ³J_{H-H} = 4 Hz), 2.80-1.87 (broad, 10H, -BH), 1.15 (d, 2H, H-C(CH₃), ³J_{H-H} = 4 Hz), 0.35 (s, 36H, -Si(CH₃)₃) ppm. ¹³C{¹H} NMR (100 MHz, CDCl₃): $\delta = 162.4$, 63.2 (H-C(CH₃)), 18.4 (H-C(CH₃)), 1.0 (-Si(CH₃)₃) ppm. ¹¹B NMR (128 MHz, CDCl₃): $\delta = -6.8$ (-BH₂), -23.4 (-BH₃) ppm. HRMS (AP⁺) *m/z* calcd for C₂₀H₅₈B₄N₁₀Si₄: 594.4313 [M]⁺; found: 594.4339 and *m/z* calcd for C₂₀H₅₃B₂N₁₀Si₄: 567.3727 [M-(2BH₃)+H]⁺; found: 567.3702.

Synthesis of bis(trimethylsilyl)-N,N'-2,4-diamino-1,3,5-triazine (BDT) (3): To a solution of 2,4-N,N'-diaminotriazine (0.04 mol, 4.5 g) in acetonitrile, triethylamine (22.0 mL, 0.16 mol) was added, then chlorotrimethylsilane (15.0 mL, 0.32 mol) was added dropwise at 0 °C results in a cloudy yellowish orange solution. The flask was removed from the ice bath and allowed to warm to room temperature and then refluxed for overnight at 85-90 °C under nitrogen atmosphere. All the volatiles were removed under vacuum, leaving an orange sticky solid. Further, the product was extracted in THF under nitrogen and washed with hexane/pentane to purify it. Yield 0.8 g, 7.8 %. ¹H NMR (400 MHz, CDCl₃): δ = 8.11 (s, 2H, CH₂), 4.93 (s, 2H, N-H) 0.28 (s, 36H, -Si(CH₃)₃) ppm. ¹³C{¹H} NMR (100 MHz, CDCl₃): δ = 168.2, 166.0, 0.3 (-Si(CH₃)₃) ppm. ²⁹Si NMR (79.5 MHz, CDCl₃): δ = 6.1 ppm. HRMS (AP+) *m/z* calcd. for C₉H₂₂N₂Si₂: 256.1414 [M+H]⁺; found: 256.1422.

Synthesis of the dimer, [2,4-(NHSiMe₃)₂{C₃N₃H₂}(μ-BH₂)]₂·(BH₃)₂ (4): BH₃·SMe₂ (7.5 mmol, 0.75 mL) was added slowly to a stirred solution of and *bis*(trimethylsilyl)-N,N'-2,4-diamino-1,3,5-triazine (BDT) (3) (3.0 mmol, 0.8 g,) in toluene (30 mL) at 0 °C. The reaction mixture was allowed to come to room temperature and stirred for 3 h. All the volatiles were removed under vacuum to give a white solid. This solid was crystallized at -10 °C from pentane. Yield 0.15 g, (17.0 %). Mp: 90-93 °C. IR (Nujol) *v*: 3484, 3371 (N-H), 2952, 2927, 2855, 2359, 2248 (B-H), 1632, 1460, 1380, 1246, 1166, 10533, 810, 726 cm⁻¹. ¹H NMR (400 MHz, CDCl₃): δ = 5.81 (s, 4H, -NH), 4.02 (d, 2H, H-C-H, ³J_{H-H} = 12 Hz), 3.94 (d, 2H, H-C-H, ³J_{H-H} = 12 Hz), 2.80-1.85 (broad, 10H, -BH), 0.36 (s, 36H, -Si(CH₃)₃) ppm; ¹³C{¹H} NMR (100 MHz, CDCl₃): δ = 163.4, 57.7 (H-C-H), 0.7 (-Si(CH₃)₃) ppm; ¹¹B NMR (128 MHz, CDCl₃): δ = -8.0 (-BH₂), -24.2 (-BH₃) ppm. HRMS (AP⁺) *m/z* calcd for C₁₈H₅₄B₄N₁₀Si₄: 566.4000 [M]⁺; found:

566.4026 and m/z calcd. for $C_{18}H_{49}B_2N_{10}Si_4$: 539.3414 $[M-(2BH_3)+H]^+$; found: 539.3437.

Synthesis of the dimer, [2,4-(SiMe₃)₂{CH(Me)C₂N₃}(μ-BH₂)₂·(BH₂Cl)₂ (5): BH₂Cl·SMe₂ (6.0 mmol, 0.6 mL) was added slowly to a stirred solution of BDMT (3.72 mmol, 1.0 g) in hexane/toluene (30 mL) at 0 °C. The reaction mixture was allowed to come to room temperature and stirred for 3 h. All volatiles were removed under vacuum to give a white solid. This solid was crystallized at -20 °C from pentane. Yield 0.2 g, (12.0 %). Mp: 110-113 °C. ¹H NMR (400 MHz, CDCl₃): δ = 5.89 (s, 4H, -NH), 4.32 (q, 2H, H-C(CH₃), ³J_{H-H} = 4 Hz), 3.17-2.84 (broad signal, 8H, BH), 1.19 (d, 6H, H-C(CH₃), ³J_{H-H} = 4 Hz), 0.35 (s, 36H, -Si(CH₃)₃) ppm; ¹³C{¹H} NMR (100 MHz, CDCl₃): δ = 162.2, 63.8 (H-C-Me), 16.2 (H-C(CH₃)), 0.5 (-Si(CH₃)₃) ppm; ¹¹B NMR (128 MHz, CDCl₃): δ = -7.5 (-BH₂) ppm. HRMS (AP+) m/z calcd. for $C_{20}H_{51}B_2N_{10}Si_4$: 565.3571 $[M-2BH_2Cl]^+$; found: 565.3542.

2B.5 Crystallographic Data

Table 2B.5.1. Crystallographic data for compounds 2 and 3.

Compound	2	3
Chemical formula	C ₁₀ H ₂₉ B ₂ N ₅ Si ₂	C ₉ H ₂₁ N ₅ Si ₂
molar mass	297.18	255.49
Crystal system	monoclinic	Tetragonal
Space group	<i>P</i> 2 ₁ / <i>c</i>	I-42d
<i>T</i> [K]	100(2)	100(2)
<i>a</i> [Å]	7.7951(5)	15.6433(15)
<i>b</i> [Å]	17.4706(13)	15.6433(15)
<i>c</i> [Å]	13.3888(6)	15.6433(15)
α [°]	90	90
β [°]	96.212(5)	90
γ [°]	90	90
<i>V</i> [Å ³]	1812.6(2)	2951.2(7)
<i>Z</i>	4	8
<i>D</i> (calcd.) [g·cm ⁻³]	1.089	1.150
μ (Mo-K α) [mm ⁻¹]	0.191	0.226
Reflections collected	15968	13089
Independent reflections	3204	2674
Data/restraints/parameters	3204/0/207	2674/12/80
<i>RI</i> , <i>wR</i> ₂ [<i>I</i> > 2 σ (<i>I</i>)] ^[a]	0.0798, 0.2019	0.0994, 0.2321
<i>RI</i> , <i>wR</i> ₂ (all data) ^[a]	0.1026, 0.2383	0.2008, 0.2885
GOF	1.079	0.953

[a] $RI = \sum ||Fo| - |Fc|| / \sum |Fo|$. $wR2 = [\sum w(|Fo^2| - |Fc^2|)^2 / \sum w|Fo^2|^2]^{1/2}$

Table 2B.5.2. Crystallographic data for compounds 4 and 5.

Compound	4	5
Chemical formula	C ₉ H ₂₇ B ₂ N ₅ Si ₂	C _{20.61} H _{57.23} B ₄ Cl ₂ N ₁₀ Si ₄
molar mass	283.15	671.87
Crystal system	monoclinic	Monoclinic
Space group	<i>P</i> 2 ₁ / <i>c</i>	<i>P</i> 2 ₁ / <i>c</i>
<i>T</i> [K]	100(2)	100(2)
<i>a</i> [Å]	6.8574(3)	10.1328(3)
<i>b</i> [Å]	18.7934(8)	16.1919(3)
<i>c</i> [Å]	13.1776(5)	23.5278(5)
α [°]	90	90
β [°]	99.246(4)	101.790(2)
γ [°]	90	90
<i>V</i> [Å ³]	1676.18(12)	3778.75(16)
<i>Z</i>	4	4
<i>D</i> (calcd.) [g·cm ⁻³]	1.122	1.181
μ (Mo-K α) [mm ⁻¹]	0.203	0.327
Reflections collected	19241	83488
Independent reflections	5908	13690
Data/restraints/parameters	5908 /0/170	13690/0/391
<i>RI</i> , <i>wR</i> ₂ [<i>I</i> >2 σ (<i>I</i>)] ^[a]	0.0501, 0.1310	0.0604, 0.1536
<i>RI</i> , <i>wR</i> ₂ (all data) ^[a]	0.0758, 0.1490	0.0950, 0.1805
GOF	1.052	1.097

[a] $RI = \Sigma||Fo| - |Fc||/\Sigma|Fo|$. $wR2 = [\Sigma w(|Fo^2| - |Fc^2|)^2/\Sigma w|Fo^2|^2]^{1/2}$

2B.6 References

1. (a) T. Eicher, and S. Hauptmann in *The Chemistry of Heterocycles-Structure, Reactions, Syntheses and Applications*, 2nd ed., Wiley-VCH, Weinheim, **2003**.
2. (a) B. D. Shaw, *J. Chem. Soc.*, **1925**, 215; (b) B. D. Shaw, *J. Chem. Soc.*, **1937**, 300; (c) S. Danishefsky, and A. Nagel, *Chem. Commun.*, **1972**, 373; (d) A. J. Birch, and E. A. Karakhanov, *Chem. Commun.*, **1975**, 480; (e) T. J. Donohoe, A. J. McRiner, and P. Sheldrake, *Org. Lett.*, **2000**, 2, 3861; (f) T. J. Donohoe, A. J. McRiner, M. Helliwell, and P. Sheldrake, *J. Chem. Soc. Perkin Trans. I*, **2001**, 1435; (g) G. W. Gribble, *Chem. Soc. Rev.*, **1998**, 27, 395; (h) M. R. Pitts, J. R. Harrison, and C. J. Moody, *J. Chem. Soc. Perkin Trans. I*, **2001**, 955; (i) P. N. Rylander, *Academic Press, New York*, **1979**; (j) *Handbook of Homogeneous Hydrogenation* (Eds.: J. G. de Vries, C. J. Elsevier), Wiley-VCH, Weinheim, **2007**; (k) D. S. Wang, Q. A. Chen, S. M. Lu, and Y. G. Zhou, *Chem. Rev.*, **2012**, 112, 2557; (l) L. Hounjet, D. W. Stephan, *Org. Process Res. Dev.*, **2014**, 18, 385; (m) Y. Liu, and H. Du, *J. Am. Chem. Soc.*, **2013**, 135, 12968; (n) M. Rueping, and A. P. Antonchick, *Angew. Chem. Int. Ed.*, **2007**, 46, 4562; *Angew. Chem.*, **2007**, 119, 4646.
3. (a) T. M. Krygowski, and M. K. Cryanski, *Chem. Rev.*, **2001**, 101, 1385; (b) A. T. Balaban, D. C. Oniciu, and A. R. Katritzky, *Chem. Rev.*, **2004**, 104, 2777; (c) A. R. Pape, K. P. Kaliappan, and E. P. Kgdig, *Chem. Rev.*, **2000**, 100, 2917
4. (a) P. G. Andersson, and I. J. Munslow, *Modern Reduction Methods*, Wiley, New York, **2008**; (b) B. Marciniec, *Chem. Rev.*, **2005**, 249, 2374; (c) K. Revunova, and G. I. Nikonov, *Dalton Trans.*, **2015**, 44, 840; (d) C. C. Chong, and R. Kinjo, *ACS Catal.*, **2015**, 5, 3238; (e) R. Lavilla, *J. Chem. Perkin Trans. I*, **2002**, 1141; (f) C. Cheng, and J. F. Hartwig, *Chem. Rev.*, **2015**, 115, 8946; (g) S. Park and S. Chang,

- Angew. Chem. Int. Ed.*, **2017**, *56*, 7720; (h) Sehoon Park, *ChemCatChem.*, **2020**, *12*, 3170.
5. (a) H. C Brown, and B. C. SubbaRao, *J. Am. Chem. Soc.*, **1956**, *78*, 5694; (b) M. Davidson, A. K. Hughes, T. B. Marder, and K. Wade; *Contemporary Boron Chemistry; Eds.; Royal Society of Chemistry: Cambridge, U.K.*, **2000**, 371; (c) A. Suzuki, *Angew. Chem., Int. Ed.*, **2011**, *50*, 6722.
6. (a) M. Arrowsmith, M. S. Hill, T. Hadlington, G. Kociok-Köhn, and C. Weetman, *Organometallics*, **2011**, *30*, 5556; (b) J. Intemann, M. Lutz, and S. Harder, *Organometallics*, **2014**, *33*, 5722; (c) D. Mukherjee, S. Shirase, T. P. Spaniol, K. Mashima, and J. Okuda, *Chem. Commun.*, **2016**, *52*, 13155; (d) P. Ji, T. Sawano, Z. Lin, A. Urban, D. Boures, and W. Lin, *J. Am. Chem. Soc.*, **2016**, *138*, 14860; (e) M. Rauch, S. Ruccolo, and G. Parkin, *J. Am. Chem. Soc.*, **2017**, *139*, 13264; (f) L. E. Lemmerz, T. P. Spaniol, and J. Okuda, *Dalton Trans.*, **2018**, *47*, 12553; (g) P. Eisenberger, A. M. Bailey, and C. M. Crudden, *J. Am. Chem. Soc.*, **2012**, *134*, 17384; (h) X. Fan, J. Zheng, Z. Hua Li, and H. Wang, *J. Am. Chem. Soc.*, **2015**, *137*, 4916; (i) Z.-Y. Liu, Z.-H. Wen, and X.-C. Wang, *Angew Chem Int Ed Engl.*, **2017**, *56*, 5817; (j) E. N. Keyzer, S. S. Kang, S. Hanf and D. S. Wright, *Chem. Commun.*, **2017**, *53*, 9434;
7. (a) Z. Nairoukh, M. Wollenburg, C. Schlepfforst, K. Bergander, and F. Glorius, *Nature Chem.*, **2019**, *11*, 264; (b) A. S. Dudnik, V. L. Weidner, A. Motta, M. Delferro, and T. J. Marks, *Nature Chem.*, **2014**, *6*, 1100; (c) A. Kaithal, B. Chatterjee, and C. Gunanathan, *Org. Lett.*, **2016**, *18*, 3402; (d) J. L. Lortie, T. Dudding, B. Gabidullin, and G. I. Nikonov, *ACS Catal.*, **2017**, *7*, 8454; (e) P. Ji, X. Feng, S. S. Veroneau, Y. Song, and W. Lin, *J. Am. Chem. Soc.*, **2017**, *139*, 15600; (f) F. Zhang, H. Song, X. Zhuang, C.-Ho Tung, and W. Wang, *J. Am.*

- Chem. Soc.*, **2017**, *139*, 17775; (g) S. R. Tamang, A. Singh, D. K. Unruh, and M. Findlater, *ACS Catal.*, **2018**, *8*, 6186; (h) X. Feng, Y. Song, J. S. Chen, Z. Li, E. Y. Chen, M. Kaufmann, C. Wang, and W. Lin, *Chem. Sci.*, **2019**, *10*, 2193.
8. (a) T. Hynes, E. N. Welsh, R. McDonald, M. J. Ferguson, and A. W. H. Speed, *Organometallics*, **2018**, *37*, 841; (b) B. Rao, C. C. Chong, and R. Kinjo, *J. Am. Chem. Soc.*, **2018**, *140*, 652; (c) E. Jeong, J. Heo, S. Park and S. Chang, *Chem. Eur. J.*, **2019**, *25*, 6320; (d) H. C. Brown, *Boranes in Organic Chemistry*; *Cornell University Press: Ithaca, NY*, **1972**; (e) P. R. Jones, *J. Org. Chem.*, **1972**, *37*, 1886.
9. (a) K. Oshima, T. Ohmura, and M. Suginome, *Chem. Commun.*, **2012**, *48*, 8571; (b) B.-X. Leong, J. Lee, Y. Li, M.-C. Yang, C.-K. Siu, M.-D. Su, and C. W. So, *J. Am. Chem. Soc.*, **2019**, *141*, 17629.
10. H. Liu, M. Khononov, and M. S. Eisen, *ACS Catal.*, **2018**, *8*, 3673.
11. (a) A. Nzila, *J. Antimicrob. Chemother.*, **2006**, *57*, 1043; (b) V. Francesconi, L. Giovannini, M. Santucci, E. Cichero, M. P. Costi, L. Naesens, F. Giordanetto, and Michele Tonelli, *European Journal of Medicinal Chemistry*, **2018**, *155*, 229; (c) M. Kidwai, P. Mothsra, R. Mohana, and S. Biswas, *Bioorg. Med. Chem. Lett.*, **2005**, *15*, 915; (d) N. P. Jensen, A. L. Ager, R.A. Bliss, C. J. Canfield, B. M. Kotecka, K.H. Rieckmann, J. Terpinski, and D. P. Jacobus, *J. Med. Chem.*, **2001**, *44*, 3925.
12. (a) N. Fujita, S. Shinkai, and T. D. James, *Chem. Asian J.*, **2008**, *3*, 1076; (b) V. Barba, P. Ramos, D. Jiménez, A. Rivera, and A. Meneses, *Inorganica Chimica Acta*, **2013**, *401*, 30; (c) A. González-Hernández, G. Serrano-Melgar, R. Villamil-Ramos, and V. Barba, *Heteroatom Chem.*, **2017**, *28*, 1; (d) V. Barba, R. Hernández, H. Höpfl, R. Santillan, and N. Farfan, *J. Organomet. Chem.*, **2009**, *694*, 2127; (e) V. Barba, and I. Betanzos, *J. Organomet. Chem.*, **2007**, *692*, 4903.

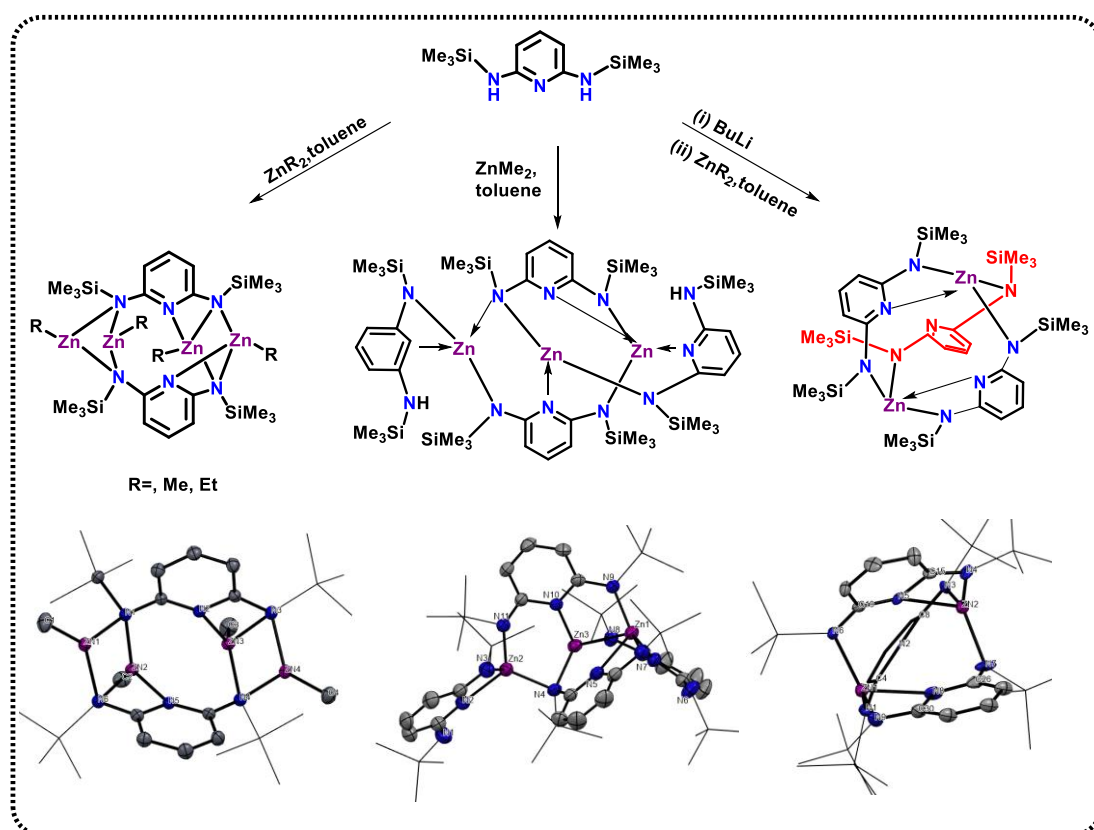
13. (a) F. García, A. D. Hopkins, R. A. Kowenicki, M. McPartlin, J. S. Silvia, J. M. Rawson, M. C. Rogers, and D. S. Wright, *Chem. Commun.*, **2007**, 586; (b) D. Salazar-Mendoza, J. Guerrero-Alvarez, and H. Höpfl, *Chem. Commun.*, **2008**, 6543; (c) J. Cruz-Huerta, D. Salazar-Mendoza, J. Hernández-Paredes, I. F. H. Ahuactzic, and H. Höpfl, *Chem. Commun.*, **2012**, 48, 4241; (d) A. Widera, E. Filbeck, H. Wadepohl, E. Kaifer, and H. J. Himmel, *Chem. Eur. J.*, **2020**, 26, 3435; (e) B. Icli, E. Sheepwash, T. Riis-Johannessen, K. Schenk, Y. Filinchuk, R. Scopelliti, and K. Severin, *Chem. Sci.*, **2011**, 2, 1719; (f) (h) D. Salazar-Mendoza, J. Cruz-Huerta, H. Höpfl, I. F. Hernández-Ahuactzi, and M. Sanchez, *Cryst. Growth Des.*, **2013**, 13, 2441; (g) S. Wakabayashi, M. Kuse, A. Kida, S. Komeda, K. Tatsumic, and Y. Sugiharad, *Org. Biomol. Chem.*, **2014**, 12, 5382.
14. (a) W. Iwanek, A. Iwanek, K. Woźniak, and M. Malińska, *Tetrahedron Lett.*, **2012**, 53, 4526; (b) M. Yalpani, R. Boese, and R. Koster, *Chem. Ber.*, **1990**, 123, 1275; (c) M. Yalpani, R. Koster, and R. Boese, *Chem. Ber.*, **1991**, 124, 1699.
15. (a) D. Bawari, C. Negi, K. Jaiswal, B. Prashanth, A. R. Choudhury, and S. Singh, *Chem. Commun.*, **2018**, 54, 8857; (b) D. Bawari, C. Negi, V. K. Porwal, S. Ravi, K. R. Shamasundar, and S. Singh, *Dalton Trans.*, **2019**, 48, 7442; (c) “New Molecular Topologies from Main Group Elements: P/N, B/N and Al/N Containing Macrocycles and Pyridinophanes”, D. Bawari, **2018**, *Ph.D. Thesis*, IISER Mohali, India.
16. (a) S. Trofimenko, *J. Am. Chem. Soc.*, **1967**, 89, 4948; (b) S. Trofimenko, *J. Am. Chem. Soc.*, **1967**, 3165; (c) M. A. Tehfe, S. Schweizer, A.-C. Chany, C. Ysacco, J.-L. Clément, D. Giges, F. Morlet-Savary, J.-P. Fouassier, M. Neuburger, T. Tschamber, N. Blanchard, and J. Lalevéé, *Chem. Eur. J.*, **2014**, 20, 5054.

17. (a) A. Weiss, H. Pritzkow, and W. Siebert, *Angew. Chem. Int. Ed.*, **2000**, *39*, 547; (b) A. Weiss, V. Barba, H. Pritzkow, and W. Siebert, *J. Organomet. Chem.*, **2003**, *680*, 294; (c) H. M. Bass, S. A. Cramer, A. S. McCullough, K. J. Bernstein, C. R. Murdock, and D. M. Jenkins, *Organometallics*, **2013**, *32*, 2160.
18. B. Parker, and D. Y. Son, *Inorg. Chem. Commun.*, **2002**, *5*, 516.
19. (a) J. V. B. Kanth, and H. C. Brown, *J. Org. Chem.*, **2001**, *66*, 5359; (b) H. C. Brown, and N. Ravindran, *Inorganic Chemistry*, **1977**, *16*, 2938.
20. (a) C. Remenyi, and M. Kaupp, *J. Am. Chem. Soc.*, **2005**, *127*, 11399; (b) J. L. Boyer, J. Rochford, M. K. Tsai, J. T. Muckerman, and E. Fujita, *Coord. Chem. Rev.*, **2010**, *254*, 309; (c) J. Rochford, M. K. Tsai, D. J. Szalda, J. L. Boyer, J. T. Muckerman, and E. Fujita, *Inorg. Chem.*, **2010**, *49*, 860; (d) I. V. Rostov, R. D. Amos, R. Kobayashi, G. Scalmani, and M. J. J. Frisch, *Phys. Chem. B.*, **2010**, *114*, 5547; (e) D. Jacquemin, C. Michaux, E. A. Perpète, F. Maurel, and A. Perrier, *Chem. Phys. Lett.*, **2010**, *488*, 193; (f) M. M. Mikolajczyk, R. Zalesny, Z. Czyznikowska, P. Toman, J. Leszczynski, and W. J. Bartkowiak, *Mol. Model.*, **2011**, *17*, 2143.
21. (a) CrystalClear 2.0; Rigaku Corporation: Tokyo, Japan, **2013**. (b) O. V. Dolomanov, L. J. Bourhis, R. J. Gildea, J. A. K. Howard, and H. J. Puschmann, *Appl. Crystallogr.*, **2009**, *42*, 339; (c) G. M. Sheldrick, *Acta Cryst. A*, **2015**, *71*, 3. (d) G. M. Sheldrick, *Acta Cryst. A.*, **2008**, *64*, 112; (e) G. M. Sheldrick, *Acta Cryst. A.*, **2015**, *71*, 3.

Chapter 3

Modular Approach to Macrocycles and Cluster Topologies

Assembled Around Zinc Centers



C. Negi, M. Goyal, S. Singh*; Modular approach to macrocycles and cluster topologies assembled around zinc centers, *Unpublished results*.

Abstract

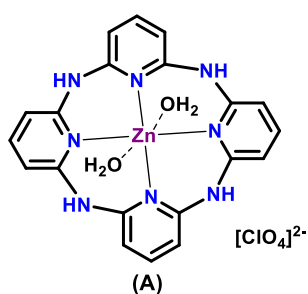
This chapter of the thesis presents the first report of targeted synthesis of zinc containing pyridinophanes by the condensation reaction of bis(trimethylsilyl)-N,N'-2,6-diaminopyridine (bap) with organozinc and zinc halides. In the present approach, zinc plays a key role in successfully assembling the macrocycle by providing a template where zinc is a constituent member of the cyclic core and, unlike in previous attempts, where Zn coordinates within the multidentate cavity of a pre-assembled macrocyclic framework. Further, by varying the relative stoichiometry of the building block bap and zinc reagents, different molecular entities (mononuclear, dinuclear, trinuclear, and tetranuclear complexes) containing zinc centers have been synthesized. The 1:1 reaction of bap with ZnMe₂/ZnEt₂ leads to the formation of dinuclear zinc complexes [$\{2-(\text{Me}_3\text{SiN})-6-(\text{Me}_3\text{SiNH})\text{C}_5\text{H}_3\text{N}\}(\text{ZnMe})\}_2$ (1) and [$\{2-(\text{Me}_3\text{SiN})-6-(\text{Me}_3\text{SiNH})\text{C}_5\text{H}_3\text{N}\}(\text{ZnEt})\}_2$ (2) respectively, which further converted to pyridinophanes [$\{2,6-(\text{Me}_3\text{SiN})_2\text{C}_5\text{H}_3\text{N}\}_2(\text{ZnMe})_4$] (3) and [$\{2,6-(\text{Me}_3\text{SiN})_2\text{C}_5\text{H}_3\text{N}\}_2(\text{ZnEt})_4$] (4) by addition of another equivalent of the respective zinc reagents. Trinuclear bowl-shaped zinc macrocycle **6**, the mononuclear zinc compound **7** and dinuclear complex **8** have been afforded by varying the relative stoichiometry. The bicyclic pyridinophane, [$\{2,6-(\text{Me}_3\text{SiN})_2\text{C}_5\text{H}_3\text{N}\}_3\text{Zn}_2$] (9) was obtained by the reaction of zinc halides (ZnCl₂/ZnI₂) with dilithiated N,N'-2,6-diamidopyridine. All new compounds have been characterized using multinuclear NMR, HRMS, and single crystal X-ray diffraction.

3.1 Introduction

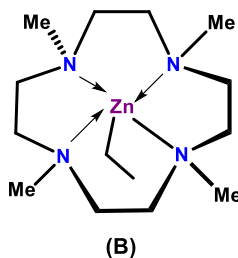
In the last decade, there has been a significant interest in zinc chemistry. The abundance of zinc is 70 mg/kg on the earth's crust and 0.004.9 mg/L in sea water near the surface.^[1] It is an indispensable trace element of the human body present in active sites of various enzymes like metallothionein, carboxypeptidase A, carbonic anhydrase, α_2 -macroglobulin, leucine aminopeptidase, etc. Most of the zinc ions in biological systems are tightly bound to proteins for structural and catalytic functions and play a vital role in more than 300 enzymatic processes.^[2] There are several reports on zinc as an active organometallic reagent for various syntheses, and their coordination complexes exhibit wide structural diversity and possess a wide range of applications in various ring opening polymerization (ROP) of cyclic esters, copolymerization of epoxides and carbon dioxide.^[2] They serve as a versatile and convenient tool for numerous biological applications, including bioimaging, molecular recognition, highly active and selective catalysts, and in material science.^[2,3]

Several N,N'-chelating organic ligands including β -diketiminato, guanidinate and amidinate anions are well known in coordination chemistry and have been investigated intensely in both main group and transition metals. The steric and electronic properties of these N,N'-chelating substituents can be modified by varying the substituents present on the nitrogen atoms, which alters the chemical properties of metal complexes and confers the diverse advancement in inorganic chemistry. Numerous N,N'-chelate zinc complexes and metallacycles have been reported by various research groups, including mono, binuclear chelated complexes, and pincer complexes containing four, five and six membered chelate rings.^[2-6] Since macrocycles are appealing multidentate ligands, the chemistry of macrocycles coordinating zinc has been studied (A-C) (Figure 3.1), but those macrocyclic frameworks are rare where zinc atom

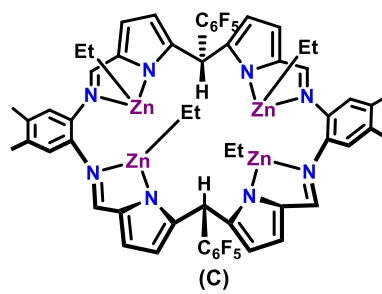
I Macrocyclic systems as a multidentate ligands coordinating zinc ions



Zn(II) complex of (NH)₄-bridged calix[4] pyridine (Wang and co-workers)

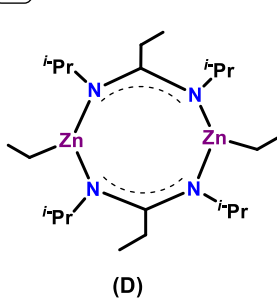


Zn-Et Complex Supported by tetramethyltetraazacyclododecane Ligand (Maron, Okuda and co-workers)

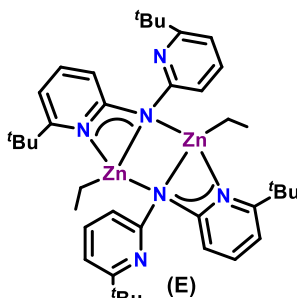


Tetranuclear Zn Complex of the Schiff-Base pyrrole macrocycles (Williams, love and co-workers)

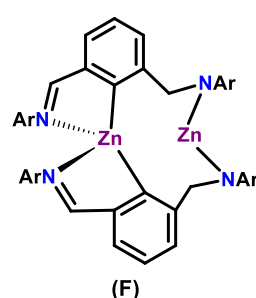
II Zinc based dimeric complexes and macrocyclic frameworks



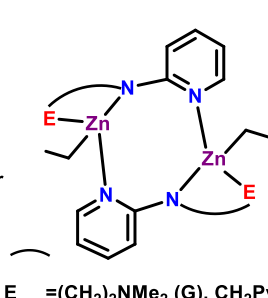
Zn-Et bridged dimeric cycle based on amidinate ligand (Schulz and co-workers)



Dimeric amidinate chelated complex forming Zn₂N₂ ring (Carpentier and co-workers)

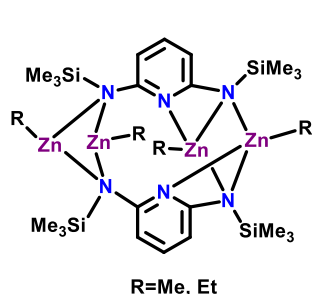


Dimeric cycle zinc complex having pincer ligand (Nikonov and co-workers)

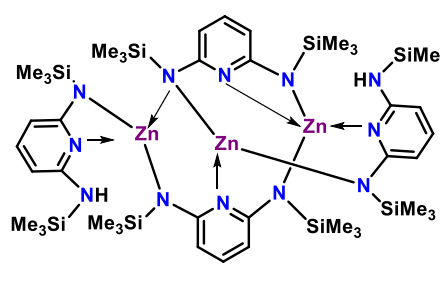
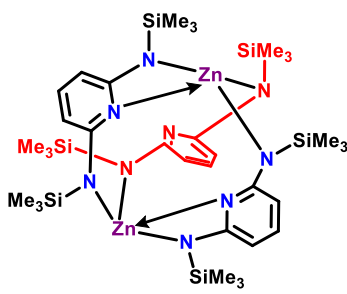


E = (CH₂)₂NMe₂ (G), CH₂Py (H)
Zn-Et bridged cyclic complex containing amidopyridinate ligands (Chen and co-workers)

III This work: Zinc bridged [3.3](2,6)pyridinophanes and a bowl shaped zinc cluster



Zinc-amide bridged [3.3](2,6)pyridinophane and bicyclic pyridinophane



Zinc-amide bridged bowl shaped pyridinophane

Figure 3.1. Examples of zinc based: (I) macrocyclic ligand systems coordinating zinc ion in cavity; (II) dimeric complexes and macrocycles; (III) this work: zinc bridged [3.3](2,6)pyridinophane, bicyclic pyridinophane and a bowl-shaped trinuclear zinc cluster.

is a constituent member of cyclic core i.e., use of zinc to assemble macrocyclic systems are less investigated. The tailoring of macrocyclic framework depends on the pre-organized orientation, i.e. the proper placement of reacting groups in the building block and the wise choice of reaction strategy. With this scenario, 2,6-disubstituted pyridine

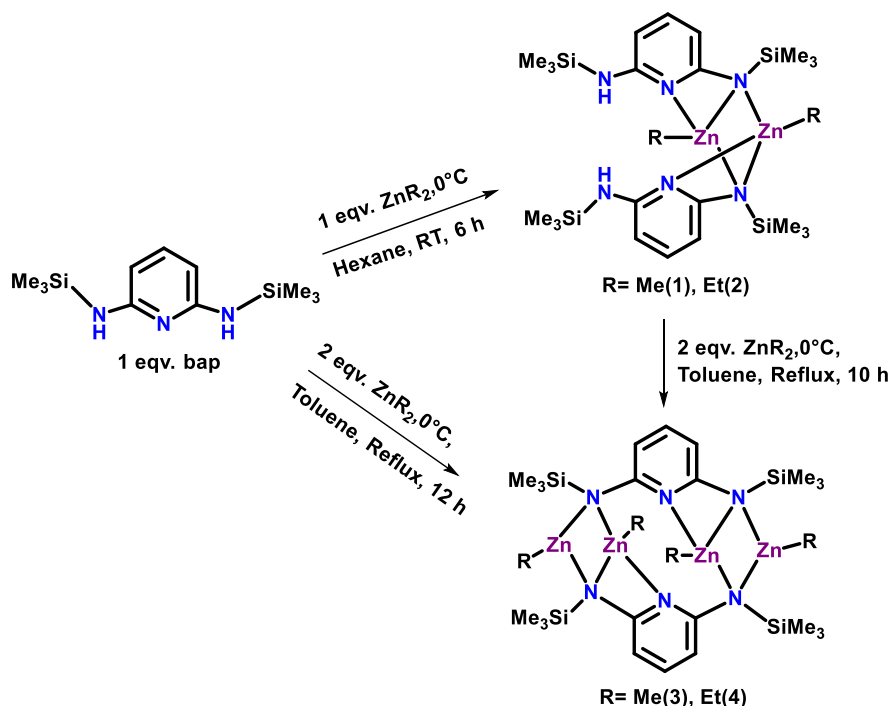
units with amine functionality [Py(NR)₂] appear to be a promising candidate, exhibiting the desired orientation of coordinating group (NR) with a rigid pyridine skeleton for assembling the macrocyclic structure.

Schulz group in 2008 reported the reaction of ZnEt₂ with *bis*(isopropyl)carbodiimide undergoes the insertion reaction to give cyclic dimeric zinc amidinate complex [EtC(N^{*i*}Pr)₂ZnEt]₂ containing eight atoms in cyclic core (**D**). Carpentier and co-workers afforded the dimeric amidinate chelated complex bridged via zinc atom forming four-membered Zn₂N₂ ring (**E**).^[7] In 2018, Nikonov and co-workers reported the zinc complex supported by pincer ligand, which rearranges at room temperature into the ten-membered binuclear zinc species (**F**).^[8] In 2019, Chen and co-workers assembled zinc bridged dimeric macrocycles (**G**) and (**H**) supported by amidopyridinate ligand system (Figure 2.1). The macrocyclic framework (**G**) and (**H**) show distorted tetrahedron geometry around the zinc center. Further, the activity of these complexes for the ROP of L-lactide and ϵ -caprolactone using benzyl alcohol as the initiation reagent was also demonstrated.^[9]

Previously, we reported on several aluminum containing complexes and pyridinophanes involving donor-acceptor (Npy-Al) interactions.^[15-17] Herein, utilizing similar strategy we have synthesized some zinc containing macrocycles by varying the relative stoichiometry of bap and ZnMe₂/ZnEt₂ as the first examples of organozinc bridged tetranuclear neutral pyridinophanes [{2,6-(Me₃SiN)₂C₅H₃N}(ZnR)₂]₂ (R= Me, Et) and trinuclear bowl shaped zinc cluster [{2-(Me₃SiN)-6-(Me₃SiNH)C₅H₃N}₂ {2,6-(Me₃SiN)₂C₅H₃N}₂ Zn₃] (**6**). The bicyclic pyridinophane, [{2,6-(Me₃SiN)₂C₅H₃N}₃Zn₂] (**9**) was obtained by the reaction of zinc halides (ZnCl₂/ZnI₂) with dilithiated N,N'-2,6-diamidopyridine.

3.2 Results and Discussion

The 1:1 stoichiometric reaction between bis(trimethylsilyl)-N,N'-2,6-diamidopyridine (bap) and ZnMe_2 at room temperature was expected to yield a symmetrical zinc bridged pyridinophane, $[\{2,6-(\text{Me}_3\text{SiN})_2\text{C}_5\text{H}_3\text{N}\}_2(\text{ZnMe})_2]$ like in the case of boron and aluminum (chapter 2A, Figure 2A.4).^[13] Rather in this case a dinuclear zinc methyl bridged complex $[\{2-(\text{Me}_3\text{SiN})-6-(\text{Me}_3\text{SiNH})\text{C}_5\text{H}_3\text{N}\}(\text{ZnMe})_2]$ (**1**) obtained (Scheme 3.1). The signal in the HRMS spectrum of **1** at $m/z = 665.1815$ (calcd. 665.1809 for $\text{C}_{24}\text{H}_{51}\text{Zn}_2\text{N}_6\text{Si}_4$), for $[\text{M}+\text{H}]^+$ indicates the formation of a dinuclear zinc methyl complex. The presence of methyl group on the zinc center was seen as a singlet at -0.68 ppm in its ^1H NMR spectrum, and the corresponding carbon signal appeared at -0.34 ppm in its $^{13}\text{C}\{^1\text{H}\}$ NMR spectrum.



Scheme 3.1. Syntheses of dinuclear zinc complexes, $[\{2-(\text{Me}_3\text{SiN})-6-(\text{Me}_3\text{SiNH})\text{C}_5\text{H}_3\text{N}\}(\text{ZnMe})_2]$ (**1**), $[\{2-(\text{Me}_3\text{SiN})-6-(\text{Me}_3\text{SiNH})\text{C}_5\text{H}_3\text{N}\}(\text{ZnEt})_2]$ (**2**), tetranuclear zinc [3.3](2,6)pyridinophanes $[\{2,6-(\text{Me}_3\text{SiN})_2\text{C}_5\text{H}_3\text{N}\}(\text{ZnMe})_2]_2$ (**3**) and $[\{2,6-(\text{Me}_3\text{SiN})_2\text{C}_5\text{H}_3\text{N}\}(\text{ZnEt})_2]_2$ (**4**).

Two equal intensity doublets in the aromatic region at 5.98 and 5.69 ppm and different sets of signals for SiMe_3 groups in ^1H (0.19 and 0.16 ppm each for 18H), $^{13}\text{C}\{^1\text{H}\}$ and ^{29}Si NMR spectra gave an indication of an asymmetric disposition of the ligand units around Zn centers in such a way that both the Zn centers are still symmetric with respect to each other. The signal at 3.24 ppm corresponding to N-H in the ^1H NMR spectrum indicates the presence of one unreacted NHSiMe_3 group per bap unit. Later single crystal X-ray diffraction analysis confirmed the dinuclear zinc methyl complex as speculated based on the NMR data, where two zinc centers bridging two bap units through $\text{N}_{\text{py}}\text{-Zn(Me)-N}_{\text{py}}$ while leaving another NHSiMe_3 of bap unreacted (Figure 3.2).

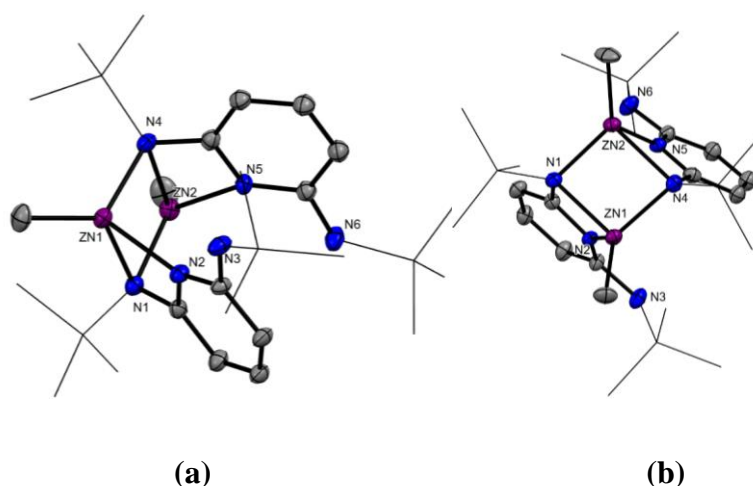


Figure 3.2. Solid-state structure of dinuclear zinc complex $[\{2\text{-(Me}_3\text{SiN)-6-(Me}_3\text{SiNH)C}_5\text{H}_3\text{N}\}(\text{ZnMe})_2$ (**1**); **(a)** Front view showing parallel orient of pyridine units and two four membered chelated rings $[\text{N}_2\text{ZnC}]$ and showing $\text{N}_{\text{py}}\text{-Zn}$ interaction; **(b)** side view showing four membered $[\text{N}_2\text{Zn}_2]$ ring; All hydrogen atoms have been omitted for clarity. Selected bond lengths [\AA] and bond angles [$^\circ$]: Zn1-Zn2 2.9156(10), Zn1-N1 2.193(5), Zn1-N2 2.103(5), Zn1-N4 2.068(5), Zn1-C4 2.595(6), Zn1-C23 1.970(7), Zn2-N1 2.074(5), Zn2-N4 2.221(5), Zn2-N5 2.118(5), Zn2-C24 1.962(7), N1-C4 1.399(8), N2-C4 1.362(8), N2-C8 1.346(8), N3-C8 1.405(8); N1 Zn1 C4 32.63(19), N2-Zn1-N1 64.04(18), N4-Zn1-N1 94.3(2), N4-Zn1-N2 101.6(2), N4-Zn1-C4 101.5(2), C23-Zn1-N1 125.9(3), C23-Zn1-N2 125.1(3), C23-Zn1-N4 127.2(3), C23-Zn1-C4 131.1(3), N1-Zn2-N4 93.3(2), N1-Zn2-N5 100.1(2), N5-Zn2-N4 63.91(19), C24-Zn2-N1 127.6(3), C24-Zn2-N4 126.3(4), C24-Zn2-N5 126.2(3).

The dinuclear zinc complex **1** crystallized in the orthorhombic system with $P2_12_12_1$ space group. The single crystal X-ray structure showed that zinc atoms are tetracoordinated and have a distorted tetrahedral geometry, where zinc is bonded to three nitrogen and one methyl group. This structure consists of two parallel four-membered $[N_2CZn]$ rings where pyridyl and amino sites of bap bind to zinc centers. The two zinc and amino nitrogen atoms form a four-membered ring N_2Zn_2 $[Zn1N1Zn2N4]$, as illustrated in Figure 3.2.

Similarly, the reaction of bap with diethylzinc was also performed, and similar observations were spotted. The 1:1 stoichiometric reaction of bap and $ZnEt_2$ was performed at room temperature. The presence of ethyl group on the zinc center was seen as a triplet (1.66 ppm, CH_3CH_2-) and a quartet (0.80 ppm, CH_3CH_2-) in its 1H NMR spectrum, and the corresponding carbon signals appeared at 13.73 and 1.42 ppm in its $^{13}C\{^1H\}$ NMR spectrum. Further, only one triplet at 6.85 ppm and two equal intensity doublets in the aromatic region at 6.06 and 5.56 ppm in 1H NMR and different sets of signals for $SiMe_3$ groups in 1H , $^{13}C\{^1H\}$ and ^{29}Si NMR spectra indicated unsymmetrical linkage of bap unit with zinc. The signal at 3.45 ppm in the 1H NMR spectrum and the IR spectrum showed -NH stretch at 3382 cm^{-1} indicating the presence of NH group. The signal in the HRMS spectrum at $m/z = 692.2047$ (calcd. 692.2045) for $[M]^+$ also supports the dinuclear zinc ethyl complex. Later, the X-ray diffraction analysis confirmed the solid-state structure of **2** where both the zinc coordinated with only one NH of each bap unit, leaving another NH unreacted with the molecular composition $[\{2-(Me_3SiN)-6-(Me_3SiNH)C_5H_3N\}(ZnEt)]_2$ (**2**) (Figure 3.3).

Dinuclear zinc complex **2** crystallized in the orthorhombic system with $Pna2_1$ space group. The single crystal X-ray structure shows that zinc atoms are tetracoordinated and have a distorted tetrahedral geometry. This structure consists of

two four-membered $[N_2CZn]$ rings where pyridyl and amino sites of bap bind to the zinc center. Two zinc atoms and two amino nitrogen atoms of bap form a four-membered ring N_2Zn_2 $[Zn_1N_3Zn_2N_4]$, illustrated in Figure 3.3.

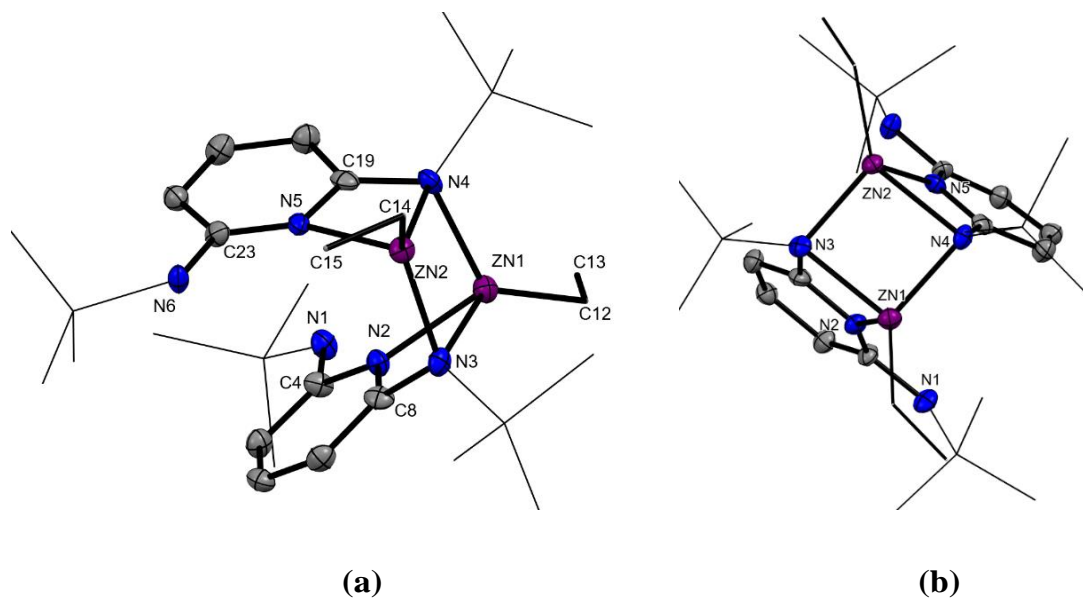


Figure 3.3. Solid-state structure of dinuclear zinc complex $[\{2-(Me_3SiN)-6-(Me_3SiNH)C_5H_3N\}(ZnEt)_2$ (**2**); (a) view showing parallel orient of pyridine units and Zn-ethyl groups and two four-membered chelated rings showing $N_{py}\text{-Zn}$ interaction $[N_2ZnC]$; (b) side view showing four-membered $[N_2Zn_2]$ ring; All hydrogen atoms have been omitted for clarity. Selected bond lengths [Å] and bond angles [°]: Zn2-Zn1 2.9501(13), Zn2-N5 2.122(6), Zn1-N3 2.235(7), Zn1-N4 2.063(7), Zn2-N3 2.060(6), Zn2-N4 2.199(7), Zn1-N2 2.117(7), Zn2-C14 1.987(8), Zn1-C12 1.976(11), Zn1-C12 1.976(11); N3-Zn2-N5 99.9(2), N3-Zn2-N4 92.9(3), N3-Zn2-C19 99.5(2), N4-Zn1-N2 99.8(3), N4-Zn1-N3 91.8(2), N5-C19-N4 113.8(7), N2-C8-N3 112.0(7)

In order to synthesize the full cyclic zinc pyridinophane, two more equivalents of dimethylzinc were added to **1** at 0 °C in toluene, and the reaction was refluxed for another 10 hours. The colourless solution changed to yellowish, which after workup gave a white fluffy compound whose composition was established as $[\{2,6-(Me_3SiN)_2C_5H_3N\}(ZnMe)_2\}_2$ (**3**) (Scheme 3.1). Alternatively, one-pot synthesis was also performed, based on the above reaction stoichiometry and solid state X-ray

structure of **1**, the relative stoichiometric of *bap* and ZnMe_2 taken as 1:2 in toluene and reflux for 12 hours afforded the tetranuclear zinc [3.3](2,6)pyridinophane, $[\{2,6\text{-(Me}_3\text{SiN)}_2\text{C}_5\text{H}_3\text{N}\}(\text{ZnMe})_2]_2$ (**3**). The presence of four methyl groups on the zinc center in **3** was seen as a singlet at -0.37 ppm in its ^1H NMR spectrum, and the corresponding carbon signal appeared at -0.68 ppm in its $^{13}\text{C}\{^1\text{H}\}$ NMR spectrum. Signals in ^1H NMR (at 0.19 ppm), $^{13}\text{C}\{^1\text{H}\}$ NMR (at 1.27 ppm), and ^{29}Si NMR (at 3.65 ppm) spectra of **3** were attributed to four chemically equivalent SiMe_3 groups. The absence of the signal for *-NH* in the ^1H NMR spectrum and N-H stretching frequency in IR are indicative of complete deprotonation of NHSiMe_3 .

The solid-state structure of **3** as tetranuclear zinc pyridinophane was confirmed by the single crystal X-ray diffraction analysis (Figure 3.4). Tetranuclear zinc pyridinophane **3** crystallized in the monoclinic system with $P2_1/c$ space group. The single crystal X-ray structure showed that all zinc atoms are tetracoordinated (three nitrogen atoms and one methyl group), having distorted tetrahedral geometry. This structure consists of two four-membered $[\text{N}_2\text{Zn}_2]$ rings bridging two pyridine units in nearly *syn* orientation. The pyridinophane is composed of twelve atoms in a cyclic core $\text{Zn}_2\text{C}_4\text{N}_6$, and two four-membered rings $[\text{CN}_2\text{Zn}]$ on the diagonally opposite side of the central core ring formed *via* amidinate linkage by engaging the pyridine nitrogen $\text{N}\rightarrow\text{Zn}$ (Figure 3.4).

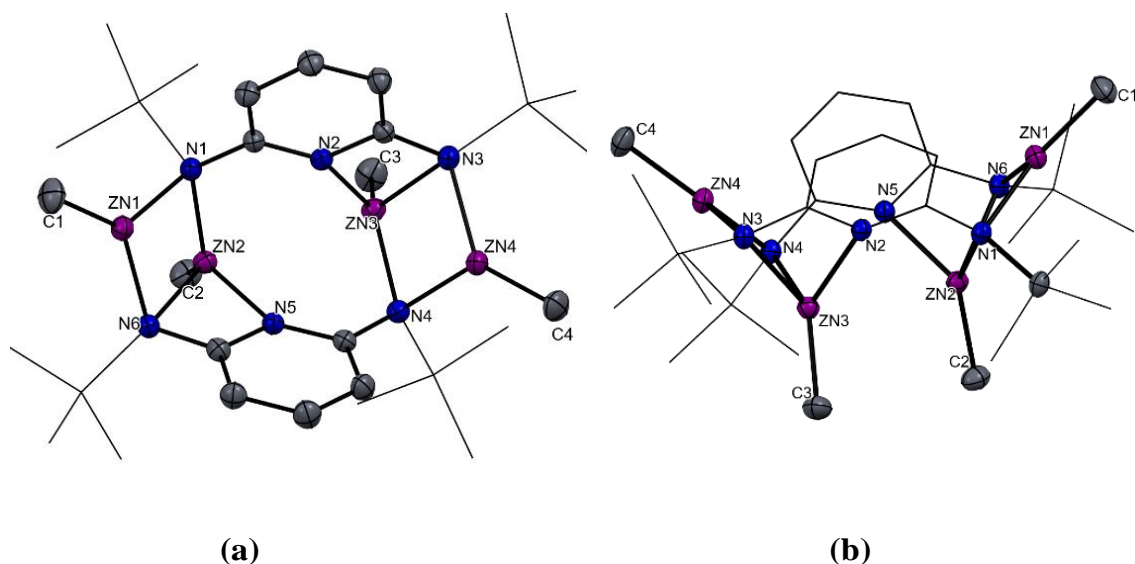


Figure 3.4. Solid-state structure of tetranuclear zinc [3.3](2,6)pyridinophane **3**; (a) Front view showing twelve membered pyridinophane and two four-membered chelated rings [N₂ZnC] having N_{py}-Zn interaction and two four-membered rings [Zn₂N₂]; (b) side view showing *syn* orientation of pyridine rings and *cis* orientation of methyl groups; All hydrogen atoms have been omitted for clarity. Selected bond lengths [Å] and bond angles [°]: Zn1-Zn2 2.9594(5), Zn1-N1 2.081(2), Zn1-N6 2.012(2), Zn1-C1 1.952(4), Zn2-N1 2.090(2), Zn2-N5 2.092(2), Zn2-N6 2.281(3), Zn2-C2 1.976(3), Zn3-Zn4 2.9352(5), Zn3-N2 2.089(2), Zn3-N3 2.305(3); N6-Zn1-N1 94.07(10), C1-Zn1-Zn2 167.16(13), C1-Zn1-N1 131.56(15), C1-Zn1-N6 134.15(15), N1-Zn2-N5 99.04(9), N1-Zn2-N6 86.40(9), N5-Zn2-N6 63.30(9), C2-Zn2-N1 129.09(12), C2-Zn2-N5 129.42(12).

Learning from the above observations for the conversion of **1** to **3**, analogously to synthesize full pyridinophane from **2**, two more equivalents of diethylzinc were added to **2** at 0 °C, and the reaction mixture was set to reflux for another 10 h. The colourless reaction mixture changed to neon green, which gave a fluffy compound after workup. Alternatively, the 1:2 reaction of bap and ZnEt₂ was performed in toluene at 0 °C (Scheme 3.1), and after achieving room temperature the reaction was refluxed for

another 12 h, which resulted in the change of colourless solution to neon green. After evaporating all volatiles, a fluffy compound was obtained which was further crystallized from dry pentane at $-20\text{ }^{\circ}\text{C}$ to afford colourless crystals of tetranuclear zinc [3.3](2,6)pyridinophane (**4**) (Scheme 3.1). The absence of N-H stretching in IR as well as the absence of signal in ^1H NMR spectra of **4** corroborates the complete deprotonation of all HNSiMe_3 groups with the liberation of ethane gas. The triplet at 1.63 ppm, CH_3CH_2 - and quartet at 0.87 ppm, CH_3CH_2 - in the ^1H NMR spectrum and the corresponding carbon signals appeared at 13.21 and 4.13 ppm in its $^{13}\text{C}\{^1\text{H}\}$ NMR spectrum indicates the presence of ethyl groups on the zinc centers. The single peak in ^1H NMR (0.28 ppm), $^{13}\text{C}\{^1\text{H}\}$ NMR (1.07 ppm), and ^{29}Si NMR (6.61 ppm) spectra for SiMe_3 of **4** specify the chemically equivalent environment of four SiMe_3 groups. The formation of **4** as tetranuclear zinc was confirmed by the single crystal X-ray diffraction analysis shown in Figure 3.5, where two bap units were bridged *via* zinc atoms and the composition was also supported by HRMS signal at $m/z = 882.1393$ (calcd. 882.1367) for $[\text{M}+2\text{H}]^+$.

Tetranuclear zinc pyridinophane **4** crystallized in the monoclinic system with $I2/a$ space group. The single crystal X-ray structure showed that all zinc atoms are tetracoordinated (three nitrogen atoms and one methyl group), having distorted tetrahedral geometry. This structure consists of two four-membered $[\text{N}_2\text{Zn}_2]$ rings bridging the two pyridine units in *syn* fashion. The pyridinophane contains twelve atoms $\text{Zn}_2\text{C}_4\text{N}_6$ in cyclic core and two four-membered rings $[\text{CN}_2\text{Zn}]$ on diagonally opposite sides of the central core ring formed through amidinate linkage by engaging the pyridine ring nitrogen, illustrated in Figure 3.5 (Table 3.5.2).

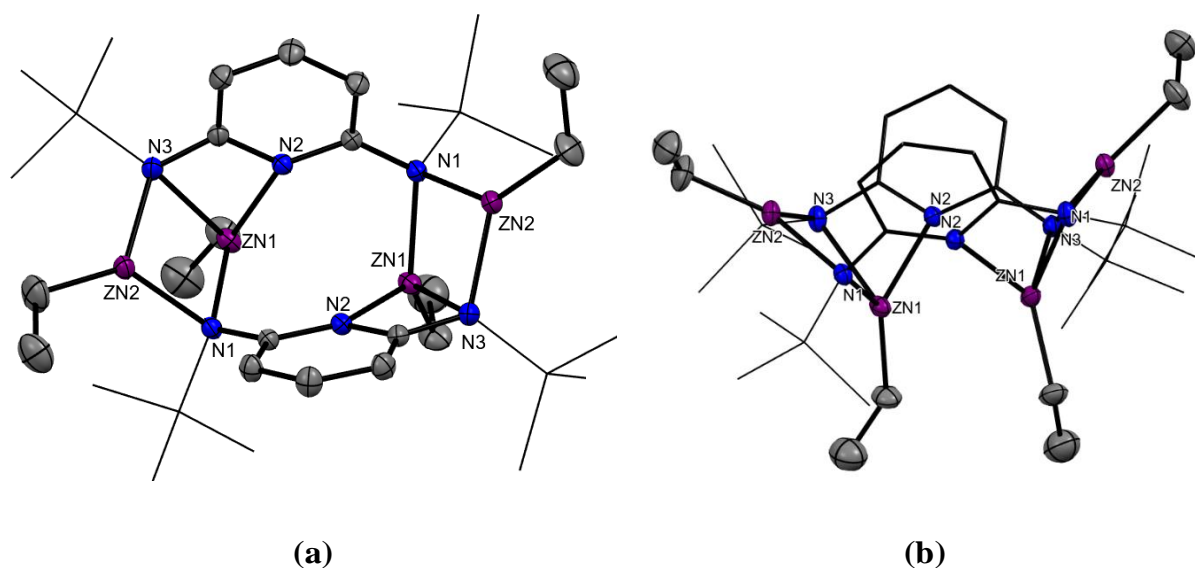
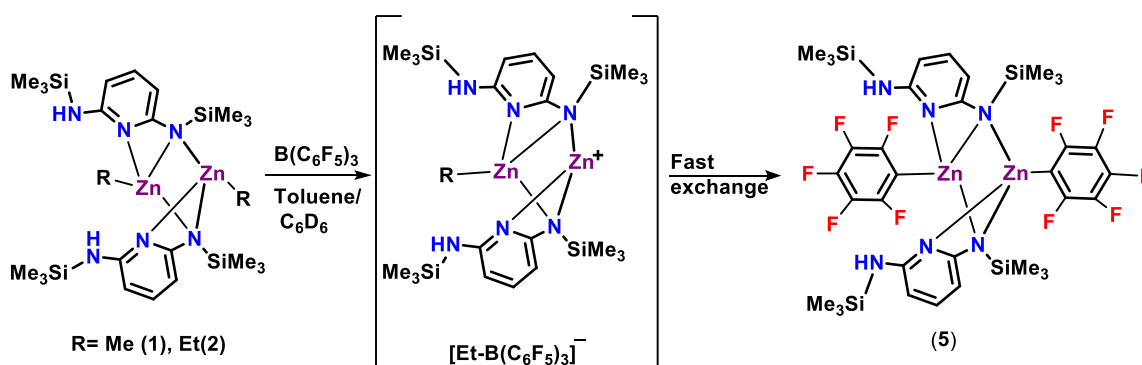


Figure 3.5. Single crystal X-ray structure of and tetranuclear zinc pyridinophane [$\{2,6-(\text{Me}_3\text{SiN})_2\text{C}_5\text{H}_3\text{N}\}(\text{ZnEt})_2\}_2$ (**4**); (a) Front view showing twelve membered cyclic core $[\text{Zn}_2\text{C}_4\text{N}_6]$ of pyridinophane and two four-membered rings $[\text{N}_2\text{ZnC}]$ having $\text{N}_{\text{py}}\text{-Zn}$ interaction and two four-membered rings $[\text{Zn}_2\text{N}_2]$; (b) Top view showing syn orientation of pyridine rings. All hydrogen atoms have been omitted for clarity. Selected bond lengths [\AA] and bond angles [$^\circ$]: Zn2-Zn1 2.9505(4), Zn2-N2 2.1039(19), Zn2-N1 2.293(2), Zn2-N3 2.0893(19), Zn2-C14 1.984(3), Zn1-N1 2.023(2), Zn1-N3 2.077(2), Zn1-C2 1.966(3); N2-Zn2-N1 62.95(7), N1-Zn1-N3 94.22(8), N3-Zn2-N2 97.63(7), N3-Zn2-N1 86.44(8), C2-Zn1-N1 130.35(14)

Zn complexes have gained importance as highly active and selective catalysts for a wide variety of transformations. There are also many examples of a considerable increase in activity by the cationization of Zn catalysts.^[11] Based on literature reports, attempts were made to synthesize the mono cationic zinc species, and the reaction was performed with Lewis acid $\text{B}(\text{C}_6\text{F}_5)_3$. The presence of reactive ethyl and methyl groups on zinc in compounds **1-4** encouraged us to synthesize the cationic zinc species. Attempts to synthesize cationic Zn complexes with $\text{B}(\text{C}_6\text{F}_5)_3$ may take place either by the abstraction of hydride from ethyl group forming $[\text{H-B}(\text{C}_6\text{F}_5)_3]^-$ anion and ethylene gas (for **2, 4**) or by abstraction of the methyl and ethyl group (for **1,2** and **3,4** respectively) from Zn center forming $[\text{Me-B}(\text{C}_6\text{F}_5)_3]^-$ or $[\text{Et-B}(\text{C}_6\text{F}_5)_3]^-$ anions

respectively, and the corresponding Zn cation. Although the formation of Zn cation took place however, due to its high reactivity, it underwent an unexpected rapid cleavage of the B-C₆F₅ bond and formation of neutral Zn and borane complexes owing to the fast exchange of C₆F₅ group from B to the Zn center.^[22,23] To monitor the reaction progress NMR tube experiments were performed, and the formation of fast exchange products was seen by the disappearance of B(C₆F₅)₃ signal and appearance of characteristic signals at -114.77, -154.89 and -160.59 in ¹⁹F NMR and missing of ethyl and methyl signals in ¹H NMR spectra. Complete exchange product was isolated in case of **1** and **2** as [{2-(Me₃SiN)-6-(Me₃SiNH)C₅H₃N}{Zn(C₆F₅)}]₂ (**5**) and a mixture of products was obtained in the case of **3** and **4** on reaction with the Lewis acid B(C₆F₅)₃. This extraordinary reactivity is likely related to the high Lewis acidity of Zn centers. The single crystal X-ray structure analysis also showed the exchange product with composition [{2-(Me₃SiN)-6-(Me₃SiNH)C₅H₃N}{Zn(C₆F₅)}]₂ (**5**) and supported the spectroscopic data.



Scheme 3.2. Attempted syntheses of cationic Zn complex and isolation of [{2-(Me₃SiN)-6-(Me₃SiNH)C₅H₃N}{Zn(C₆F₅)}]₂ (**5**) due to rapid exchange of methyl/ethyl groups with the C₆F₅ groups between the ion pairs of the intermediate cationic Zn complex.

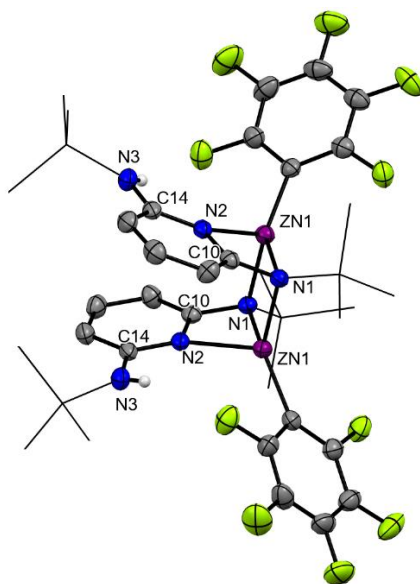
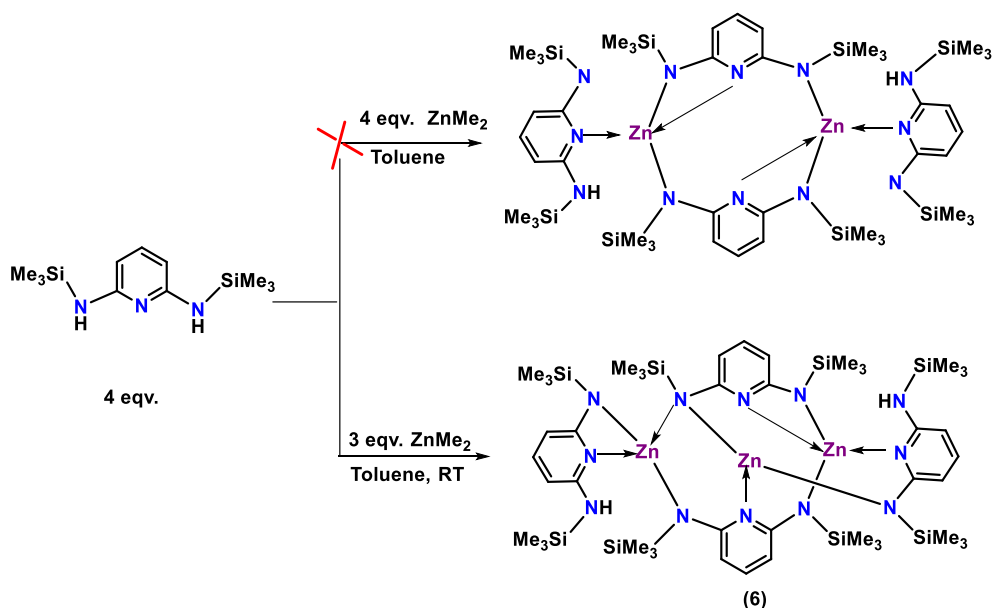


Figure 3.6. Solid-state structure of $[\{2-(\text{Me}_3\text{SiN})-6-(\text{Me}_3\text{SiNH})\text{C}_5\text{H}_3\text{N}\}\{\text{Zn}(\text{C}_6\text{F}_5)\}_2]$ (**5**); Hydrogen atoms except those bonded to N have been omitted for clarity. Selected bond lengths [\AA] and bond angles [$^\circ$]: Zn1-Zn'1 2.9156(11), Zn1-N1 2.067(4), Zn1-N1 2.133(4), Zn1-N2 2.105(4), Zn1-C10 2.559(5), Zn1-C6 1.996(5), F1-C5 1.357(6), F5-C1 1.364(6), N1-C10 1.407(6), N2-Zn1 2.105(4), N2-C10 1.349(6), F2-C4 1.356(7); N1-Zn1-N1 92.09(15), N1-Zn1-N2 104.25(14), N1-Zn1-C10 33.35(14), N1-Zn1-C10 100.68(14), C6-Zn1-N1 121.70(18), C6-Zn1-N2 119.69(17).

Compound **5** crystallized in the monoclinic system with $I2/a$ space group. Zinc atoms are tetracoordinated (bonded to three nitrogen atoms and one C_6F_5 group), having distorted tetrahedral geometry. This structure consists of two four-membered chelated rings $[\text{N}_1\text{C}_{10}\text{N}_2\text{Zn}_1]$ where pyridyl and amino sites of bap bind to the zinc center. Two zinc atoms and two amino nitrogen atoms of bap form a four-membered ring $[\text{Zn}_1\text{N}_1\text{Zn}_1'\text{N}_1']$ as illustrated in Figure 3.6.

Further exploring the dependency of the product formation on the relative stoichiometry of the reagents, we varied the stoichiometry of bap and ZnMe_2 to 3:2 and reverse stoichiometry 2:3 to synthesize the zinc containing bicyclic pyridinophane and

bowl-shaped cage complexes,^[16] unfortunately a mixture of products was obtained that could not be separated.



Scheme 3.3. Synthesis of bowl shaped pyridinophane [$\{2-(\text{Me}_3\text{SiN})-6-(\text{Me}_3\text{SiNH})\text{C}_5\text{H}_3\text{N}\}_2 \{2,6-(\text{Me}_3\text{SiN})_2\text{C}_5\text{H}_3\text{N}\}_2 \text{Zn}_3\}$ (**6**).

In our further investigation on the reaction stoichiometry based on the coordination demands of zinc, we performed a 2:1 reaction of bap and ZnMe₂, anticipating the full cyclic dinuclear zinc pyridinophane (Scheme 3.3, *top*) rather gave the trinuclear bowl-shaped cage complex [$\{2-(\text{Me}_3\text{SiN})-6-(\text{Me}_3\text{SiNH})\text{C}_5\text{H}_3\text{N}\}_2 \{2,6-(\text{Me}_3\text{SiN})_2\text{C}_5\text{H}_3\text{N}\}_2 \text{Zn}_3\}$ (**6**) (Scheme 3.3, *bottom*). Later, when we performed a 4:3 reaction of bap and ZnMe₂, we obtained compound **6** in 40% yield at room temperature, and it was found to be highly soluble in hexane and pentane. The ¹H NMR spectrum of **6** showed a series of doublets and merged triplets indicating the presence of more than two magnetically different bap units, similar corresponding signals in the aromatic region in ¹³C{¹H} NMR spectrum also supported the observations made based on ¹H NMR spectrum. The ¹H NMR spectrum also showed signals at 3.5 ppm that indicate the presence of N-H groups. The careful observation of the aromatic region in the ¹H NMR spectrum showed

the triplets in 7.07 - 7.09 ppm region for four protons and a set of eight doublets (two merged doublets) at 5.49, 5.62, 5.76, 5.83, 5.98, 5.99, 6.16 and 6.21 ppm for a total of eight protons with a coupling of 4 Hz each (Figure 3.7).

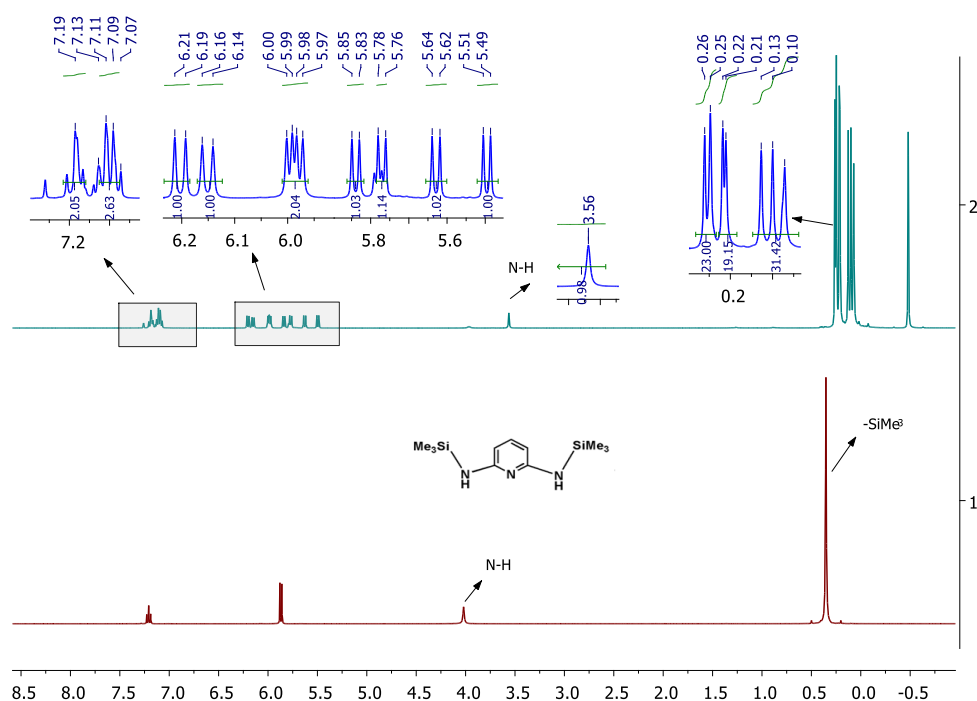


Figure 3.7. ¹H NMR spectrum (400 MHz, CDCl₃) of [{2-(Me₃SiN)-6-(Me₃SiNH)C₅H₃N}₂{2,6-(Me₃SiN)₂C₅H₃N}₂Zn₃] (**6**) (top) comparison with 2,6-(Me₃SiNH)₂C₅H₃N (bottom). Insets in the top NMR spectrum show expanded aliphatic and aromatic spectral regions.

The triplet (4H) and doublets (8H) in 1:2 ratio in the aromatic region indicate the presence of four bap units. Multiple signals in the aliphatic region 0.07 - 0.26 ppm for seventy-two protons shows the presence of eight SiMe₃ and eight separate signals in ¹³C{¹H} NMR at -0.50, -0.06, 0.31, 1.43, 2.03, 2.40, 2.57 and 2.80 for SiMe₃ also supports the presence of four bap units. The absence of signals in the upfield region shows the absence of Zn-Me group. Further, the structure of compound **6** as a trinuclear zinc complex with four ligand units was confirmed by the single-crystal X-ray diffraction analysis (Figure 3.8).

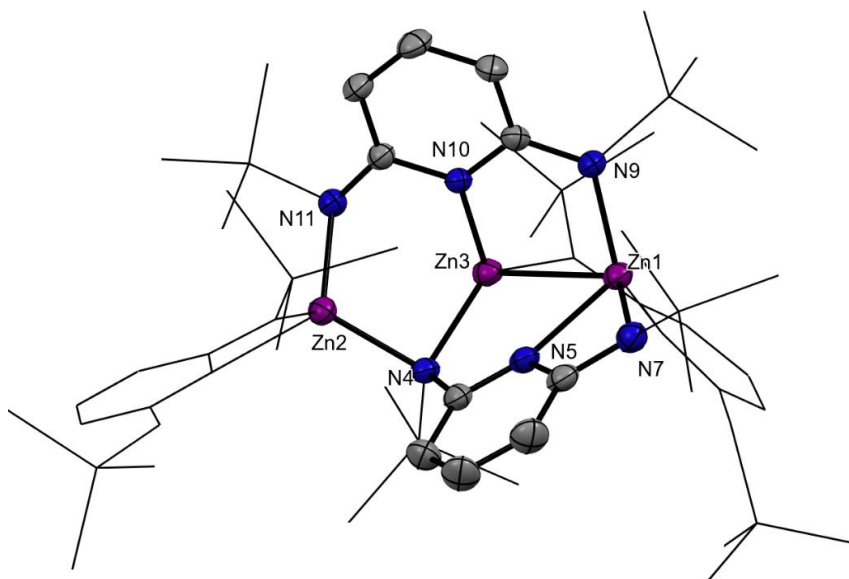
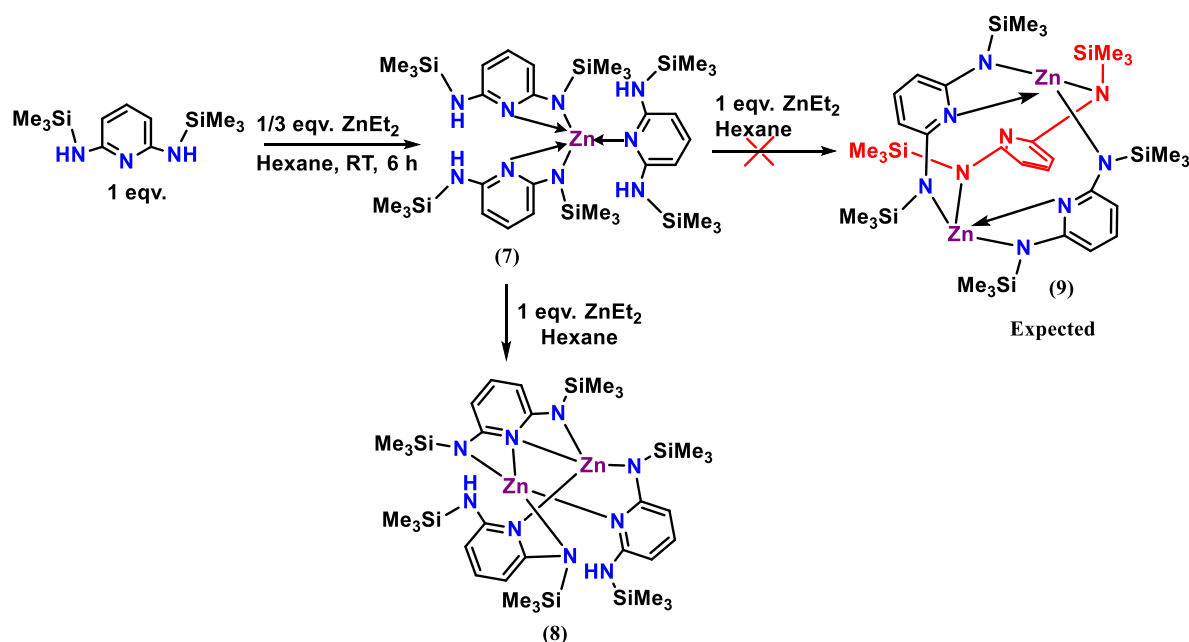


Figure 3.8. Single crystal X-ray structure of $[\{2-(\text{Me}_3\text{SiN})-6-(\text{Me}_3\text{SiNH})\text{C}_5\text{H}_3\text{N}\}_2 \{2,6-(\text{Me}_3\text{SiN})_2\text{C}_5\text{H}_3\text{N}\}_2 \text{Zn}_3]$ (**6**). All hydrogen atoms have been omitted for clarity. Selected bond lengths [\AA] and bond angles [$^\circ$]: Zn1-Zn3 2.7899(5), Zn1-N5 2.166(2), Zn1-N7 2.059(2), Zn1-N9 1.947(2), Zn1-C19 2.521(3), Zn2-N2 2.138(2), Zn2-N3 2.006(2), Zn2-N4 2.073(2), Zn2-N11 1.993(2), Zn3-Zn2 3.0457(5), Zn3-N4 2.032(2); N7-Zn1-Zn3 78.35(6), N7-Zn1-N5 96.21(9), N7-Zn1-C19 108.68(9), N9-Zn1-Zn3 79.13(7), N9-Zn1-N5 118.08(9), N9-Zn1-N7 123.35(9), N9-Zn1-C19 124.86(9), C19-Zn1-Zn3 95.89(7), N2-Zn2-Zn3 156.19(6), N2-Zn2-C8 33.59(9), N3-Zn2-Zn3 133.28(7), N3-Zn2-N2 66.12(9), N3-Zn2-C8 32.68(9).

Compound **6** crystallized in the triclinic system with $P\bar{1}$ space group. The colourless crystals of **6** were obtained from pentane, and the solid-state structure of **6** showed a bowl-shaped trinuclear zinc cage compound, where one zinc is penta-coordinated (Zn1), while the other two zinc centers are tetra-coordinated (Zn2 and Zn3) (Figure 3.8). Among the three zinc centers, Zn1 and Zn2 are part of the main cyclic backbone, whereas the third zinc center (Zn3) is located at the center of the molecule. The molecule is composed of a $[\text{N}_6\text{Zn}_2\text{C}_4]$ twelve-membered ring having one tetra-coordinated zinc at the center. Only two bap units are part of the cyclic core, while the other two bap units are coordinated to zinc with N_{py} , and one of the $-\text{NSiMe}_3$ group while another $-\text{NHSiMe}_3$ group remains unreacted. The signal for N-H proton in the ^1H

NMR spectrum was also seen in the expected chemical shift range. The Zn1-Zn3 distance is 2.7899(5) Å. The tetra-coordinated Zn2 showed Zn-N distance in 1.993(2) - 2.138(2) Å range (Table 3.5.2).

Based on our previous experience, emulating the dependency of the product formation on the relative stoichiometry of the reagents and the coordination demand of zinc, we varied the relative stoichiometry of bap and ZnEt₂.^[15,16] Subsequently, the 3:1 reaction of bap and ZnEt₂ gave mononuclear zinc complex, [$\{2-(\text{Me}_3\text{SiN})-6-(\text{Me}_3\text{SiNH})\text{C}_5\text{H}_3\text{N}\}_2\{2,6(\text{Me}_3\text{SiNH})_2\text{C}_5\text{H}_3\text{N}\}\text{Zn}\}$ (**7**) *via* ethane evolution (Scheme 3.4). The ¹H NMR spectra of complex **7** showed a triplet and a doublet for the pyridine hydrogens at 7.02 and 5.80 ppm, and their corresponding carbons were observed as three signals in their ¹³C{¹H} NMR spectrum at 160.4, 139.4 and 98.4 ppm.



Scheme 3.4. Syntheses of mononuclear zinc complex, [$\{2-(\text{Me}_3\text{SiN})-6-(\text{Me}_3\text{SiNH})\text{C}_5\text{H}_3\text{N}\}_2\{2,6(\text{Me}_3\text{SiNH})_2\text{C}_5\text{H}_3\text{N}\}\text{Zn}\}$ (**7**) and dinuclear zinc complex, [$\{2-(\text{Me}_3\text{SiN})-6-(\text{Me}_3\text{SiNH})\text{C}_5\text{H}_3\text{N}\}_2\{2,6(\text{Me}_3\text{SiNH})_2\text{C}_5\text{H}_3\text{N}\}\text{Zn}_2\}$ (**8**).

Signal for all SiMe₃ groups as a singlet appeared in ¹H NMR (0.22 ppm, ¹³C{¹H} NMR (0.11 ppm) and ²⁹Si NMR (-1.10 ppm) spectra showed chemically equivalent environment in solution state around zinc center and anticipated as a symmetrical homoleptic complex. The stretching frequency for N-H bond in the IR spectrum was observed at 3388 cm⁻¹, and the signal at 4.46 ppm for four protons in the ¹H NMR spectrum indicated the presence of unreacted proton on -NHSiMe₃.

The solid-state structure was elucidated by single crystal X-ray diffraction analysis and the composition was confirmed as the mononuclear *tris*-bap complex, [{2-(Me₃SiN)-6-(Me₃SiNH)C₅H₃N}₂ {2,6-(Me₃SiNH)₂C₅H₃N}Zn], surprisingly it was found to be an unsymmetrical mononuclear zinc complex.

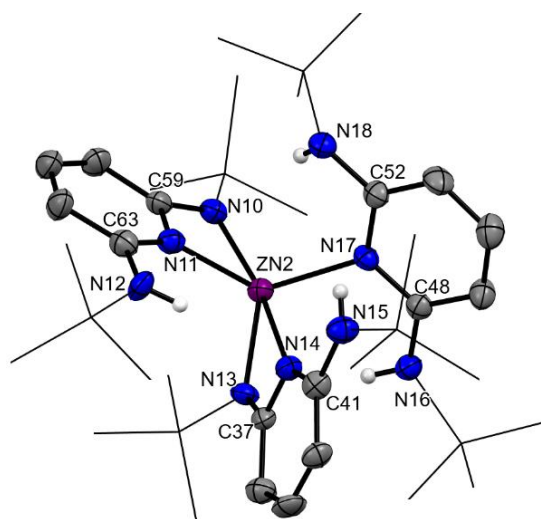


Figure 3.9. Solid-state structure of [{2-(Me₃SiN)-6-(Me₃SiNH)C₅H₃N}₂ {2,6-(Me₃SiNH)₂C₅H₃N}Zn] (**7**). All hydrogen atoms, except those bonded to N, have been omitted for clarity. Selected bond lengths [Å] and bond angles [°]: Zn2-N17 2.099(4), Zn2-N11 2.109(4), Zn2-N13 1.979(4), Zn2-N14 2.470(4), Zn2-N10 2.071(4), N11-C59 1.372(6), N10-C59 1.355(6); N17-Zn2-N11 125.18(15), N17-Zn2-N14 82.39(14), N17-Zn2-C59 122.62(15), N11-Zn2-N14 96.20(14), N11-Zn2-C59 32.74(15), N13-Zn2-N17 116.08(16), N13-Zn2-N11 109.99(16), N13-Zn2-N14 60.61(15), N13-Zn2-N10 126.94(16), N13-Zn2-C59 121.19(16), N14-Zn2-C59 128.91(15).

Out of three bap units, two bap units were bonded to zinc through one of their amino nitrogen as well as coordinating through their N_{py} (pyridine nitrogen), forming two four-membered chelated rings, while the third bap unit provided coordination only through N_{py} (pyridine nitrogen) and both of its amino ($NHSiMe_3$) sites remain unreacted. The single signal in 1H , $^{13}C\{^1H\}$ and ^{29}Si NMR spectra might be due to identical behaviour in solution. The Zn center in **7** is pentacoordinated (two amino and three N_{py} coordination). The bond lengths of N11-C59 and N10-C59 are 1.372(6) and 1.355(6) Å in the double bond range indicating the amidinate type coordination in chelated rings $[Zn_2N_{10}C_{59}N_{11}]$ (Figure 3.9).

To synthesize the bicyclic molecule, one more equivalent of diethyl zinc was added to **7**, anticipating the formation of bicyclic pyridinophane, $[\{(2,6-(Me_3SiN)_2C_5H_3N)_3 Zn_2\}]$ (**9**) (Scheme 3.4). The 1H NMR spectra of the product showed a triplet and a doublet for the pyridine hydrogens at 7.03 and 5.77 ppm, and their corresponding carbon signals appeared at 159.9, 139.2, and 98.3 ppm in their $^{13}C\{^1H\}$ NMR spectra. A singlet for all $SiMe_3$ groups in 1H (0.22 ppm) and $^{13}C\{^1H\}$ NMR (0.11 ppm) spectra showed chemically equivalent environment of $NSiMe_3$ groups in the assembly. The presence of signal in the 1H NMR spectrum at 4.39 ppm and IR stretching band (for N-H) at 3384 cm^{-1} indicates the presence of -NH group. Later the solid-state structure confirmed the unsymmetrical dinuclear complex, $[\{2-(Me_3SiN)-6-(Me_3SiNH)C_5H_3N\}_2\{2,6-(Me_3SiNH)_2C_5H_3N\}Zn_2]$ (**8**) for this product. The symmetry in the NMR of **8** could be due to the identical behaviour in the solution caused by the fast change in $[N \rightarrow Zn]$ coordination in different bap units. The HRMS spectra of the complex showed m/z value at 883.2599 (calcd. 883.2562 for $C_{33}H_{65}N_9Si_6Zn_2$) corresponding to the molecular ion peak $[M]^+$.

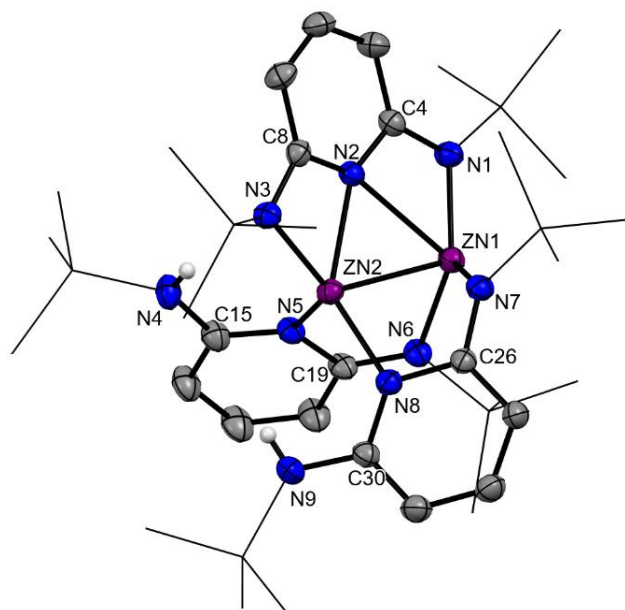
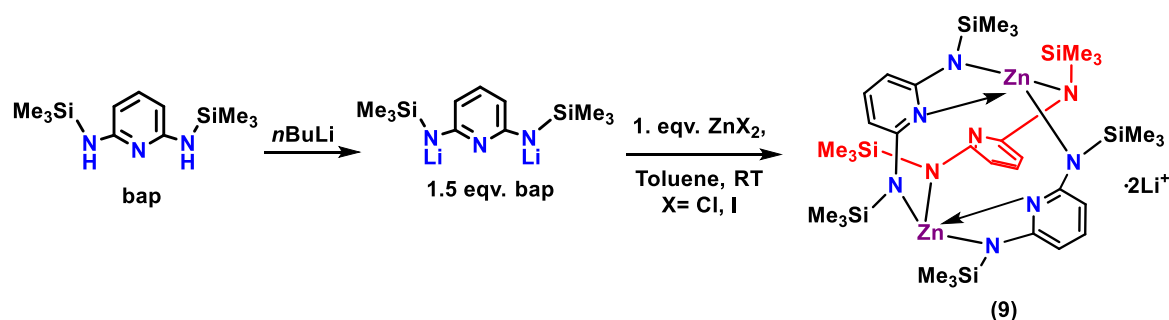


Figure 3.10. Solid-state structure of $[\{2-(\text{Me}_3\text{SiN})-6-(\text{Me}_3\text{SiNH})\text{C}_5\text{H}_3\text{N}\}_2\{2,6(\text{Me}_3\text{SiNH})\text{C}_5\text{H}_3\text{N}\}\text{Zn}_2]$ (**8**); All hydrogen atoms, except those bonded to N, have been omitted for clarity. Selected bond lengths [\AA] and bond angles [$^\circ$]: Zn1-Zn3 2.666(6), Zn2-N2 2.205(3), Zn2-N5 2.065(3), Zn2-N8 2.017(3), Zn2 N3 1.988(3), Zn2-C8 2.529(3) Zn1-N2 2.489(3), Zn1-N6 1.986(3), Zn1-N7 2.027(3), Zn1-N1 1.960(3), N1-C4 1.374(5), N2-C4 1.365(4), N2-C8 1.361(4), N3-C8 1.387(4); N2-Zn2-Zn1 60.59(8), N1-Zn1-N2 60.97(11), N1-Zn1-N6 128.76(13), N1-Zn1-N7 122.02(12), N3-Zn2-N2 65.60(11), N2-C8-N3 112.0(3), N2-C4-N1 114.5(3).

Compound **8** crystallized in the monoclinic system with $P2_1/n$ space group. The solid-state structure of $[\{2-(\text{Me}_3\text{SiN})-6-(\text{Me}_3\text{SiNH})\text{C}_5\text{H}_3\text{N}\}_2\{2,6(\text{Me}_3\text{SiNH})\text{C}_5\text{H}_3\text{N}\}\text{Zn}_2]$ (**8**) (Figure 3.10) contains two zinc centers, where both the zinc atom are pentacoordinate with a Zn-Zn separation of 2.666(6) \AA . The Zn-Zn bond distance in **8** is longer than those of previously reported, this distance is substantially longer than twice Pauling's single-bond metallic radius 2.50 \AA and therefore indicating no actual covalent bonding interaction between zinc centers.^[22]

Attempts to synthesize the bicyclic pyridinophane using organozinc reagents (dimethyl zinc and diethyl zinc) were unsuccessful. Consequently, the alternative zinc

halide reagents were examined. Lithiation of *bap* was carried out by the reaction of *bap* with 2 equivalents of *n*BuLi in hexane, using the reported procedure^[16]. The colourless crystals of dilithium *bis*(trimethylsilyl)-*N,N'*-2,6-diamidopyridine (*bap*Li₂) were obtained at -4 °C. The stoichiometric reaction of *bap*Li₂ with ZnCl₂ and ZnI₂ in toluene afforded a solid, which on crystallization with pentane gave colourless crystals of [2,6(Me₃SiN)₂C₅H₃N]₃Zn₂ (**9**) (Scheme 3.5).



Scheme 3.5. Synthesis of bicyclic pyridinophane, {[2,6(Me₃SiN)₂C₅H₃N]₃Zn₂} (**9**).

In the ¹H NMR spectrum, the presence of two triplets at 7.70 and 6.97 ppm in 1:2 intensity and two signals at 0.32 and 0.36 ppm for SiMe₃ in 1:2 intensity indicate that one pyridine ring has a different orientation than the other two, similar intensity ratio was observed for doublets also. The doublet at 6.03 ppm for two protons corresponds to a triplet at 7.09 ppm (1H), and two close doublets at 5.86 and 5.89 ppm (4H) corresponds to the triplet at 6.97 ppm (2H) (Figure 3.11). In the ¹³C{¹H} NMR spectrum, the eight different signals for pyridine ring carbons appeared at 166.3, 166.3, 163.9, 143.6, 140.4, 103.2, 103.1, and 101.7 ppm (Figure 3.12). The presence of different sets of triplets and doublets in the ¹H NMR spectrum clearly indicates that the environment of one *bap* is different from the other two rings, and these two pyridines also have slightly different environments as observed from the close doublets in ¹H NMR and eight signals in ¹³C{¹H} NMR spectra. In ²⁹Si NMR, three signals were observed at 1.90, -2.57, and -3.50 ppm for SiMe₃ groups (Figure 3.12). The composition of compound **9** also

supported by the HRMS spectrum, m/z values at 885.2568 (calcd. 885.2539) corresponding to $[M+2H]^+$ and the bicyclic nature of **9** was confirmed by its single crystal X-ray diffraction analysis (Figure 3.13).

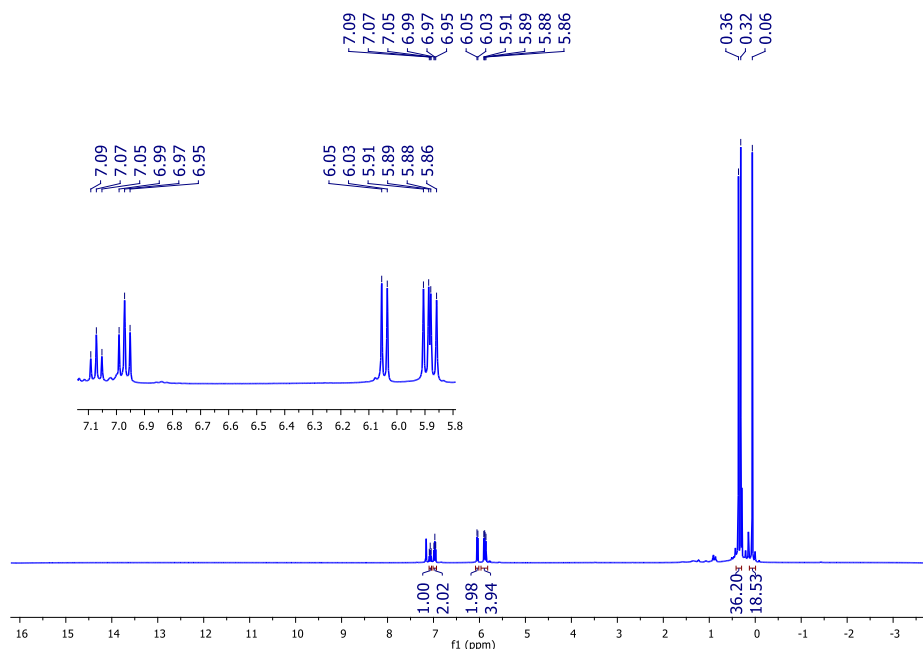


Figure 3.11. ^1H NMR spectrum (400 MHz, C_6D_6) of bicyclic pyridinophane $\{[2,6(\text{Me}_3\text{SiN})_2\text{C}_5\text{H}_3\text{N}]_3\text{Zn}_2\}$ (**9**).

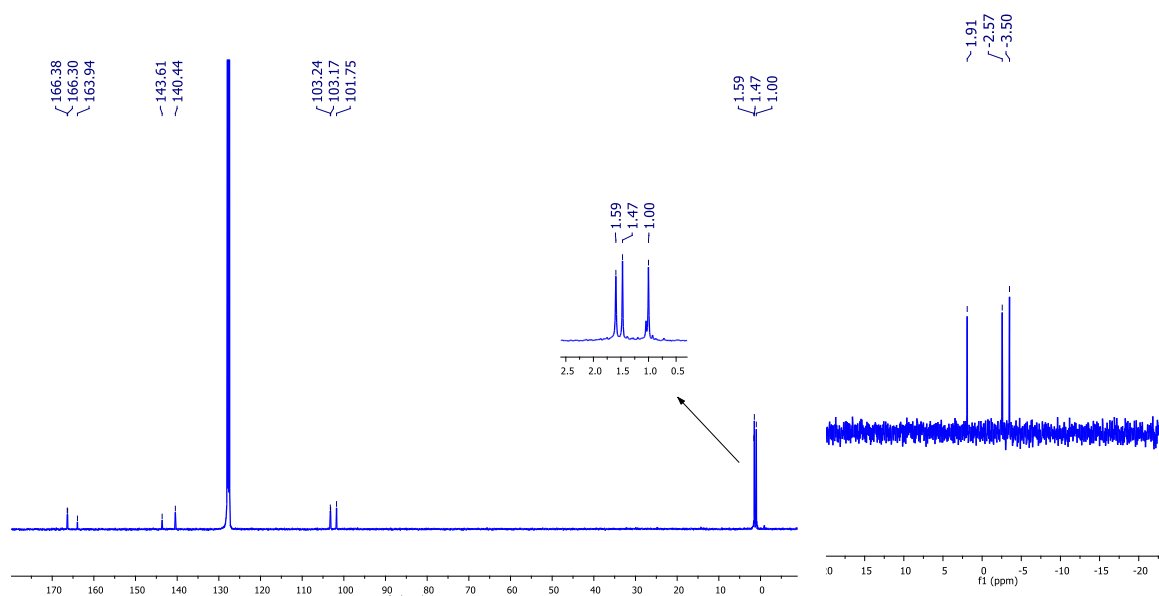


Figure 3.12. $^{13}\text{C}\{^1\text{H}\}$ (left) and ^{29}Si (right) NMR spectrum (400 MHz, C_6D_6) of bicyclic pyridinophane $\{[2,6(\text{Me}_3\text{SiN})_2\text{C}_5\text{H}_3\text{N}]_3\text{Zn}_2\}$ (**9**).

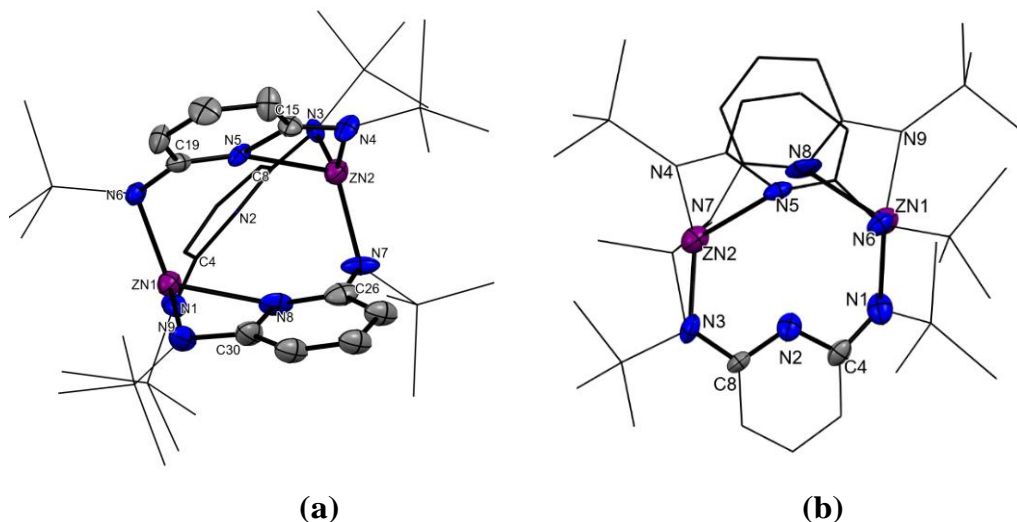


Figure 3.13. Solid-state structure of bicyclic pyridinophane, {[2,6(Me₃SiN)₂C₅H₃N]₃}Zn₂ (**9**). (a) Front view showing two parallel pyridine units and third bap on the back side; (b) top view showing *syn* orientation of pyridine ring. Selected bond lengths [Å] and bond angles [°]: Zn2-N5 2.498(11), Zn2-N4 1.981(11), Zn2-N3 1.997(13), Zn2-N7 1.983(12), Zn1-N6 1.997(11), Zn1-N1 2.099(13), Zn1-N8 2.330(14), Zn1-N9 2.093(17), N1-C4 1.378(19), N2-C8 1.376(18), N2-C4 1.387(17), N3-C8 1.376(16), N8-C30 1.33(2), N9-C30 1.36(2), N7-C26 1.41(2); N4-Zn2-N5 59.7(4), N4-Zn2-N3 128.0(5), N4-Zn2-N7 113.7(5), N3-Zn2-N5 107.4(4), N7-Zn2-N5 109.0(5), N7-Zn2-N3 117.8(5), N6 Zn1 N1 113.2(5), N6 Zn1 N8 115.3(5), N6 Zn1 N9 112.4(6), N1 Zn1 N8 102.5(5).

Compound **9** crystallized in the triclinic system with $P\bar{1}$ space group. The solid-state structure of **9** showed a bicyclic nature of dinuclear zinc pyridinophane, where each zinc is tetracoordinated in a distorted tetrahedral geometry. Two pyridine rings have nearly parallel *syn* orientation with a slight distortion which may be due to two four-membered (ZnN₂C) chelated rings at diagonally opposite edges of the central core ring, while the third bap unit coordinates from the back side and its pyridine ring nitrogen is not involved in the coordinate bond formation. The bond distance N9-C30 1.36(2) Å and N7-C26 1.41(2) Å was found to be in the range of double and single bond characters respectively, which indicates that in N9-C30 bond the delocalization of electrons occurs in four-membered amidinate type chelated ring (Zn₁N₈N₉C₃₀).

3.3 Conclusions

In conclusion, a variety of organozinc species have been synthesized by changing the stoichiometry of bap and zinc reagents. These macrocyclic structures present the unexplored pyridinophanes assembly containing inorganic linkages. The use of bis(trimethylsilyl)-N,N'-2,6-diaminopyridine (bap) with ZnMe₂ and ZnEt₂ gave mono-, di, tri and tetranuclear zinc complexes. These complexes include the dinuclear zinc complex **1** and **2**, which are further converted into pyridinophanes **3** and **4**, respectively. Further on varying the stoichiometry of bap and ZnMe₂ (4:3) afforded zinc containing bowl shaped pyridinophane $[\{2-(\text{Me}_3\text{SiN})-6-(\text{Me}_3\text{SiNH})\text{C}_5\text{H}_3\text{N}\}_2 \{2,6-(\text{Me}_3\text{SiN})_2\text{C}_5\text{H}_3\text{N}\}_2 \text{Zn}_3]$ (**6**). In an attempt to synthesize the cationic zinc species, an unexpected fast exchange of the C₆F₅ group from B to the Zn center owing to high reactivity results in the formation of the neutral zinc complex **5**. We have also shown the facile synthesis of zinc-containing bicyclic pyridinophane. The reaction of dilithium bis(trimethylsilyl)-N,N'-2,6-diamidopyridine with ZnCl₂ and ZnI₂ afforded bicyclic pyridinophane $\{[2,6(\text{Me}_3\text{SiN})\text{C}_5\text{H}_3\text{N}]_3\text{Zn}_2\}$ (**9**). The results, taken together, demonstrate that the synthesis of macrocycles containing main group elements are conceivable if the reaction strategy and conditions are carefully selected.

3.4 Experimental section

3.4.1 General methods

All syntheses were carried out under an inert atmosphere of dinitrogen in oven-dried glassware using standard Schlenk techniques or a glovebox where O₂ and H₂O levels were maintained, usually below 0.1 ppm. All the glassware were dried at 150 °C in an oven for at least 12h. Solvents were purified by MBRAUN solvent purification system MB SPS-800.

3.4.2 Starting materials

All chemicals were purchased from Sigma-Aldrich and used without further purification. The starting materials, bis(trimethylsilyl)-N,N'-2,6-diaminopyridine and lithium bis(trimethylsilyl)-N,N'-2,6-diamidopyridine^[20] were prepared by following the reported procedures.

3.4.3 Physical measurements

The ¹H and ¹³C{¹H} NMR spectra were recorded with a Bruker 400 MHz spectrometer with tetramethyl silane (TMS) as an external reference; chemical shift values are reported in ppm. FT-IR spectra of complexes were recorded (in the range 4000-400 cm⁻¹) with a Perkin-Elmer Lambda 35-spectrophotometer using Nujol mull. High resolution mass spectrometry (HRMS) was performed with Waters SYNAPT G2-S. Melting points were measured in a sealed glass tube on a Büchi B-540 melting point apparatus.

Single crystal X-ray diffraction data of compounds **1-9** were collected using a Rigaku XtaLAB mini diffractometer equipped with Mercury375 M CCD detector. The data were collected with MoK α radiation ($\lambda = 0.71073 \text{ \AA}$) using omega scans. During the data collection, the detector distance was 49.9 mm (constant), and the detector was placed at $2\theta = 29.85^\circ$ (fixed) for all the data sets. The data collection and data reduction were done using the Crystal Clear suite.^[23] All the crystal structures were solved through OLEX2.^[23b] All non-hydrogen atoms were refined anisotropically. All figures were generated using mercury 2022.1.0

3.4.4 Synthetic procedures

Synthesis of [{2-(Me₃SiN)-6-(Me₃SiNH)C₅H₃N}(ZnMe)]₂ (**1**):

A solution of ZnMe₂ (3.8 mmol, 2.6 mL, 1.5 M in heptane) was added slowly at 0 °C to a stirred solution of bis(trimethylsilyl)-N,N'-2,6-diaminopyridine (3.8 mmol, 1.0 g) in

toluene/hexane. The reaction mixture was allowed to come to room temperature and stirred for 6 h. All the volatiles were removed under vacuum to give a white solid that afforded transparent crystals of **1** on crystallization from pentane at -30 °C. Yield: 0.66 g (51 %). Mp: 168-170 °C. IR (nujol) ν : 3269 (N-H), 2953, 2923, 2853, 1616, 1565, 1490, 1460, 1378, 1256, 1239, 1173, 1042, 846, 779, 643, 629, 522, 479, 436 cm^{-1} . ^1H NMR (400 MHz, C_6D_6): δ = 7.12 (t, 2H, *p*-ArH, $^3J_{\text{H-H}} = 8$ Hz), 6.00 (d, 2H, *m*-ArH, $^3J_{\text{H-H}} = 8$ Hz), 5.71 (d, 2H, *m*-ArH, $^3J_{\text{H-H}} = 8$ Hz), 3.24 (s, 2H, NH), 0.19 (s, 18H, SiMe₃), 0.16 (s, 18H, SiMe₃), -0.68 (s, 6H, Zn-CH₃) ppm; $^{13}\text{C}\{^1\text{H}\}$ NMR (100 MHz, C_6D_6): δ = 165.5, 155.6, 140.3, 103.8, 99.1, 1.3 (SiMe₃), 1.0 (SiMe₃), -0.3 (Zn-CH₃) ppm; ^{29}Si NMR (79.5 MHz, C_6D_6): δ = 4.0, 3.4 (SiMe₃) ppm. HRMS (AP⁺): *m/z* calcd for C₂₄H₅₁Zn₂N₆Si₄: (665.1809) [M+H]⁺; found: (665.1815).

Synthesis of [{2-(Me₃SiN)-6-(Me₃SiNH)C₅H₃N}(ZnEt)]₂ (**2**):

A solution of ZnEt₂ (3.8 mmol, 3.8 mL, 1.0 M in hexane) was slowly added at 0 °C to a stirred solution of bis(trimethylsilyl)-N,N'-2,6-diaminopyridine (3.8 mmol, 1.0 g) in toluene/hexane (40 mL). The reaction mixture was allowed to come to room temperature and stirred for 6 h. All the volatiles were removed under vacuum to give a white solid that afforded transparent crystals of **2** on crystallization from pentane/DCM at -30 °C. Yield: 0.7 g (50 %). Mp: 161–163 °C. IR (nujol) ν : 3282 (N-H), 2956, 2859, 2719, 1569, 1445, 1378, 1299, 1255, 1162, 1094, 1048, 842, 751, 686 cm^{-1} . ^1H NMR (400 MHz, C_6D_6): δ = 6.85 (t, 2H, *p*-ArH, $^3J_{\text{H-H}} = 8$ Hz), 6.08 (d, 2H, *m*-ArH, $^3J_{\text{H-H}} = 8$ Hz), 5.58 (d, 2H, *m*-ArH, $^3J_{\text{H-H}} = 8$ Hz), 3.45 (s, 2H, -NH), 1.66 (t, 6H, -CH₂CH₃, $^3J_{\text{H-H}} = 8$ Hz), 0.80 (q, 4H, -CH₂CH₃, $^3J_{\text{H-H}} = 8$ Hz), 0.43 (s, 18H, SiMe₃), -0.04 (s, 18H, SiMe₃) ppm; $^{13}\text{C}\{^1\text{H}\}$ NMR (100 MHz, C_6D_6): δ = 166.8, 155.7 (Py-C2, Py-C6), 140.3 (Py-C4), 103.7 (Py-C3), 98.9 (Py-C5), 13.7 (CH₂CH₃), 1.4, 0.9 (SiMe₃) ppm; ^{29}Si NMR (79.5

MHz, C₆D₆): δ = 3.5, 3.3 (SiMe₃) ppm. HRMS (AP⁺): m/z calcd for C₂₆H₅₄Zn₂N₆Si₄: (692.2045) [M]⁺; found: (692.2047).

Synthesis of tetranuclear zinc [3.3](2,6)pyridinophane {2,6-(Me₃SiN)₂C₅H₃N₂(ZnMe)₄} (3):

A solution of ZnMe₂ (7.6 mmol, 5.0 mL, 1.5 M in heptane) was slowly added to a stirred solution of bis(trimethylsilyl)-N,N'-2,6-diaminopyridine (3.8 mmol, 1.0 g) in toluene/hexane (40 mL) at 0 °C. The reaction mixture was allowed to come to room temperature, followed by 10 h of reflux. All volatiles were removed under vacuum to give a white solid that afforded transparent crystals of **3** on crystallizing from pentane at -20 °C. Yield 0.65 g (38 %).

Alternative approach for the synthesis of 3: To a solution of **1** (1.0 mmol, 0.67 g) in toluene (40 mL), a solution of ZnMe₂ (2.0 mmol, 1.4 mL, 1.5 M in heptane) was added slowly at 0 °C, the reaction mixture was allowed to come to room temperature followed by 10 h of reflux. Subsequently, all volatiles were removed under vacuum to give a white solid that afforded transparent crystals of **3** on crystallizing from pentane at -30 °C. Yield 0.58 g (33%). Mp: 146–150 °C. IR (nujol) ν : 3388, (N-H), 3248 (N-H), 2925, 2855, 1599, 1572, 1459, 1377, 1336, 1296, 1256, 1160, 1097, 1075, 1047, 846, 781, 723, 693, 639, 599, 517, 463 cm⁻¹. ¹H NMR (400 MHz, C₆D₆): δ = 7.23 (t, 2H, *p*-ArH, ³J_{H-H} = 8 Hz), 6.25 (d, 4H, *m*-ArH, ³J_{H-H} = 8 Hz), 0.16 (s, 18H, SiMe₃), -0.37 (s, 12H, CH₃) ppm; ¹³C{¹H} NMR (100 MHz, C₆D₆): δ = 164.3 (Py-C2, Py-C6), 140.3 (Py-C4), 112.8 (Py-C3, Py-C5), 1.2 (SiMe₃), -0.6 (CH₃), 34.4, 22.7, 14.3 (pentane) ppm;. ²⁹Si NMR (79.5 MHz, C₆D₆): δ = 3.6 (SiMe₃) ppm.

Synthesis of tetranuclear zinc [3.3](2,6)pyridinophane, {[2,6-(Me₃SiN)₂C₅H₃N]₂(ZnEt)₄} (4):

ZnEt₂ (7.6 mmol, 7.6 mL, 1.0 M in hexane) was added slowly to a stirred solution of bap (3.8 mmol, 1.0 g) in toluene (40 mL) at 0 °C. The reaction mixture was allowed to come to room temperature, followed by 10 h reflux. All volatiles were removed under vacuum to give a white solid, which afforded transparent crystals of **4** on crystallizing from pentane at -30 °C. Yield: 0.61 g (37 %).

Alternative approach for the synthesis of 4: To a solution of **2** (1.0 mmol, 0.7 g) in toluene (40 mL) at 0 °C was slowly added a solution of ZnEt₂ (2.0 mmol, 2.0 mL 1.0 M in hexane), the reaction mixture was allowed to come to room temperature followed by 10 h of reflux. Subsequently, all the volatiles were removed under vacuum to give a white solid that afforded transparent crystals of **4** on crystallizing from pentane at -30 °C. Yield: 0.55 g (34 %). Mp: 184-186 °C. IR (nujol) ν : 2924, 2723, 1575, 1559, 1462, 1377, 1301, 1262, 1248, 1159, 1043, 871, 843, 802, 747, 723, 679, 597, 506, 488, 466, 446, 429, 407 cm⁻¹. ¹H NMR (400 MHz, CDCl₃): δ = 6.69 (t, 2H, *p*-ArH, ³J_{H-H} = 8 Hz), 6.14 (d, 2H, *m*-ArH, ³J_{H-H} = 8 Hz), 1.63 (t, 12H, -CH₂CH₃, ³J_{H-H} = 8 Hz), 0.89 (q, 8H, -CH₂CH₃, ³J_{H-H} = 8 Hz), 0.28 (s, 36H, SiMe₃) ppm; ¹³C{¹H} NMR (100 MHz, CDCl₃): δ = 164.2 (Py-C2, Py-C6), 140.6 (Py-C4), 112.2 (Py-C3, Py-C5), 13.2 (CH₂CH₃), 4.1 (-CH₂CH₃), 1.0 (SiMe₃) ppm; ²⁹Si NMR (79.5 MHz, CDCl₃): δ = 6.6 (SiMe₃) ppm. HRMS (AP⁺): *m/z* calcd for C₃₀H₆₄N₆Si₄Zn₄: (882.1367) [M]⁺; found: (882.1393).

Synthesis of exchange product with B(C₆F₅)₃ [{2-(Me₃SiN)-6-(Me₃SiNH)C₅H₃N}{Zn(C₆F₅)}]₂ (5).

To a stirred solution of **1** (0.3 mmol, 0.2 g) in toluene (10 mL) at room temperature was added the Lewis acid B(C₆F₅)₃ (0.6 mmol, 0.3 g) and stirred for 1h, the volume of the

filtrate was reduced to 4 mL and stored at $-20\text{ }^{\circ}\text{C}$ to afford transparent crystals of $[\{2-(\text{Me}_3\text{SiN}),6-(\text{Me}_3\text{SiNH})\text{C}_5\text{H}_3\text{N}\}\{\text{Zn}(\text{C}_6\text{F}_5)\}]_2$ (**5**). Yield: 0.55 g (34 %). (0.1 g) Mp: $206\text{-}208\text{ }^{\circ}\text{C}$. IR (nujol) ν : 3397 (N-H), 2929, 2863, 1583, 1455, 1371, 1256, 1048, 950, 809, 734, 596 cm^{-1} . ^1H NMR (400 MHz, C_6D_6): $\delta = 6.88$ (t, 2H, *p*-ArH, $^3J_{\text{H-H}} = 8$ Hz), 6.31 (d, 2H, *m*-ArH, $^3J_{\text{H-H}} = 8$ Hz), 5.65 (d, 2H, *m*-ArH, $^3J_{\text{H-H}} = 8$ Hz), 3.24 (s, 2H, NH), 0.33 (s, 18H, SiMe₃), 0.04 (s, 18H, SiMe₃) ppm; $^{19}\text{F}\{^1\text{H}\}$ NMR (376 MHz, C_6D_6): $\delta = -114.77, -154.89, -160.59$ ppm; $^{13}\text{C}\{^1\text{H}\}$ NMR (100 MHz, C_6D_6): $\delta = 166.0$ (Py-C2), 156.3 (Py-C6), 141.5 (Py-C4), 103.1 (Py-C3), 101.0 (Py-C5), 0.7, -1.1 (SiMe₃) ppm; ^{29}Si NMR (79.5 MHz, C_6D_6): $\delta = 7.3, 4.4$ (SiMe₃) ppm.

Synthesis of zinc containing bowl shaped pyridinophane, $[\{2-(\text{Me}_3\text{SiN})-6-(\text{Me}_3\text{SiNH})\text{C}_5\text{H}_3\text{N}\}]_2 [\text{2,6-(Me}_3\text{SiN)}_2\text{C}_5\text{H}_3\text{N}]_2 \text{Zn}_3$ (6**):**

To a stirred solution of bap in toluene (3.8 mmol, 1.0 g) in toluene/hexane (40 mL) at $0\text{ }^{\circ}\text{C}$ was slowly added a solution of ZnMe₂ (2.9 mmol, 2.0 mL, 1.5 M in heptane). The reaction mixture was allowed to come to room temperature and stirred for another 12 h at room temperature. All volatiles were removed under vacuum to give a white solid that afforded transparent crystals of **6** on crystallizing from pentane at $-20\text{ }^{\circ}\text{C}$. Yield: 0.49 g (40 %). Mp: $247\text{-}249\text{ }^{\circ}\text{C}$ (decomposition). IR (nujol) ν : 3415, 3154, 2926, 2855, 1562, 1451, 1376, 1343, 1313, 1292, 1251, 1209, 1166, 1073, 1053, 972, 899, 846, 773, 728, 687, 629, 587, 556 cm^{-1} . ^1H NMR (400 MHz, CDCl_3): $\delta = 7.09$ (merged triplet, 2H, *p*-ArH, $^3J_{\text{H-H}} = 8$ Hz), 7.19 (merged triplet, 2H, *p*-ArH) 6.21 (doublets, 1H, *m*-ArH), 6.16 (doublets, 1H, *m*-ArH), 5.97-6.00 (merged doublets, 2H, *m*-ArH), 5.85 (doublets, 1H, *m*-ArH), 5.78 (doublets, 1H, *m*-ArH), 5.64 (doublets, 1H, *m*-ArH), 5.51 (doublets, 1H, *m*-ArH), 0.26, 0.22, 0.13, 0.10 (s, 72H, SiMe₃) ppm; $^{13}\text{C}\{^1\text{H}\}$ NMR (100 MHz, CDCl_3): $\delta = 167.9, 167.3, 166.0, 165.9, 165.2, 159.8, 159.5, 155.9, 145.1, 140.8, 140.1, 139.5, 106.4, 105.8, 105.7, 105.0, 104.5, 99.5, 97.3, 92.0$ and 2.6, 2.4, 2.2,

1.8, 1.2, 0.1, -0.2, -0.6 (SiMe₃) ppm; ²⁹Si NMR (79.5 MHz, CDCl₃): δ = 10.5, 4.0, 3.7, 1.6, 1.1, -0.5, -1.6, -4.8 ppm. HRMS (AP⁺): *m/z* calcd for C₄₄H₈₆N₁₂Si₈Zn₃: (1198.3127) [M]⁺; found: (1198.3148).

Synthesis of [{2-(Me₃SiN)-6-(Me₃SiNH)C₅H₃N}₂{2,6-(Me₃SiNH)₂C₅H₃N}Zn] (7):

To a solution of **bap** (3.8 mmol, 1.0 g) in toluene (30 mL) at 0 °C was slowly added a solution of ZnEt₂ (1.3 mmol, 1.3 mL, 1.0 M in hexane). The reaction mixture was allowed to come to room temperature and stirred for 6h. All the volatiles were removed under vacuum to give a white solid that afforded transparent crystals of **7** on crystallization from pentane at -30 °C. Yield 0.56 g (52 %). Mp: 215-217 °C. IR (nujol) *v*: 3388 (N-H), 2923, 2853, 2720, 1593, 1462, 1377, 1353, 1298, 1256, 1154, 1084, 1054, 974, 894, 842, 796, 726, 682, 620, 574, 508 cm⁻¹. ¹H NMR (400 MHz, C₆D₆): δ = 7.02 (t, 3H, *p*-ArH, ³J_{H-H} = 8 Hz), 5.80 (d, 6H, *m*-ArH, ³J_{H-H} = 8 Hz), 4.46 (s, 4H, -NH-), 0.22 (s, 27H, SiMe₃), 0.22 (s, 24 H, SiMe₃) ppm; ¹³C{¹H} NMR (100 MHz, C₆D₆): δ = 160.4 (Py-C2/C6), 139.3 (Py-C4), 98.3, (Py-C3/C5), 0.9 (SiMe₃) ppm; ²⁹Si NMR (79.5 MHz, C₆D₆): δ = -1.1 (SiMe₃) ppm.

Synthesis of [{2-(Me₃SiN)-6-(Me₃SiNH)C₅H₃N}₂{2-6-(Me₃SiNH)C₅H₃N}Zn₂] (8):

To a solution of **7** (0.5 mmol, 0.4 g) in toluene (30 mL) at 0 °C was slowly added a solution of ZnEt₂ (0.5 mmol, 0.5 mL, 1.0 M in hexane). The reaction mixture was allowed to come to room temperature and stirred for 6 h. All the volatiles were removed under vacuum to give a white solid that afforded transparent crystals of **8** on crystallization from DCM at -20 °C. Yield: 0.20 g (42 %). Mp: 276-278 °C (decomposition). IR (nujol) *v*: 3384, 2923, 2855, 2720, 1589, 1457, 1457, 1372, 1257, 1156, 1053, 847, 1044, 730, 686 cm⁻¹. ¹H NMR (400 MHz, C₆D₆): δ = 7.03 (t, 3H, *p*-ArH, ³J_{H-H} = 8 Hz), 5.79 (d, 6H, *m*-ArH), 4.39 (s, 2H, -NH-) 0.22 (s, 54H, SiMe₃) ppm;

$^{13}\text{C}\{^1\text{H}\}$ NMR (100 MHz, C_6D_6): $\delta = 159.9, 139.2, 98.3, 0.07$ (SiMe_3) ppm. HRMS (AP^+): m/z calcd for $\text{C}_{33}\text{H}_{65}\text{N}_9\text{Si}_6\text{Zn}_2$: (883.2562) $[\text{M}]^+$; found: (883.2599).

Synthesis of bicyclic pyridinophane {[2,6(Me_3SiN) $\text{C}_5\text{H}_3\text{N}$] $_3\text{Zn}_2$ } (**9**):

The 1:2 reaction of *bap* and *n*BuLi in hexane gave dilithium bis(trimethylsilyl)-*N,N'*-2,6-diamidopyridine compound in good yield. To a solution of *bap*Li₂ (3.8 mmol, 1.0 g) in toluene (30 mL), a solution of (2.5 mmol) ZnCl₂ (0.34 g) or ZnI₂ (0.8 g) in toluene (30 mL) was added slowly at 0 °C. The reaction mixture was allowed to warm to room temperature and stirred further for 12 h at rt. The mixture was then filtered to remove salt LiX (X = Cl, I), and all the volatiles were removed under vacuum to give a solid which on further crystallization from pentane at -20 °C for 3 days, gave transparent crystals of **9**. Yield: 0.35 g (31 %). Mp: 149-152 °C. IR (nujol) ν : 2958, 2853, 1586, 1457, 1374, 1253, 1156, 1089, 1036, 847, 783, 728, 624, 584 cm^{-1} . ^1H NMR (400 MHz, C_6D_6): $\delta = 7.07$ (triplet, 1H, *p*-ArH, $^3J_{\text{H-H}} = 8$ Hz), 6.97 (triplet, 2H, *p*-ArH, $^3J_{\text{H-H}} = 8$ Hz), 6.05 (doublets, 2H, *m*-ArH), 5.91 and 5.88 (closely overlapped doublets, 4H, *m*-ArH, $^3J_{\text{H-H}} = 8$ Hz), 0.36, 0.32, 0.06 (s, 18H each, SiMe_3) ppm; $^{13}\text{C}\{^1\text{H}\}$ NMR (100 MHz, C_6D_6): $\delta = 166.3, 166.3, 163.9, 143.6, 140.4, 103.2, 103.1, 101.7, 1.5, 1.4, 1.00$ (SiMe_3) ppm; ^{29}Si NMR (79.5 MHz, C_6D_6): $\delta = 1.9, -2.5, -3.5$ (SiMe_3) ppm. HRMS (AP^+): m/z calcd for $\text{C}_{30}\text{H}_{65}\text{Zn}_2\text{N}_9\text{Si}_6$: (885.2539) $[\text{M}+2\text{H}]^+$; found: (885.2545).

3.5 Crystallographic Data

Table 3.5.1 Crystallographic data of Compounds 1-3.

Compound	1	2	3
Chemical formula	C ₂₄ H ₅₀ N ₆ Si ₄ Zn ₂	C ₂₆ H ₅₂ N ₆ Si ₄ Zn ₂	C ₂₆ H ₅₄ N ₆ Si ₄ Zn ₄
molar mass	615.40	691.84	824.59
Crystal system	Orthorhombic	Orthorhombic	Monoclinic
Space group	<i>P2₁2₁2₁</i>	<i>Pna2₁</i>	<i>P2₁/c</i>
<i>T</i> [K]	150.00(10)	150.00(10)	150.00(10)
<i>a</i> [Å]	13.1654(6)	15.601(2)	12.7790(5)
<i>b</i> [Å]	15.6019(7)	13.1808(14)	15.8345(5)
<i>c</i> [Å]	17.9741(7)	18.391(3)	19.8594(7)
α [°]	90	90	90
β [°]	90	90	108.533(4)
γ [°]	90	90	90
<i>V</i> [Å ³]	3692.0(3)	3781.8(9)	3810.1(2)
<i>Z</i>	4	4	4
<i>D</i> (calcd.) [g·cm ⁻³]	1.107	1.215	1.437
μ (Mo-K α) [mm ⁻¹]	1.447	1.418	2.635
Reflections collected	54557	13827	53548
Independent reflections	13258	6030	13691
Data/restraints/parameters	13258/0/325	6030/1/357	13691/0/377
<i>RI</i> , <i>wR</i> ₂ [<i>I</i> >2 σ (<i>I</i>)] ^[a]	0.0745, 0.2005	0.0647, 0.1503	0.0428,0.1020
<i>RI</i> , <i>wR</i> ₂ (all data) ^[a]	0.1050, 0.2393	0.0856, 0.1731	0.0613,0.1191
GOF	1.046	1.083	1.154

$$[a] \text{ } RI = \frac{\sum ||Fo| - |Fc||}{\sum |Fo|}, \text{ } wR2 = \left[\frac{\sum w(|Fo|^2 - |Fc|^2)^2}{\sum w|Fo|^2} \right]^{1/2}$$

Table 3.5.2 Crystallographic data of Compounds 4-6.

Compound	4	5	6
Chemical formula	C ₃₀ H ₆₂ N ₆ Si ₄ Zn ₄	C ₃₄ H ₄₄ F ₁₀ N ₆ Si ₄ Zn ₂	C ₃₃ H ₆₃ N ₉ Si ₆ Zn ₃
molar mass	880.69	969.85	1098.24
Crystal system	Monoclinic	monoclinic	Triclinic
Space group	<i>I2/a</i>	<i>I2/a</i>	<i>P</i> $\bar{1}$
<i>T</i> [K]	150.0(10)	200.00(10)	200.00(10)
<i>a</i> [Å]	25.7368(9)	17.2087(8)	12.9696(16)
<i>b</i> [Å]	8.6682(3)	12.2702(7)	15.6204(19)
<i>c</i> [Å]	19.5243(7)	21.7666(11)	17.254(2)
α [°]	90	90	106.853(2)
β [°]	101.613(3)	95.993(5)	91.862(2)
γ [°]	90	90	102.828(2)
<i>V</i> [Å ³]	4266.5(3)	4571.0(4)	3244.2(7)
<i>Z</i>	4	4	4
<i>D</i> (calcd.) [g·cm ⁻³]	1.371	1.409	1.235
μ (Mo-K α) [mm ⁻¹]	2.361	1.226	1.286
Reflections collected	24451	16588	53891
Independent reflections	7364	4042	14920
Data/restraints/parameters	7364/12/211	4042/0/263	14920/0/623
<i>RI</i> , <i>wR</i> ₂ [<i>I</i> > 2 σ (<i>I</i>)] ^[a]	0.0488, 0.1378	0.0664, 0.1704	0.0412, 0.1046
<i>RI</i> , <i>wR</i> ₂ (all data) ^[a]	0.0610, 0.1538	0.0869, 0.2006	0.0682, 0.1205
GOF	1.040	1.083	1.047

[a] $RI = \sum ||Fo| - |Fc|| / \sum |Fo|$. $wR2 = [\sum w(|Fo|^2 - |Fc|^2)^2 / \sum w|Fo|^2]^1/2$

Table 3.5.3 Crystallographic data of Compounds 7-9.

Compound	7	8	9
Chemical formula	C ₃₃ H ₆₇ N ₉ Si ₆ Zn	C ₃₃ H ₆₅ N ₉ Si ₆ Zn ₂	C ₃₃ H ₆₃ N ₉ Si ₆ Zn ₂
molar mass	823.86	887.22	885.20
Crystal system	monoclinic	Monoclinic	Triclinic
Space group	<i>P2₁/c</i>	<i>P2₁/n</i>	<i>P$\bar{1}$</i>
<i>T</i> [K]	150.00(10)	250.00(10)	200.00(10)
<i>a</i> [Å]	36.841(3)	13.1375(14)	11.9821(5)
<i>b</i> [Å]	21.0080(18)	21.0080(18)	18.0824(6)
<i>c</i> [Å]	22.906(2)	19.224(2)	23.5279(8)
<i>α</i> [°]	90	90	92.016(3)
<i>β</i> [°]	106.416(9)	105.811(11)	90.834(3)
<i>γ</i> [°]	90	90	93.951(3)
<i>V</i> [Å ³]	9717.8(15)	5104.8(9)	5081.7(3)
<i>Z</i>	8	4	4
<i>D</i> (calcd.) [g·cm ⁻³]	1.126	1.154	1.157
<i>μ</i> (Mo-K _α) [mm ⁻¹]	0.685	1.111	1.116
Reflections collected	40135	72170	71505
Independent reflections	17112	18103	18000
Data/restraints/parameters	17112/228/950	18103/0/477	18000/144/901
<i>RI</i> , <i>wR</i> ₂ [<i>I</i> >2σ(<i>I</i>)] ^[a]	0.0711, 0.1698	0.0715, 0.1941	0.2272,0.5569
<i>RI</i> , <i>wR</i> ₂ (all data) ^[a]	0.1149, 0.2136	0.1365, 0.2536	0.2597,0.5998
GOF	1.073	1.045	2.664

$$[a] RI = \frac{\sum ||Fo| - |Fc||}{\sum |Fo|}, wR2 = \left[\frac{\sum w(|Fo|^2 - |Fc|^2)^2}{\sum w|Fo|^2} \right]^{1/2}$$

3.6 References

1. (a) R. S. Carmichael, *Ed.*, *CRC Practical Handbook of Physical Properties of Rocks and Minerals*, CRC Press, Boca Raton, FL, **1989**; (b) I. Bodek, I., *Environmental Inorganic Chemistry*, Pergamon Press, New York, **1988**; (c) A. B. Ronov, and A. A. Yaroshevsky, "Earth's Crust Geochemistry," in *Encyclopedia of Geochemistry and Environmental Sciences*, Fairbridge, R. W., *Ed.*, Van Nostrand, New York, **1969**; (d) X. Tian, S. Hussain, C.D. Pace, L. R.-Prez, and G. Battaglia, *Chem. Asian J.* **2019**, *14*, 509.
2. (a) E-X. Zhang, D-X. Wang, Z-T. Huang, and M-X. Wang; *J. Org. Chem.*, **2009**, *74*, 22; (b) H.C. Freake, and K. Sankavaram, *Biomedical science*, **2013**, 437; (c) M. Mesquita, V. Andre, C. V. Esteves, T. Palmeira, M. N. Berberan-Santos, P. Mateus, and R. Delgado, *Inorg. Chem.*, **2016**, *55*, 2212; (d) U. Lehmann, and B. Kersting, *Z. Anorg. Allg. Chem.*, **2013**, *639*, 1543.
3. (a) A. Rit, T. P. Spaniol, L. Maron, and J. Okuda, *Organometallics*, **2014**, *33*, 2039; (b) A. Ross, J. H. Choi, T. M. Hunter, C. Pannecouque, S. A. Moggach, S. Parsons, E. D. Clercq, and P. J. Sadler, *Dalton Trans.*, **2012**, *41*, 6408.
4. (a) T. Cadenbach, J.S. R. Pankhurst, T.A. Hofmann, M. Curcio, P. L. Arnold, and J. B. Love, *Organometallics*, **2015**, *34*, 2608; (b) J. R. Pankhurst, S. Paul, Y. Zhu, C. K. Williams, and J. B. Love; *Dalton Trans.*, **2019**, *48*, 4887; (c) J. A. Marafie, D. D. C. Bradley, and C. K. Williams, *Inorg. Chem.*, **2017**, *56*, 5688.
5. S. Schmidt, B. Gutschank, S. Schulz, D. Bläser, R. Boese, and C. Wölper; *Eur. J. Inorg. Chem.*, **2011**, 4464.
6. Z. Zheng, M. K. Elmekdem, C. Fischmeister, T. Roisnel, C. M. Thomas, J. F. Carpentier, and J. L. Renaud; *New J. Chem.*, **2008**, *32*, 2150.

7. M. T. Nguyen, B. Gabidullin, and G. I. Nikonov, *Dalton Trans.*, **2018**, 47, 4607.
8. M-T. Chen, Y-Y. Chen, G-L. Li, and C-T. Chen; *Front. Chem.*, **2019**, 6, 615.
9. (a) S. Enthaler, and X.-F. Wu; Zinc Catalysis; Eds.; *Wiley-VCH*: **2015**; (b) M. Rauch, S. Kar, A. Kumar, L. Avram, L. J. W. Shimon, and D. Milstein, *J. Am. Chem. Soc.*, **2020**, 142, 14513.
10. P. A. Lummis, M. R. Momeni, M. W. Lui, R. McDonald, M. J. Ferguson, M. Miskolzie, A. Brown, and E. Rivard; *Angew. Chem., Int. Ed.*, **2014**, 53, 9347.
11. A. Rit, A. Zanardi, T. P. Spaniol, L. Maron, and J. Okuda, *Angew. Chem., Int. Ed.*, **2014**, 53, 13273.
12. R. Chambenahalli, A. P. Andrews, F. Ritter, J. Okuda, and A. Venugopal, *Chem. Commun.*, **2019**, 55, 2054.
13. D. Bawari, C. Negi, K. Jaiswal, B. Prashanth, A. R. Choudhury, and S. Singh, *Chem. Commun.*, **2018**, 54, 8857.
14. D. Bawari, C. Negi, V. K. Porwal, S. Ravi, K. R. Shamasundar, and S. Singh, *Dalton Trans.*, **2019**, 48, 7442.
15. C. Negi, D. Bawari, S. K. Thakur, A.R. Chaudhary, and S. Singh, *J. Organomet. Chem.*, **2019**, 901, 120943.
16. L. Beer, J. F. Britten, J. L. Brusso, A. W. Cordes, R. C. Haddon, M. E. Itkis, D. S. MacGregor, R. T. Oakley, R. W. Reed, and C. M. Robertson, *J. Am. Chem. Soc.*, **2003**, 125, 14394.
17. G. G. Skvortsov, G. K. Fukin, S. Y. Ketkov, A. V. Cherkasov, K. A. Lyssenko, and A. A. Trifonov, *Eur. J. Inorg. Chem.*, **2013**, 4173.
18. B. Parker, and D.Y. Son, *Chem. Commun.*, **2002**, 5, 516.

19. M. J. C. Dawkins, E. Middleton, C. E. Kefalidis, D. Dange, M. M. Juckel, L. Maron, and C. Jones, *Chem. Commun.*, **2016**, 52, 10490.
20. (a) K. Huse, C. Wölper, and S. Schulz, *Organometallics*, **2021**, 40, 12, 1907; (b) G. Ballmann, J. Martin, J. Langer, C. Farber, and S. Harder, *Z. Anorg. Allg. Chem.*, **2020**, 593; (c) F. Ritter, T. P. Spaniol, I. Douair, L. Maron, and J. Okuda, *Angew. Chem., Int. Ed.*, **2020**, 59, 23335.
21. (a) CrystalClear 2.0; Rigaku Corporation: Tokyo, Japan, **2013**; (b) O. V. Dolomanov, L. J. Bourhis, R. J. Gildea, J. A. K. Howard, and H. Puschmann, *J. Appl. Crystallogr.*, **2009**, 42, 339; (c) G. M. Sheldrick, *Acta Cryst. A*, **2015**, 71, 3.
22. (a) I. Resa, E. Carmona, E. Gutierrez-Puebla, and A. Monge, *Science*, **2004**, 305, 1136; (b) R. K. Sahoo, S. Rajput, A. G. Patro and Sharanappa Nembenna, *Dalton Trans.*, **2022**, 51; (c) L. Pauling, *The Nature of the Chemical Bond* (Cornell Univ. Press, Ithaca, NY, ed. 3, **1960**), chap. 7.

List of Publications

1. C. Negi, ‡ D. Bawari, ‡ S. K. Thakur, A.R. Choudhury, S. Singh,* Concise access to aluminum containing [3.3](2,6)pyridinophane and molecular bowl using 2,6-diamidopyridine modules; *J. Organomet. Chem.*, **2019**, *901*, 120943 (‡ equal contribution).
2. D. Bawari, C. Negi, K. Jaiswal, B. Prashanth, A.R. Choudhury, S. Singh,* Group 13 element containing conformationally rigid “N–E–N” heteroatomic bridged [3.3](2,6)pyridinophanes (E = B, Al); *Chem. Commun.*, **2018**, *54*, 8857-8860.
3. D. Bawari, C. Negi, V.K. Porwal, S. Ravi, K. R. Shamasundar, S. Singh,* Aluminum containing molecular bowls and pyridinophanes: use of pyridine modules to access different molecular topologies; *Dalton Trans.*, **2019**, *48*, 7442-7450.
4. C. Negi, D. Bawari, V. K. Porwal, S. Singh,* Catalyst free dearomative hydroboration of triazine. Unprecedented synthesis of -BH₂- bridged macrocycles. *Manuscript to be submitted*.
5. C. Negi, M. Goyal, S. Singh,* Modular approach to macrocycles and cluster topologies assembled around zinc centers. *Manuscript to be submitted*
6. C. Negi, ‡ M. Goyal, ‡ S. Singh,* New Members in Cryptand family: Cyclophosphazane based Bicyclic Macrocyces. *Manuscript under preparation*